Regional Modelling of Particulate Matter for the Netherlands

This is a publication of the Netherlands Research Program on Particulate Matter

Netherlands Environmental Assessment Agency

ECN

rivm

TNO

Technical background report BOP

Regional Modelling of Particulate Matter for the Netherlands

M. Schaap, TNO; A.M.M. Manders, TNO; E.C.J. Hendriks, TNO; J.M. Cnossen, PBL;
A.J.S. Segers, TNO; H.A.C. Denier van der Gon, TNO; M. Jozwicka, TNO;
F. Sauter, RIVM; G. Velders, PBL; J. Matthijsen, PBL; P.J.H. Builtjes, TNO

Netherlands Environmental Assessment Agency

ECN
Energy research Centre of the Netherlands

TNO

rivm
National Institute
for Public Health
and the Environment

Regional Modelling of Particulate Matter for the Netherlands
This is a publication of the Netherlands Research Program on Particulate Matter
Report 500099008
M. Schaap, A.M.M. Manders, E.C.J. Hendriks, J.M. Cnossen, A.J.S. Segers, H.A.C. Denier van der Gon, M. Jozwicka, F.J. Sauter, G.J.M. Velders, J. Matthijsen, P.J.H. Builtjes
Contact: karin.vandoremalen@pbl.nl
ISSN: 1875-2322 (print) ISSN: 1875-2314 (on line)

This is a publication in the series: BOP reports

Project assistant: Karin van Doremalen

English editing: Annemarieke Righart
Figure editing: PBL editing and production team
Layout and design: RIVM editing and production team
Cover design: Ed Buijsman (photographer: Sandsun)

ECN Energy Research Centre of the Netherlands
PBL Netherlands Environmental Assessment Agency
TNO Built Environment and Geoscieces
RIVM National Institute for Public Health and the Environment

This study has been conducted under the auspices of the Netherlands Research Program on Particulate Matter (BOP), a national program on PM10 and PM2.5 funded by the Dutch Ministry of Housing, Spatial Planning and the Environment (VROM).

A comprehensive reference to the report reads as ' Schaap M., Manders A.M.M., Hendriks E.C.J., Cnossen J.M., Segers A.J.S., Denier van der Gon H.A.C., Jozwicka M., Sauter F.J., Velders G.J.M., Matthijsen J., Builtjes P.J.H. (2009) Regional modelling of particulate matter for the Netherlands:
The complete publication, can be downloaded from the website www.pbl.nl, or a copy may be requested from reports@pbl.nl, citing the PBL publication number.

Netherlands Environmental Assessment Agency, (PBL)
P.O. BOX 303, 3720 AH Bilthoven, the Netherlands;
Tel: +31-30-274 274 5;
Fax: +31-30-274 4479;
www.pbl.nl/en

Rapport in het kort

Dit rapport is een technisch achtergrond rapport over het modelleren van fijnstof. Voor het beleid is het noodzakelijk om de relatie tussen emissies, atmosferische omstandigheden en de concentraties van luchtverontreinigende stoffen te kwantificeren. In Nederland worden voor dit doel twee modellen gebruikt. Dit document beschrijft de twee modellen en recente ontwikkelingen die binnen het BOP onderzoeksprogramma bereikt zijn. LOTOS-EUROS berekent de luchtkwaliteit op Europese schaal terwijl OPS gericht is op Nederland. Het LOTOS-EUROS model is gevalideerd met metingen en verder ontwikkeld door de toevoeging van verbeterde en nieuwe routines voor het berekenen van de bijdrage van zeezout, bodemstof en biogene secundaire organische aërosolen aan fijnstof. Daarnaast is een koppeling gerealiseerd tussen het mondiale chemietransport model TM5 en LOTOS-EUROS. Tenslotte worden LOTOS-EUROS en OPS getest in vergelijking met het UNIFIED EMEP model voor ammonium, nitraat, sulfaat en primaire deeltjes.

Contents

Abstract

Particulate Matter (PM) causes adverse health effects. Therefore, it is subject to regulations. For policy support, it is necessary to quantify the relation between emissions, atmospheric conditions and concentrations of air pollutants; this is done by using models. Generally, models describe only about half of the PM_{10} concentration, which can be attributed to the known anthropogenic sources. Although sources and dispersion of the other half, like sea salt and mineral dust, are understood, in general terms, understanding by means of modelling is still rather poor. This forms a major handicap for source apportionment of PM concentrations. The Netherlands Research Program on Particulate Matter (BOP) aims for a better understanding of PM by improving models especially with respect to sea salt and mineral dust.

This report is a background document which describes the two models used in the Netherlands and their recent developments accomplished within the BOP research programme. The LOTOS-EUROS model, which calculates air quality on a European scale, and the OPS model, which focuses on the Netherlands, both belong to the main model instruments for policy support in the Netherlands. The LOTOS-EUROS model is further developed for PM by including (improved) parameterisations for the contribution of sea salt, mineral dust and biogenic secondary organic aerosol. In addition, a coupling was realised between the global air quality model TM5 and LOTOS-EUROS. This coupling allowed for calculating the effects of global emission changes on European air quality. Finally, the LOTOS-EUROS model and the OPS model were tested in an intercomparison together with the EMEP model for ammonium, nitrate and sulphate, particles, which are chemically formed in the air from gases, and the fine primary particles, which are directly emitted into the air.

As a base case, the performance of the original operational LOTOS-EUROS version, without the new developments, was investigated and compared with observations within the Netherlands. The time correlation of total PM_{10} was reasonable, but absolute concentrations were underestimated, especially for the highest concentrations. Secondary inorganic aerosols were well represented, both in time and space. Elemental carbon and sea salt concentrations could not be validated well, and components such as mineral dust and secondary organic aerosol were not modelled. A simple bias correction was proposed to improve the modelling of total PM_{10}.

Three adaptations were made to improve the model description of sea salt:

1. The particle-size resolution was doubled
2. The source function for the smallest sea salt particles was now according to Mårtensson (2003).
3. A new dry deposition scheme was introduced according to Zhang (2001).

The new sea salt parameterisation resulted in an improved representation of the model sea salt processes. However, sea salt concentrations which result from the improved parameterisation were an overestimation in comparison with European observations (between 50% and 100%). The modelled overestimation occurred especially at high wind speeds. Large uncertainties (by a factor of 10) in the sea salt source function formulations were likely to be the main cause of our overestimation.

Hereafter, mineral dust was included in the LOTOS-EUROS model as a new PM fraction. A description was made of three different mineral dust sources.

4. The emission of wind-blown dust (wind-induced abrasion) was included, taking soil texture, soil moisture and precipitation into account. Dust which originates from large deserts outside the LOTOS-EUROS domain was included through coupling with the global model, TM5.
5. Resuspension of mineral dust due to traffic circulation was also included. The description includes the effects of precipitation and a regional dependence in terms of climatic conditions on the basis of soil moisture information and observed PM concentrations.
6. A first effort was made to model the emission of mineral dust due to agricultural activity. The source function describes emission of mineral dust from agricultural land, based on the agricultural activity calendar and taking the effects of precipitation into account.

Furthermore, the modelling of biogenic volatile organic carbon emissions was improved. These emissions have an impact on the formation of secondary organic aerosol (SOA), for which the chemical formation scheme was also extended.

The intercomparison was based on modelled concentration levels and results from source receptor matrices (SRM) per model. Overall, the results of the LOTOS-EUROS model are closer too those of the EMEP model version 2.8 than those of the OPS model. The model intercomparison showed that

per PM fraction model results were different for each model considered. The results from the models form a range, which can be seen as a margin of uncertainty when using models for policy support, provided that the models are equally fit.

The OPS model is currently used for calculating average annual concentrations of primary particulate matter (PPM) and the secondary inorganic aerosol (SIA) for the specific air quality situation in the Netherlands. OPS is not always suitable for scenarios studies on the effect of emission reductions of SO_2, NO_x and NH_3, due to the absence of non-linear chemistry modelling. This is confirmed in this report by the SRM results, in particular, by those for NH_3. The accuracy of the spatial distribution of ammonium with OPS on a 1x1 km^2 grid is limited due to the linear approach. Source-receptor data, generated with OPS, are reliable when NO_x, SO_2, and NH_3 emissions are reduced proportionally and simultaneously.

The SRM results of LOTOS-EUROS, OPS and EMEP v2.8 could be generalised as follows. The relative reaction of the average particulate matter concentration in the Netherlands to 15% reduction in $PPM_{2.5}$, NH_3 and NO_x was about the same for all three (several percents reduction). 15% emission reductions of SO_2 lead to less than 1% reduction of PM. The reaction per kiloton emission change gave an impression of the effectiveness of emission changes. Reducing $PPM_{2.5}$ was most effective, naturally, followed by NH_3, NO_x and SO_2. The reaction per kiloton of emission reduction, for all pollutants considered, was largest in the Netherlands, followed by Belgium, Germany and France, and was the smallest in Great Britain.

1 Introduction

1.1 Background

While air quality in Europe has improved substantially over the past decades, air pollution still poses a significant threat to human health (EEA, 2007). Health effects of air pollution are dominated by particulate matter, both $PM_{2.5}$ and PM_{10}. Short-term exposure to PMx has frequently been associated with increased human morbidity and mortality (e.g., Brunekreef and Holgate, 2002). Although the effects of long-term exposure to PM are much more uncertain than the effects of short-term exposure, they are believed to have a much greater effect on health loss (Dockery *et al.,* 1993; Pope *et al*., 1995). Therefore, the European air quality standards currently focus on the total mass of the unspecified combined particles smaller than 10 µm in diameter (PM_{10}), which cover the inhalable size fraction of PM. At present, many European countries, including the Netherlands, have problems attaining the daily limit value for PM_{10}.

Mass and composition of PM_{10} tend to divide into two principal groups: fine and coarse mode. The fine particles (typically smaller than 2.5 microns) contain secondary inorganic aerosols (SIA), elemental carbon and organic material. The larger particles usually contain sea salt, earth crust materials and fugitive dust from roads and industries. To quantify the relation between emissions, atmospheric conditions and concentrations of air pollutants one depends on chemistry transport models (CTMs). For a robust application of a regional CTM in policy support studies such as the evaluation of mitigation strategies, it is important that the model can represent the air pollutant concentration and the most important processes affecting the concentration in a satisfactory way. However, for particulate matter the current CTMs underestimate the PM_{10} concentrations by about 40 to 50%. This so-called non-modelled fraction comprises a number of PM components: sea salt, crustal material, secondary organic material and water. To gain more insight in the variability of the PM_{10} concentrations and the mechanisms that lead to concentrations above the daily mean threshold of 50 µg/m³ one needs to incorporate these components in the model. This report describes the effort to develop or incorporate a modelling framework for sea salt, dust and secondary organic aerosol for use in the CTM LOTOS-EUROS.

1.2 Goals and approach

This report aims to provide a technical background document to the modelling work performed in the project of the Netherlands Research Program on Particulate Matter (BOP). To put the work into the perspective of the BOP programme, we describe several research questions that contribute to the main purpose of the programme. Each research question was translated into a question relating to modelling (placed in italics). The motivation and the approaches used for answering these questions are described below each research question. The methodologies for answering the research questions are described in this report. The use of the LOTOS-EUROS model to answer these policy and science related questions is described in the main thematic reports of the project.

What are the mechanisms that lead to an exceedance of the daily limit value and which sources and/or components contribute the most to these high pollution days? *Can we use modelled particulate matter distributions to address exceedance days?*

Chemistry transport models provide a relation between emissions, atmospheric conditions and concentrations of air pollutants. However, for PM_{10} CTMs underestimate the total concentrations. First we examined the performance of LOTOS-EUROS for PM_{10} by a comparison between modelled and measured PM_{10} concentrations in the Netherlands. To detail the model performance, making a comparison between the PM components was mandatory. Hence, we performed the analysis to the furthest extent possible, which is described in Chapter 3.

What is the contribution of sea salt to the PM_{10} and $PM_{2.5}$ concentration on an annual basis and on days with limit value exceedances? *How well does the model perform for sea salt? How sensitive are the modelled sea salt contributions to the choice of emission and dry deposition parameterisation?*

Sea salt is modelled in all models used in the Netherlands. However, models use different methodologies for the emission parameterisation. These different modules may have a large impact on the modelled distribution. Here, we update the model description to the combination of emission parameterisations that is considered to be state-of-the-art. In addition, the model results for sea salt have not been extensively validated for both Dutch and European conditions. For the Netherlands, validation and

assessments of sea salt concentrations have relied largely on chloride measurements which are not well defined. Therefore, the BOP measurements and the efforts to compile foreign data provide the first opportunity for a more extensive validation. Furthermore, the coarse mode sea salt distribution is sensitive to the parameterisation used for the dry deposition, which largely determines the transport distance. We tested the impact of a scheme based on theory to compare the results to the empirical approach that was used up to now. This work is described in Chapter 4.

What is the contribution of soil dust to the PM_{10} and $PM_{2.5}$ concentration on an annual basis and on days with limit value exceedances? *How can we model crustal matter emissions and to which extent can we estimate the source strength of this component?*

Crustal material or soil particles typically contribute between 5 and 20% to the ambient PM_{10} mass. Despite the importance of crustal material in total PM_{10} mass, the sources are still scarcely understood and not (well) represented in emission inventories or air quality models. Here we aimed to develop a methodology for checking first-order estimates of the various source strengths in Europe and in the Netherlands, in particular. For this purpose, we implemented simple and therefore transparent emission functions for wind erosion, (re-)suspension by traffic and agricultural land management. Furthermore, we included boundary conditions for desert dust from the global TM5 model. A first assessment of the model performance is also given in Chapter 5.

What is the contribution of carbonaceous material to the PM_{10} and $PM_{2.5}$ concentration on an annual basis and on days with limit value exceedances? *How can we model the formation of organic material in the atmosphere?*

Chemistry transport models underestimate the concentrations of carbonaceous material. Previous studies have concluded that the emissions of elemental carbon (EC) and organic carbon (OC) are probably underestimated. In addition to primary EC and OC, secondary organic aerosol may contribute significantly to the observed OC levels. The formation of secondary organic aerosols (SOAs) is not represented in LOTOS-EUROS. Several schemes have been documented in literature. However, current understanding is so uncertain that we have incorporated a scheme that is flexible and can easily be extended in the future. The chosen approach is described in Chapter 6.

What is the contribution of non-European sources to PM levels in the Netherlands? *What is the impact of using boundary conditions from a global modelling system?*

Dutch levels of PM may be affected to some extent by sources from outside the model domain. Current practice incorporates an estimated 0.9 µg/m³ into the annual average PM_{10} concentration. For sea salt, dust and ozone, the impact is estimated to be non-negligible and we tested the use of a global CTM to provide the boundary conditions for LOTOS-EUROS. In Chapter 7, we will demonstrate that the model is capable of using boundary conditions from TM5.

Note that the model development with BOP is not performed based on the BOP measurement programme as both activities are performed simultaneously. Moreover, the observation database was not available when this report was printed. Hence, all model results shown in this report are for the year 2005. Comparison of the model results to the BOP measurements will be shown in thematic reports.

1.3 Rational model choice

In the Netherlands, two models are used for policy support. The first is the OPS model, developed by the Netherlands Environmental Assessment Agency (PBL). The second model is the LOTOS-EUROS model developed by TNO Built Environment and Geosciences and the National Insitute for Public Health and the Environment (RIVM). For the BOP project, LOTOS-EUROS was chosen over OPS to be used as the central model for development. The first reason for this is that it has full photochemistry incorporated which is necessary to address the secondary aerosols properly. Furthermore, the model incorporates a larger domain and performs calculations on an hourly basis using analysed meteorology, enabling a more extensive comparison with observations. Finally, LOTOS-EUROS is well documented with respect to its performance in comparison to other European models.

Considering the different model approaches in LOTOS-EUROS and OPS, a variability of the results between the models is expected. Therefore, an assessment was performed to find out the most important differences in the results of the models in a policy oriented application (Chapter 8). In addition to the Dutch models, the unified model from the European Monitoring and Evaluation Programme (EMEP) is also incorporated in the comparison as this model is used within the convention on trans-boundary air pollution

To guarantee that OPS also benefits from the BOP project, all developed parameterisations within this report will be made available to the developers of OPS.

2 Model descriptions

2.1 The LOTOS-EUROS model

The LOTOS-EUROS model is an operational air quality and chemical transport model of intermediate complexity focused on modelling the composition of the lower part of the troposphere. The model is used for calculating air pollutant concentrations and depositions on a regional scale [Schaap *et al.*, 2008]. The LOTOS-EUROS model has been frequently used in policy support studies for the Netherlands, Germany and Europe. Furthermore, the model has been developed and used in a large number of European research projects. The model describes the processes of emission, transport, chemical conversion and dry and wet deposition. The LOTOS-EUROS model can be characterised as an Eulerian model in which all processes are solved at an evenly distributed grid. Up to now, the LOTOS-EUROS modelling system could be applied for the following components:

- *Oxidants: O_3, VOC's, NOx, HNO_3, etc*
- *Secondary inorganic aerosol (SIA): SO_4, NO_3, NH_4*
- *Secondary organic aerosol (SOA) from terpenes*
- *Primary aerosol:* $PPM_{2.5}$, $PPM_{10\text{-}2.5}$, Black Carbon (BC), sea salt.
- *Heavy metals:* Cd, Pb and other non-volatile metals
- *POP's:* BAP, etc.

Particulate Matter in LOTOS-EUROS is modelled as the sum of the individual components as these components have different origins and atmospheric behaviour. At the start of the BOP project, PM_{10} is defined as the sum of the secondary inorganic components, the primary emitted particles and sea salt:

$$PM_{10} = SO_4 + NO_3 + NH_4 + PPM_{2.5} + PPM_{2.5\text{-}10} + EC + SS$$

Considering that $PM_{2.5}$ is part of PM_{10}, it is calculated similarly but the coarse primary and sea salt particles are excluded from the summation:

$$PM_{2.5} = SO_4 + NO_3 + NH_4 + PPM_{2.5} + EC + SS_{fine}$$

As noted before, secondary organic aerosols and crustal matter were not included in LOTOS-EUROS at the start of the project and their contributions should be added when they become available in LOTOS-EUROS.

A description of the model characteristics is given below.

Domain

The master domain of LOTOS-EUROS is bound at 35° and 70° North and 10° West and 60° East. The projection is a normal longitude–latitude and the standard grid resolution is 0.50° longitude x 0.25° latitude, approximately 25x25 kilometres. The model code is structured such that zooming (up to a factor of 8) is possible. Currently, there are three vertical dynamic layers and an optional surface layer. The model extends in a vertical direction for 3.5 kilometres above sea level. Note that, in this study, we added an extra layer of 3.5 to 5 kilometres. The lowest dynamic layer is the mixing layer, followed by two reservoir layers. The height of the mixing layer is part of the diagnostic meteorological input data. The heights of the reservoir layers are determined by the difference between the mixing layer height and 3.5 kilometres. Both reservoir layers are equally thick with a minimum of 50 metres. In some cases when the mixing layer extends near or above 3500 metres the top of the model exceeds the 3500 metres according to the abovementioned description. Simulations were performed with the optional surface layer with a fixed depth of 25 metres. Hence, this layer is always part of the dynamic mixing layer. For output purposes, the concentrations at measuring height (usually 3.6 m) are diagnosed by assuming that the flux is constant with height and equal to the deposition velocity times the concentration at height z.

Transport

The transport consists of advection in 3 dimensions, horizontal and vertical diffusion, and entrainment or detrainment. The advection is driven by meteorological field (u,v) input, every three hours. The vertical wind speed w is calculated by the model to be a result of the divergence of the horizontal wind fields. The improved and highly accurate, monotonic advection scheme developed by Walcek (2000) is used to solve the system. The number of steps within the advection scheme is chosen in such a way that the courant restriction is fulfilled. Entrainment is caused by the growth of the mixing layer during the day. Each hour, the vertical structure of the model is adjusted to the new mixing layer depth. After the new structure is set, the pollutant concentrations are redistributed by using linear interpolation.

The horizontal diffusion is described with a horizontal eddy diffusion coefficient following the approach by Liu and Durran (1977). Vertical diffusion is described using the standard Kz theory. Vertical exchange is calculated by employing the new integral scheme by Yamartino *et al.* (2004).

Chemistry

The LOTOS-EUROS model contains two chemical mechanisms, the TNO CBM-IV scheme (Schaap *et al*., 2005) and the CBM-IV by Adelman (1999). In this study we used the TNO CBM-IV scheme which is a modified version of the original CBM-IV (Whitten *et al*., 1980). The scheme includes 28 substances and 66 reactions, including 12 photolytic reactions. Compared to the original scheme steady state approximations were used to reduce the number of reactions. In addition, reaction rates have been updated regularly. The mechanism was tested against the results of an intercomparison presented by Poppe *et al*. (1996) and found to be in good agreement with the results presented for the other mechanisms. Aerosol chemistry is represented by using ISORROPIA (Nenes *et al*., 1999).

Dry and wet deposition

The dry deposition in LOTOS-EUROS is parameterised following the well-known resistance approach. The deposition speed is described as the reciprocal sum of three resistances: the aerodynamic resistance, the laminar layer resistance and the surface resistance. The aerodynamic resistance is dependent on atmospheric stability. The relevant stability parameters (u*, L and Kz) are calculated by using standard similarity theory profiles.

The laminar layer resistance and the surface resistances for acidifying components and particles are described following the EDACS system (Erisman *et al*., 1994).

Below-cloud scavenging is described by using simple scavenging coefficients for gases (Schaap *et al*., 2005) and following Simpson *et al*. (2003) for particles. In-cloud scavenging is neglected due to the limited information on clouds. Neglecting in-cloud scavenging results in wet deposition fluxes that are too low, but it has a very limited influence on ground level concentrations (see Schaap *et al*., 2004a).

Meteorological data

The LOTOS-EUROS system in its standard version is driven by 3-hourly meteorological data. These include three-dimensional fields for wind direction, wind speed, temperature, humidity and density, substantiated by two-dimensional gridded fields of mixing layer height, precipitation rates, cloud cover and several boundary layer and surface variables. The standard meteorological data for Europe are produced at the Free University of Berlin employing a diagnostic meteorological analysis system based on an optimum interpolation procedure on isentropic surfaces. The system utilises all available synoptic surface and upper air data (Kerschbaumer and Reimer, 2003). Also, as was done for this study, meteorological data obtained from ECMWF can be used to force the model.

Emissions

The anthropogenic emissions used in this study are a combination of the TNO emission database (Visschedijk and Denier van der Gon *et al*., 2005) and the Clean Air For Europe (CAFE) baseline emissions for 2000. For each source category and each country, we scaled the country totals of the TNO emission database to those of the CAFE baseline emissions. Elemental carbon (EC) emissions were derived from (and subtracted from) the primary $PM_{2.5}$ ($PPM_{2.5}$) emissions following Schaap *et al*. (2004b). Hence, we used the official emission totals as used within the protocol of long-ange transboundary air pollution (LRTAP), but we benefited from the higher resolution of the TNO emission database (0.25°x0.125° longitude–latitude). The annual emission totals were broken down to hourly emission estimates by using time factors for the emissions strength variation over the months, the days of the week and the hours of the day (Builtjes *et al*., 2003).

In LOTOS-EUROS, biogenic isoprene emissions were calculated following Veldt (1991) by using the actual meteorological data. In addition, sea salt emissions were parameterised following Monahan *et al.* (1986) from the wind speed at ten-metre heights.

Boundary conditions

The lateral boundary conditions used in this study were obtained by a simulation of the LOTOS-EUROS model with its full domain. Model top boundary concentrations were set to 0.8 ug/m3 for sulphate, and ammonium was set to neutralise the sulphate. Other aerosol substances were set to zero. Ozone concentrations were obtained from Logan (1999).

Use of the LOTOS-EUROS model

The LOTOS-EUROS model is used for air quality studies at several institutes in the Netherlands. Presently, the LOTOS-EUROS consortium consists of TNO, PBL, RIVM and KNMI. Furthermore, researchers at several universities have access to the model. In the last two years, the model has been used to perform air quality studies for VROM, PBL, EEA, UBA Germany and the EU DG Environment. Scientific studies have been performed to address aerosol nitrate (Schaap *et al*., 2004a; 2007), black carbon (2004b; 2007), heavy metals (Denier van der Gon *et al*., 2008), PM_{10} (Van Zelm *et al*., 2008); Van de Kassteele *et al*., 2007), ozone (Vautard *et al*., 2006) and POP's (Hollander *et al*., 2007). The model has frequently particpated in international model comparisons aimed at ozone (Van Loon *et al*., 2007; Hass *et al*., 200x), PM (Cuvelier *et al*., 2007; Hass *et al*., 200x; Stern *et al*., 2008; Schaap *et al*., 2008) and source Receptor Matrices (Thunis *et al*., 2008). Recently, data assimilation techniques have been used to perform a combined assessment of the air pollution levels using the model and observational data (e.g. Van Loon *et al*., 2001; Denby *et al*., 2008; Barbu *et al*., 2008). A new direction is the use of satellite data in combination with these data assimilation techniques (e.g. Koelemeijer *et al*., 2006; Timmermans *et al*., 2008).

1.2 OPS

The OPS model is used for calculating time averaged concentrations and depositions on a local to regional scale from European emissions to the atmosphere [Van Jaarsveld, 2004]. OPS model results are used in combination with air quality measurements for assessment of air pollution in the Netherlands [e.g. Velders *et al*., 2008]. The model describes the processes of emission, transport, chemical conversion and dry and wet deposition. The OPS model is a universal air quality dispersion model and is a fit for those substances for which

the atmospheric loss processes can be described as first-order loss reactions. Ozone is therefore excluded. The OPS model can be characterised as a Lagrangian model in which the transport equations are solved analytically. Contributions from the various sources are calculated independent of each other by using backward trajectories; local dispersion is introduced via a Gaussian plume formulation. Dry deposition, wet deposition and chemical conversion are incorporated as first-order processes and independent of concentrations of other substances. The only exception is the dry deposition of NH_3 and SO_2, which are mutually dependent.

The basic meteorological data needed by the model (wind direction and velocity, temperature, solar radiation and precipitation) are taken from 16 stations of national meteorological network in the Netherlands. This includes also data from the 200 meter meteorological tower at Cabauw. On the basis of these data meteorological statistics are derived with a specific pre-processor for six regions within the Netherlands. The model determines for every receptor point specific dispersion properties for every receptor point by interpolation of the regional data and depending on terrain roughness. The operational OPS model calculates long-term average (yearly) concentrations and depositions. A short-term version of the model is available.

Validation
OPS model results agree with air pollution concentrations (trends and spatial distribution) as measured by the Dutch national air quality monitoring network [LML, 2008] over the past 10 to 20 years. This is especially true, on a yearly basis, for the following substances: sulphur dioxide (SO_2) and particulate sulphate (SO_4), nitrogen oxides (NO_x) and particulate nitrate (NO_3), ammonia (NH_3) and particulate ammonium (NH_4) (with r = 0.88 to 0.93 for SO_2 and NO_x) [Van Jaarsveld, 1989, 1995 and 2004; Asman and Van Jaarsveld, 1990].

Use of the OPS model
The OPS model is widely used for air quality studies in the Netherlands [see e.g. Van Jaarsveld, 2004 and references therein]. The model has also been adapted (Mensink and Janssen, 1996) to be used in Flanders, for Belgian air quality assessments. Source receptor matrices, calculated by the OPS model, have served as input for a Dutch version of the GAINS model (Wagner *et al*., 2007), GAINS-NL (Aben *et al*., 2005). GAINS-NL combines the high resolution of the OPS model with the integrated approach of the GAINS model.

OPS differs from LOTOS-EUROS (LE)
There are several differences between the OPS and LE models.

1. Dispersion: the OPS model treats dispersion in a Lagrangian way and includes a Gaussian plume formulation for local dispersion, whereas the LE model applies a Eulerian approach on a grid. The differences have consequences for the final particulate matter results. Results following the OPS model approach are not better or worse, a priori, then when following an Eulerian approach. Lagrangian models are usually computationally more demanding. The dispersion of point source emissions, especially on the scale of the (Eulerian) grid size, are better described by using a Lagrangian approach. Primary particulate matter is emitted from point sources (e.g. chimneys or car exhausts) as well as in a diffuse manner (e.g. by sea salt).
2. Resolution: the time resolution of the operational OPS model is one year, whereas the LE model calculates concentration levels with time steps of half an hour. The OPS model therefore does not describe the day-to-day behaviour of particulate matter. It is important to understand the behaviour of particulate matter, for instance, regarding compliance to the limit value of 50 µg/m³ for daily average PM_{10} concentrations.
3. The spatial resolution of both models is also different. The OPS model calculates concentration levels for receptor points which are converted to gridded concentrations on a 5×5 km² or 1×1 km² resolution, depending on the input resolution of the gridded emissions (e.g. NH_3 emissions are gridded with a resolution of 0.5×0.5 km²). LE has a standard resolution of approximately 25×25 km², but can zoom in with a resolution of about 5×5 km². The LE model describes air-quality parameters in four layers for the lower troposphere .
4. Chemistry: the OPS model does not include complex chemical reactions, although (semi) first-order reactions for modelling some important chemical conversions are included. The LE model, however, is designed to calculate long-term ozone concentrations and therefore carries extensive oxidant and aerosol chemistry for the troposphere. It describes the non-linear behaviour of oxidants and aerosols.
5. Boundary and initial conditions: the OPS model does not apply boundary conditions to particulate matter calculations nor does it set initial conditions. The LE model uses fixed boundary conditions at the sides and the top of the domain, of around 3.5 kilometres. These conditions may vary in time and place, as if the LE model were nested into a hemispheric or global model. There is however no dynamic interaction between boundary conditions and the model.

Although other differences exist between the OPS and LE models in the description of other processes such as wet and dry deposition, basically, they are not different.

3 Base case

To quantify the relation between emissions, atmospheric conditions and concentrations of air pollutants, one depends on chemistry transport models (CTMs). For a robust application of a regional CTM, it is important that the model effectively can represent the concentration of air pollutants and the most important processes affecting the concentration. This chapter illustrates that chemistry transport models, including LOTOS-EUROS, underestimate the ambient PM_{10} concentrations. In doing so, we describe the status of LOTOS-EUROS before the implementation of new parametersations in the BOP programme. This chapter also shows the annual mean distributions as calculated by the model and examines the performance of the LOTOS-EUROS model for PM_{10} by comparing the modelled and measured concentrations for the Netherlands. To discuss the model performance in detail, a comparison between the individual PM components is necessary. Section 3.1 describes the simulation set-up and measurement data for the year under study, 2005. The modelled annual average distributions are presented in Section 3.2 and compared to observations in Section 3.3. To examine the modelled variability in PM_{10} concentrations and the possibility of having to perform a bias correction, we have incorporated more data by extending the analysis to include the period from 2004 to 2006. The model results are discussed in Section 3.4.

3.1 Methodology

3.1.1 Run description

We performed a simulation for a European domain, bound at 35° and 70° North and 10° West and 40° East. The grid resolution for this domain was 0.50° longitude x 0.25° latitude, i.e. approximately 25x25 kilometres over the Netherlands. Using a one-way zoom option, a high resolution simulation was obtained for the Netherlands and its direct surroundings, with an increase in resolution by a factor of four. The model was forced by using ECMWF meteorology and anthropogenic emissions (TNO-GEMS emission database). Natural sea salt (SS) emissions were calculated by the model, using Na as a tracer. Hourly concentrations of all particulate components were stored. The PM_{10} concentrations were diagnosed as the sum of the separate model components:

$$PM_{10} = SO_4 + NO_3 + NH_4 + PPM_{10} + SS,$$

with $PPM_{10} = PPM_{2.5} + PPM_{coarse} + EC$

From the primary $PM_{2.5}$ ($PPM_{2.5}$) the elemental carbon (EC) component was also calculated, following Schaap *et al.* (2004b). Crustal matter (CM) and secondary organic aerosols (SOAs) were not yet incorporated in the base model version, because of a lack of solid knowledge both on emission strengths for CM and formation routes for SOA.

3.1.2 Monitoring data

To verify the modelled concentrations for the Netherlands, we used monitoring data from the national air quality network as operated by the RIVM (Beijk *et al.*, 2007a). The network includes 15 rural stations for PM_{10} (see Figure 3.1). All data were corrected for sampling losses by using the standard procedures of the RIVM (Beijk *et al.*, 2007b). For the evaluation of LOTOS-EUROS, only rural background stations were used, since the resolution of LOTOS-EUROS is not high enough to produce road-level results. Furthermore, secondary inorganic aerosol concentrations were obtained for six rural locations. Finally, we used black smoke measurements to assess the model performance for EC. EC concentration data were estimated by using the empirical relation between black smoke and EC as determined by Schaap and Denier van der Gon (2007). As different analysing procedures for EC systematically yield different levels (by up to a factor of 2) (Ten Brink *et al.*, 2004), the information was mainly used for assessing the temporal performance of the model.

The results of the model at the abovementioned stations were evaluated for PM_{10} by using a range of statistical parameters. These are: average, root mean square error, residue, standard deviation of error, correlation, hit rate, hit ratio, and percentage of correct alarm (in the concentration interval of 50 to 200 µg/m³).

3.2 Modelled distributions

In this section, we present the modelled concentration data for PM_{10} and its components. In Figure 3.2, we present the modelled annual mean PM_{10} distribution for Europe as a whole and for the Netherlands, for 2005. The European domain shows maxima over the Benelux, Poland and the Po Valley (Italy). In these areas, the modelled concentrations exceeded 15 µg/m³. Similarly, large cities or agglomerations are recognisable with similar concentrations. Concentrations of 7.5 to 15 µg/m³ were found for a band over northwestern Europe, central and southeastern Europe. In general, the modelled

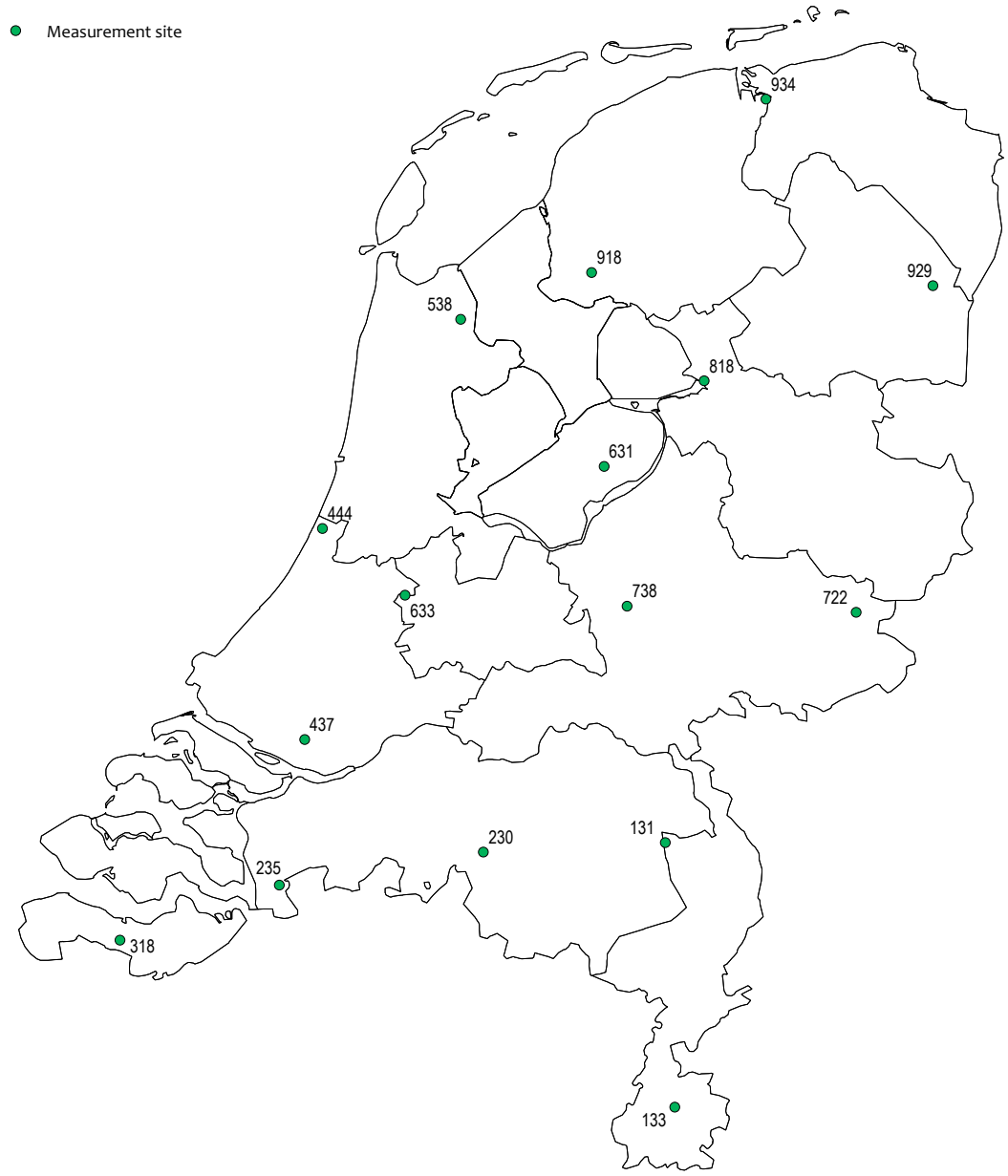

LML stations in the Netherlands used in the verification of the modelled PM_{10} distribution. All stations have been indicated by station number.

PM_{10} concentrations declined from Central Europe to northern Scandinavia and towards the Iberian Peninsula.

The modelled concentrations for the Netherlands showed levels between 10 and 20 µg/m³. The lowest concentrations were modelled for the province of Groningen. Concentrations between 14 and 18 µg/m³ were calculated for the populated western part of the Netherlands and for the river area stretching towards the Ruhr Area in Germany. Note that the modelled concentrations for the Belgian cities were (modelled to be) higher than those for the Netherlands. Minimum concentrations over the zoom area were calculated over the forest regions of the Ardennes and Germany, south-east of the Ruhr Area.

The annual average distributions of the modelled components are shown in Figure 3.3. Comparison of the distribution showed that each component had a specific distribution over the Netherlands. Sulphate contributed 1.7 to 2.2 µg/m³ to the PM_{10} concentration. It had a relatively even distribution over the Netherlands with maximum concentrations over a band connecting the Ruhr Area and the southern part of the

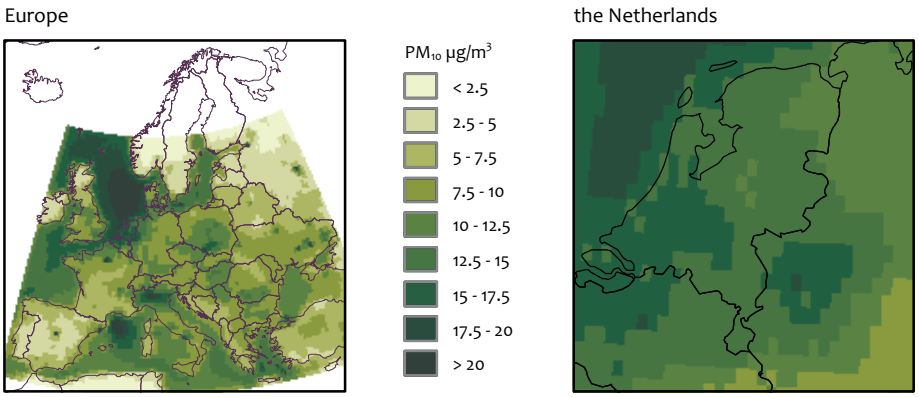

Modelled annual mean PM_{10} concentration (µg/m³) for Europe (left) and the Netherlands (right)..

Netherlands. Maximum concentrations occurred above the sea because of combined local emissions by international shipping and an efficient above-sea conversion to sulphate. Nitrate was the largest contributor (> 3 µg/m³) to PM_{10} in the model. The distribution had a strong continental signature. The reason for this was the ammonium nitrate in the model, a semi-volatile component. High concentrations of ammonia are needed to stabilise the ammonium nitrate, especially in summer. The distribution showed characteristics of the ammonia emission strength. Ammonium neutralises both sulphate and nitrate and therefore shows features of both anions. The primary PM_{10} concentration peaked at locations with the highest emission levels, that is, the cities in the Randstad and around large sources, such as the Rotterdam harbour and Corus. At these locations, the primary material exceeded the contribution of nitrate. Finally, the sodium content of sea salt is shown. Sodium showed a large gradient from open sea to locations further inland. The reason for this is the short lifespan of coarse mode aerosol, in which most of the sea salt is found, causing a limited transport distance inland. Figure 3.3 also shows the total PM_{10} again, but with a different colour scale highlighting the gradients within the country.

3.3 Verification versus measurements

To assess the performance of the model we compared its results to measurements of the Dutch national monitoring network, LML. As both PM_{10} and $PM_{2.5}$ are modelled as the sum of individual model components, we addressed the components first. Thereafter, the PM_{10} total mass was addressed. Unfortunately, there are no $PM_{2.5}$ data available for 2005 in the Netherlands. Finally, we addressed the model performance as a function of PM_{10} mass concentration.

3.3.1 PM_{10} Components

We paired the daily observations available from the LML to modelled concentrations. Before we evaluated the total PM_{10} concentration, we examined the components. Table 3.1 shows the mean and standard deviations from observed and modelled concentrations at the monitoring locations. The correlation between observations and model and the root mean square error (RMSE) are also shown. The data represent the average values for the measurement locations. Note that the observations on individual components were only available at a small number of stations.

For the modelled secondary inorganic components, the annual mean concentrations were close to those from the observations. The contribution of nitrate (NO_3) was slightly overestimated by LOTOS-EUROS, but the variability in the daily mean concentrations was quite comparable with the observations. Sulphate (SO_4) was overestimated or underestimated depending on the site, and the modelled variability was slightly too small. Ammonium aerosol (NH_4) was comparable to or slightly above the observed concentrations, with variability in accordance with the observations. The temporal correlation for nitrate was slightly better than for sulphate, which may have been due to the generally higher concentrations of nitrate (and the associated lower amount of data below the detection limit).

The comparison for sea salt was hampered by the amount of available measurement data. The measurement strategy aimed at secondary inorganic aerosols also includes an analysis of the chloride (Cl) content. However, the measurement is not ideal as the available Cl observations only approximately cover the PM_3 fraction, not the PM_{10} fraction. Moreover, Cl is lost because of chemical reactions in the atmosphere. This means that the sea salt estimate from chloride alone would be lower than the real and, therefore, also the modelled concentrations, as was indeed the case. Moreover, many of the observed concentrations were below the detection limit. Consequently, we interpreted the correlation coefficient (R=0.54) given in Table 3.1 as a lower limit. Comparison with a single month of observed Na concentrations available for 2005, showed a fairly good correspondence, although LOTOS-EUROS seemed to overestimate the concentrations for that

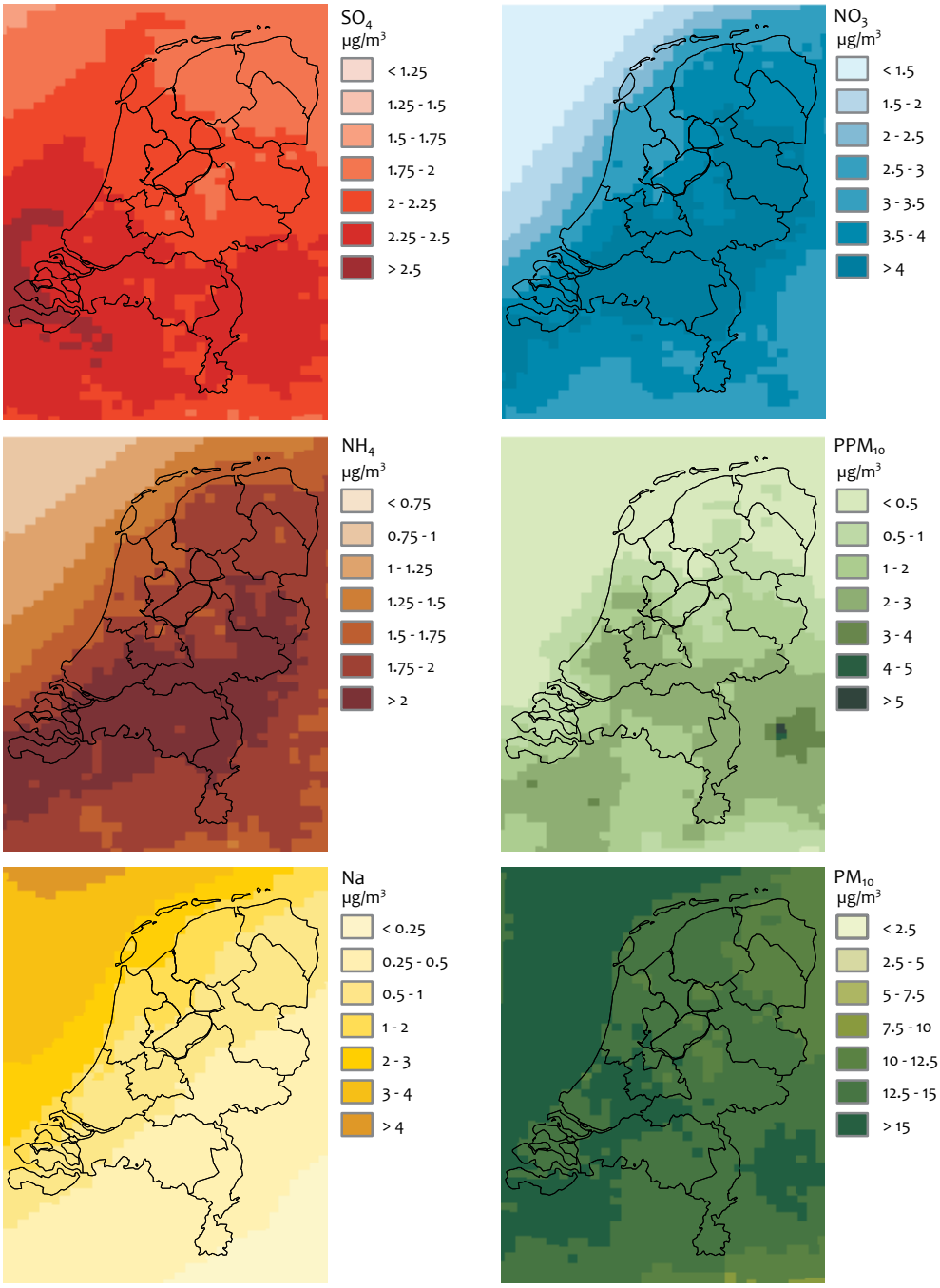

Annual mean distributions (µg/m³) of the model components sulphate (SO_4), nitrate (NO_3), ammonium (NH_4), primary PM_{10} (PPM_{10}) and sea salt sodium (Na). For completeness the distribution of PM_{10} is also shown.

month. For a more detailed discussion on sea salt we refer to Chapter 4.

Primary PM_{10} and $PM_{2.5}$ are not observed. They were modelled as direct emissions from emission databases and are presented in Table 3.1 to complete the overview of modelled concentrations. Their composition is a mixture of further unspecified substances, except for black carbon which was estimated based on an earlier study. However, black (or elemental) carbon is not routinely measured in the monitoring network. We compared the black carbon model results with black smoke observations. Black smoke is in fact not identical to black carbon but can be used as a proxy for elemental carbon, with a conversion factor which depends on the individual station because of regional differences in aerosol characteristics and differences in station type (Schaap and Denier van der Gon, 2007). By using the linear relation between black smoke (BS) and EC by Schaap and Denier van der Gon (2007),

Statistical comparison between modelled and observed concentrations of PM10 **Table 3.1**

substances	observed		LOTOS-EUROS			
	mean	stdev	mean	stdev	RMSE	correlation
total PM10	25.58	10.63	13.81	9.68	15.39	0.68
NO3	3.20	3.02	3.70	3.12	2.48	0.70
NH4	1.59	1.29	1.90	1.33	1.05	0.71
SO4	1.98	1.63	2.20	1.39	1.43	0.59
sea salt	1.42	1.19	2.81	2.84		0.54
black carbon	0.46	0.43	0.89	0.44		0.75
prim PM_{10}			0.91	0.55		
prim $PM_{2.5}$			2.39	1.23		

Statistical comparison between modelled and observed concentrations of PM_{10} and their components. We compared modelled and observed mean concentrations and standard deviations (stdev) and provided root mean square errors (RMSE) and correlation coefficients. All statistical parameters were determined based on daily data for the individual stations and were then averaged. Sea salt observations were not well constrained and only the correlation coefficient is given. The same applies to black carbon, for which the observations were estimated from black smoke observations (see text).

we estimated the annual mean EC concentration (from BS = 6.12) at the Dutch sites to be (0.056 * 6.12 + 0.12 =) 0.46. The modelled value was about twice as higher, which is within the uncertainty of the measurements on which the relation was based (Ten Brink *et al.*, 2004). For a detailed discussion on EC and OC measurement techniques we refer to the thematic report on carbonaceous particles. The temporal correlation between the estimated EC or BS and the modelled values is, however, evident.

In short, the performance of the LOTOS-EUROS system was satisfactory for secondary inorganic aerosol. We could not draw strong conclusions for sea salt nor for black carbon. Their concentrations were not unrealistic and the temporal variation was well represented. Earlier comparisons against data from other countries have confirmed these findings (Schaap *et al.*, 2008).

Below, we compared the total particulate mass to the PM_{10} measurements, to assess in how far we could explain the observed PM_{10} concentrations by using LOTOS-EUROS.

3.3.2 Bias correction for PM_{10}

The modelled PM_{10} concentration is the sum of the individual model components. Since LOTOS-EUROS does not include all PM sources and components, the model underestimated observed PM_{10} levels. This is a common feature of present day CTMs (Yu *et al.*, 2008, Stern *et al.*, 2008). As for the model components, the temporal correlation (R=0.68) for PM_{10} is quite reasonable. To use LOTOS-EUROS for assessing the variability in total PM_{10}, the missing fraction had to be compensated for. On average, LOTOS-EUROS underestimated the observed PM_{10} by 46 % or 11.7 µg/m³. In Figure 3.4, we explored the bias as a function of season, for 2004 to 2006. In the Figure, we compared all observations for all sites to the modelled value. The scatter plots indicate that the behaviour in summer differed from the other three seasons. In summer, the variability in modelled PM_{10} was lower than in the other seasons and the slope of the fit between the data was lower than 1. Hence, we used the seasonal fit parameters for estimating the bias corrected values:

$PM10_{biascor} = 1.54 * PM_{10} + 8.1$ Winter (DJF)
$PM10_{biascor} = 1.42 * PM_{10} + 7.5$ Spring (MAM)
$PM10_{biascor} = 0.76 * PM_{10} + 13.5$ Summer (JJA)
$PM10_{biascor} = 1.31 * PM_{10} + 9.1$ Autumn (SON)

We neglected the variation between stations and parts of the country to keep the procedure simple and transparent.

We assessed the quality of the LOTOS-EUROS model, including a bias correction, compared to the observations. Table 3.2 contains the values of the most important statistical parameters which are generally used to evaluate the performance of models. We also included the persistence model for comparison. The persistance model is the model in which the modelled concentration simply is the observed concentration of the day before. The mean of the bias-corrected LOTOS-EUROS simulations was very close to the observed mean (equal to the mean of persistence), as it was expected to be because of the bias correction. The bias at individual stations could be positive or negative and was typically between 0 and 4 µg/m³. The standard deviation of error, a measure for the non-systematic part of the RMS error, was comparable for the three models. The bias correction improved the skill variance of LOTOS-EUROS considerably, from 0.5 to 0.7. However, it still meant that the bias corrected LOTOS-EUROS missed variability. This could clearly be seen for Vredepeel during spring where, even with the bias correction high concentrations were not captured (see Figure 3.5). Regarding correlation, LOTOS-EUROS model results were always better than those of the persistence model. The bias-corrected LOTOS-EUROS results also had a smaller root mean squared error value (RMSE). The hit rate was determined, in this case based on the ability of the model to be within 20% of the observed value. This represented the accuracy of the observed concentrations (Beijk *et al.,* 2007b). None of the model results came close to the ideal 100% and differences were small, except for the uncorrected LOTOS-EUROS, which was always too low.

The number of values that were larger than the threshold value of 50 µg/m³ (but smaller than 200 µg/m³) was determined. To correct for data coverage issues, the observed

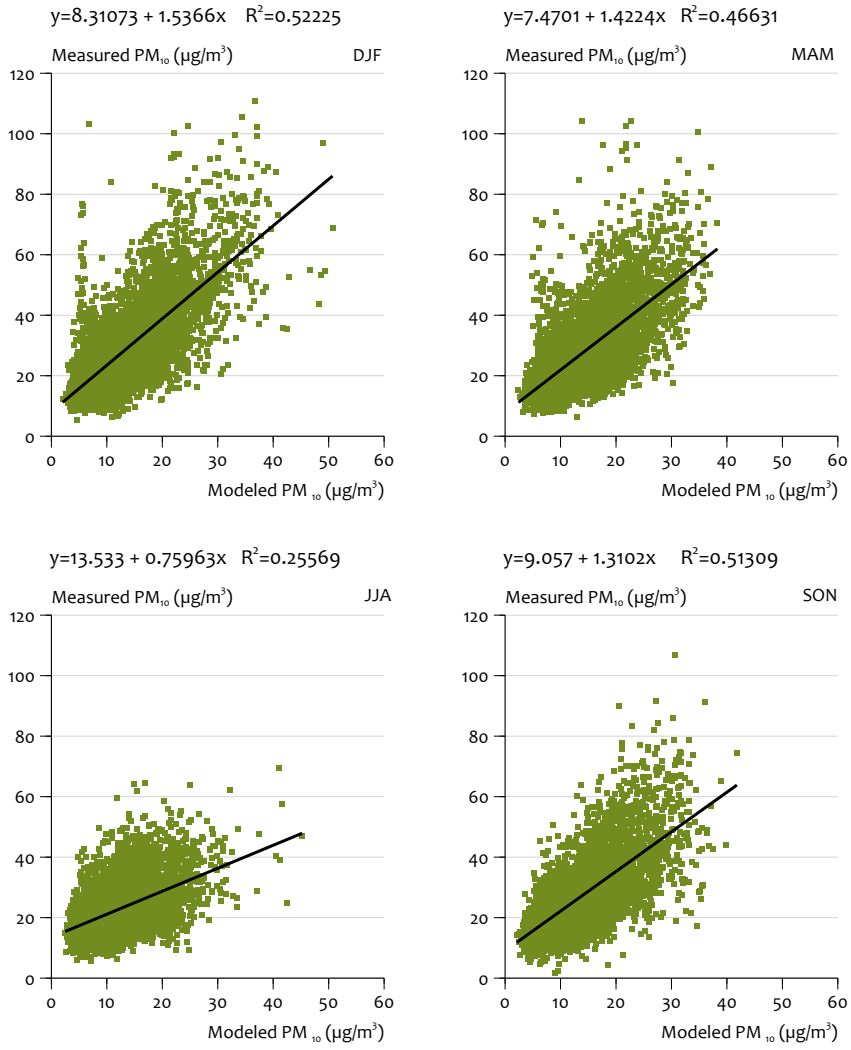

Comparison between modelled and measured PM_{10} concentrations for all LML locations. The comparison was made for every season: winter (DJF), spring (MAM), summer (JJA) and autumn (SON). The data represent all model–measurement pairs during each season for 15 LML stations. The fit parameters are given above each panel.

and modelled values were given separately for each model. LOTOS-EUROS still missed a considerable amount of exceedances, but the percentage of the correctly predicted exceedances was 60 %. Inspection of the time series and the scatter plots for PM_{10}, indicated that the periods with exceedances were generally captured in modelled high concentrations (but not above 50 µg/m³). This may be explained by the nature of a model to represent average conditions (through average emissions, parameterisations, etc). A number of exceedances was caused by sources not included in the model, such as fire works at New Year's Eve and Easter Fires. The performance of the model as a function of measured PM_{10} may indicate which components add to the underestimation as a function of PM mass, and is discussed in the next section.

The fact that the LOTOS-EUROS model performs better compared to the persistence model, may indicate that it is worthwhile to investigate if the model would be suitable for actual forecasting purposes. The model which is used now, PROPART, is only slightly better than the persistence model (Manders *et al.*, 2008). In contrast to a statistical model such as PROPART, LOTOS-EUROS provides more detailed knowledge on PM composition and origin as well as maps and time evolution, which enhances the possibility of communicating the results to the general public (Manders *et al.*, 2008).

3.3.3 Variability of composition

Here we will address if the model components show similar behaviour as a function of PM_{10} to the observed behaviour. Figure 3.6 shows the contribution of several components to PM_{10} as a function of the PM_{10} concentration. LOTOS-EUROS results showed a more or less linear relationship between PM_{10} and NO_3, SO_4 and NH_4. Observations yielded similar results. Ammonium and sulfate equally contributed to the PM mass in both the model and the observations. In the observations nitrate contributed the most with a slight increase

Observed and modelled average PM_{10} concentration **Figure 3.5**

Vredepeel, 2005

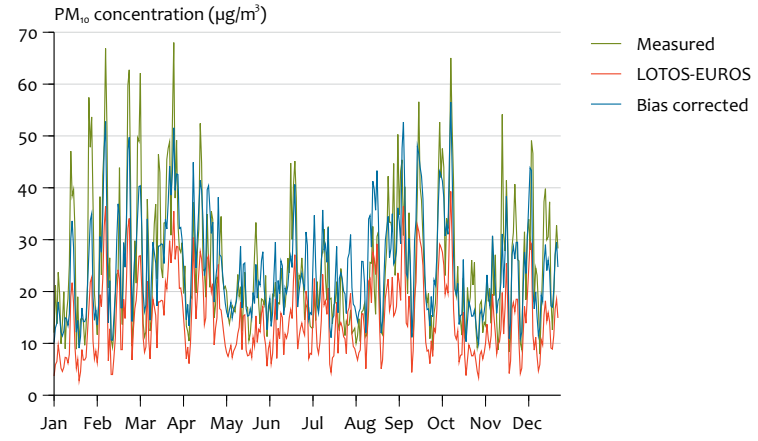

Observed and modelled average PM10 concentrations for Vredepeel (LML131), 2005. Both the LOTOS-EUROS model (red) and the bias-corrected model (blue) are shown.

Average statistical properties of the model for comparing measurements of PM10 **Table 3.2**

parameter	le_bc	le	persistence
mean	26.45	13.25	26.51
bias	-0.03	-13.23	0.02
residue	6.49	13.40	7.64
rmse	9.06	16.34	10.99
stde	9.06	9.60	10.99
skvar	0.70	0.50	1.00
correlation	0.70	0.68	0.63
hit rate	49.21	8.30	46.32
predicted 50-200	380	1.00	991
observed 50-200	1003	1003	983
%correct 50-200	61.32	100.00	42.48
datacoverage	0.96	0.96	0.94

Average statistical properties of the model for comparing measurements of PM_{10} between 2004 and 2006. All parameters were calculated for each station for the three years of daily data and subsequently averaged to provide one value for each parameter.

towards high PM concentrations. This pattern was followed by the model, although the model slightly underestimated nitrate at high concentrations. In both the model and the observations, the elemental carbon concentrations tended to be relatively higher at low concentrations ranges.

As a sea salt tracer, sodium (Na) was modelled and chloride (Cl) was observed. In Figure 3.6, neither the observed nor the modelled tracer was transformed to a sea salt equivalent. Note that the chloride-based concentrations were not reliable because of the abovementioned reasons. Nevertheless, the relative contribution to total PM_{10} could be deduced from the results. For sea salt, the contribution did not increase with increasing total PM_{10} but rather decreased. The highest concentrations were found for relatively low total PM_{10} concentrations. This behaviour was found in the observations as well as in the model, and could be easily explained by the high sea salt loads in periods with fast transport from the sea, which represents the clean sector in the Netherlands. These results indicate that sea salt did not contribute a large mass fraction on the days with high PM concentrations (exceedance days).

The analysis revealed that the model captured the variability of the substances that could be evaluated. There is no indication that these components could explain the gap between observed and modelled concentrations. In addition, there was no large mismatch between the observed and modelled contributions of these components over the full range of observed PM_{10} levels. This means that the missing mass is associated with the non-modelled components and those components that could not be evaluated through measurements.

NO_3, SO_4, NH_4, EC and sea salt in Vredepeel versus observed total PM_{10}

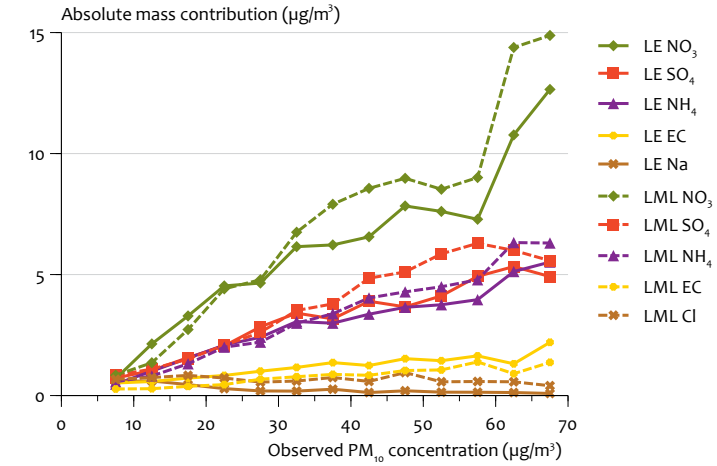

NO_3, SO_4, NH_4, EC and sea salt in Vredepeel versus observed total PM_{10}

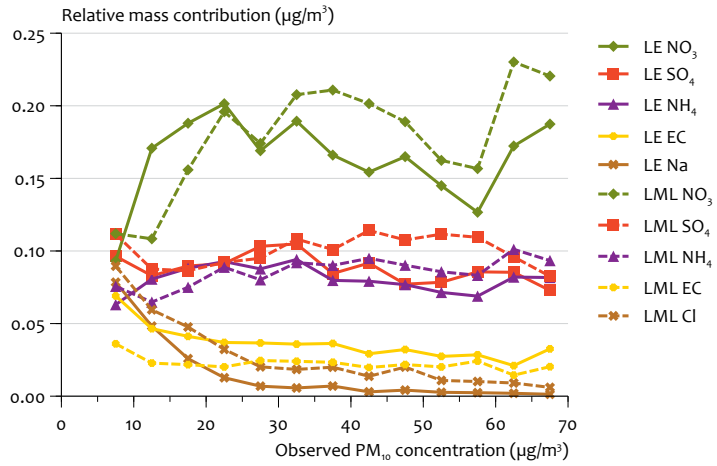

Modelled and observed absolute (top) and relative (bottom) contribution of NO_3, SO_4, NH_4, EC and sea salt in Vredepeel versus observed total PM_{10}. Note that the observed (Cl) and modelled (Na) sea salt tracers were not transformed to a sea salt equivalent and were meant to illustrate their behaviour. Observed EC concentrations were derived from black smoke measurements.

3.4 Discussion and conclusions

In this chapter, we have presented the annual mean distribution of PM_{10} and its components, as calculated by the model. Furthermore, we have examined the performance of the LOTOS-EUROS model by comparing it to observations in the Netherlands. LOTOS-EUROS was capable of modelling the temporal behaviour of PM_{10} concentrations rather well. However, the absolute concentration was not captured and a systematic bias existed between the modelled and the measured concentrations. On average, the underestimation by LOTOS-EUROS was 11.7 µg/m³. Verification of the secondary inorganic components, sea salt and EC indicated a good temporal behaviour and did not indicate that one of these components contributed largely to this bias. In addition, analysis of the model performance as a function of PM_{10} revealed that the model captured the variability of the substances that could be evaluated. This means that the missing mass is indeed associated with the non-modelled components and those components that could not be evaluated through measurements.

Similar to other models for Europe, LOTOS-EUROS has a considerable bias for PM_{10}. On average, the underestimation by LOTOS-EUROS was 11.7 µg/m³. Compared to the underestimation obtained by OPS (12 µg/m³) one could conclude that the underestimation in both models was very similar. This is no surprise, as both LOTOS-EUROS and OPS include the same components. PM_{10} is modelled as:

$PM_{10} = SO_4 + NO_3 + NH_4 + PPM_{10}$ + sea salt

In reality, PM10 consists of more substances:

$PM_{10} = SO_4 + NO_3 + NH_4 + EC + POM + SOA + PPM_{unknown}$ + sea salt + CM + water.

Crustal matter (CM) and secondary organic aerosols (SOAs) had not yet been incorporated in the model version prior the start of the BOP project, because of a lack of solid knowledge on emission strengths for CM and formation routes for SOA. Crustal matter may have contributed 3-5 µg/m³ for the Netherlands (see Chapter 5) and could explain a large fraction of the bias. In addition, but much more uncertain, SOA also could have added a significant mass. First steps were taken in Chapters 5 and 6 to include these components and pursue mass closure. Finally, it was posed that PM_{10} measurements include a portion of water, which might contribute to the systematic underestimation of the observed levels (Tsyro, 2005).

The emission data that were used here did not provide chemically speciated data, which made it hard to verify the primary components. Primary material should be distinguished in elemental carbon and primary organic matter. Furthermore, a part of the primary PM remains unidentified. This small fraction derives mainly from mechanical wear and may contain a considerable amount of metal. The distinction will be made during the BOP programme by using a chemically specified emission database for elemental carbon (EC) and primary organic matter (POM). Having data on organic matter would allow comparing model results with OC and TC measurements.

We also showed that no firm conclusions could be drawn on the model performance for sea salt. The comparison shown above was hampered by the limited usability of the chloride measurements from the LML LVS samplers. The measurements have a rather undefined cut-size and were therefore difficult to compare to the model results. In addition, chloride is replaced by sulphate and nitrate through reaction of sulphuric and nitric acid with sea salt in ambient air. Hence, without correction, the sea salt estimates based on chloride represented the lower limit. Finally, the measurements were often below the detection limit which posed a problem with the data handling and appreciation. Hence, the model results for sea salt were not extensively validated for Dutch conditions. The same applies to European conditions, because of a lack of observation data. In Chapter 4, we updated the model description to a combination of two emission parameterisations that would be considered to be state-of-the-art. The BOP measurements together with an effort of compiling foreign data, provide the first opportunity for a more extensive validation than presented above.

A CTM such as the LOTOS-EUROS model, is an approximation of reality and therefore describes average conditions (through emissions, parameterisations, etc). Observations, however, are often influenced by contributions derived from events, such as Easter Fires or fire works. Also, long-range transport of forest-fire plumes or dust storms may occasionally reach the Netherlands (Hodzic *et al.*, 2006; Birmili *et al.*, 2007). These events may be included in models using routines for wind blown dust (e.g. Bessagnet *et al.*, 2008) or satellite derived fire counts in combination with an emission module. The magnitude of the emissions and the specific conditions during such events are difficult to capture adequately. Data assimilation of both in-situ and remote sensing observations (in and upwind from the Netherlands) may therefore aid the air quality analysis. LOTOS-EUROS is equipped with a data assimilation system (e.g. Van Loon *et al.*, 2001; Barbu *et al.*, 2008; Denby *et al.*, 2008). The challenges regarding data assimilation are many but its use for air quality assessment should be investigated.

We identified three substances for which the uncertainties in the modelling needed to be reduced. These were sea salt, crustal material and organic carbon. The next three chapters describe efforts of improving the modelling of these components.

4 Sea salt

4.1 Introduction

In the recent past, sea salt contributions were estimated for the Netherlands (Hoogerbrugge *et al.,* 2005). The annual mean concentration estimates are now used for the correction of the sea salt contribution in the annual mean PM_{10} concentration. They show a considerable spatial gradient with annual means varying from high concentrations at the coast to lower concentrations inland. Maximum concentrations of PM_{10} are reached, in general, on days with weak and south-easterly winds, when the sea salt concentration is relatively low. Therefore, the corrected annual mean PM_{10} concentration cannot be used directly for estimating the number of exceedance days. The number of days on which the daily mean PM_{10} concentration exceed 50 µg/m³ due to the contribution of sea salt, was estimated at 6 days. In contrast to the annual mean sea salt concentration, its contribution on exceedance days was nearly uniform across the country.

Sea salt consists of a mixture of ions. Sodium (Na) and chloride (Cl) determine most of the sea salt mass. Of these two components, sodium is the best tracer for sea salt, as its contribution in weight is significant and it is a conserved substance. In contrast to sodium, chloride is lost in reactions of acidic gases with sea salt in ambient air and during sampling on the filter. The above-mentioned assessment of sea salt concentrations in the Netherlands by Hoogerbrugge *et al.* (2005) was based on chloride data obtained with a sampler that samples only about the PM_3 size fraction. Based on the available knowledge about the amount of chloride lost and the fine to coarse sea salt ratio, a first-order correction procedure was applied to the data. Though it was recognised that the correction factor would vary in time and space, it was used for all the data on the Netherlands as there was no means to establish the real factor. Consequently, the uncertainty in the derived sea salt distribution is rather large and calls for verification.

The goal of the work on sea salt for the BOP programme was to assess the contribution of sea salt to the PM_{10} and $PM_{2.5}$ concentrations on an annual basis and on days with limit-value exceedances. To address these questions, the LOTOS-EUROS model was applied in combination with dedicated measurements. However, the verification of LOTOS-EUROS for sea salt was limited and the modelling of sea salt is associated with considerable uncertainties. These two issues are addressed in this chapter.

To incorporate sea salt in LOTOS-EUROS one needs to describe the wind-dependent source function, transport and removal through wet and dry deposition. Below, we present the update of the model description to the combination of state-of-the-art emission parameterisations. The results were compared against a compilation of foreign data, providing the first opportunity for a more extensive validation. Furthermore, the coarse mode sea salt distribution was sensitive to the parameterisation used for the dry deposition, which largely determined the transport distance. We tested the impact in a scheme based on theory to compare the results to the empirical approach used up to now. Finally, the results are discussed.

4.2 Sea salt emission mechanisms

The generation of sea salt aerosols can be described by several physical processes. Usually, two main types are discriminated: direct and indirect mechanisms. The direct mechanism includes production of sea-salt aerosols by spumes, whereas the indirect mechanism produces sea salt particles through air bubbles.

The direct mechanism produces sea salt particles at wind speeds higher than 7 to 11 m/s. At these high wind speeds, spume drops are produced by direct tearing from the wave crests. In this way, very large (>100 µm) salt particles are emitted into the marine boundary layer (Monahan, 1986; Wu, 1993). This mechanism is not relevant for the present study, since these particles do not influence $PM_{2.5}$ and PM_{10} concentrations. Moreover, the atmospheric life time of these particles is very short, therefore they are not expected to be transported over long ranges.

The indirect mechanisms include the bursting of air bubbles which emits jet and film droplets from the sea surface into the atmosphere (Monahan *et al.*, 1986). Figure 4.1 presents a scheme of such a process. Most of the generated bubbles are produced by breaking waves which cause entrapment of air. Breaking waves are visualised by oceanic whitecaps and their amount strongly depends on wind speed. For wind speeds of 20 m/s whitecaps typically cover 10% of the sea surface (Wu, 1979).

Two types of droplets can be produced by the bursting of bubbles: (1) film droplets, ejected from the rim of the reced-

Mechanism of indirect sea-salt aerosol production by bursting air bubbles **Figure 4.1**

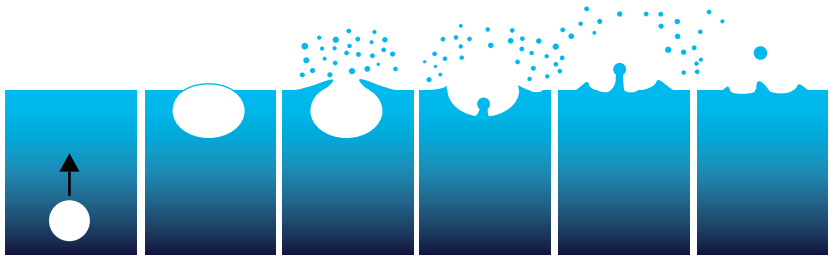

Mechanism of indirect sea salt aerosol production by bursting air bubbles.

Mass mean diameter for the bins used in the LOTOS-EUROS model. **Table 4.1**

bin sizes	0.14-1	1-2.5	2.5-5	5-10
mass mean diameter	0.56	1.75	3.75	7.5

ing film cap when the bubble film opens (Spiel, 1998) and (2) jet drops, formed from the break up of the vertically rising jet of water from the collapsing bubble cavity (e.g., Blanchard and Woodcock, 1957). The size of the bubble determines the number of film drops and jet drops produced: each bubble can generate a few hundred film drops in the sub-micron range and as much as 10 jet drops with an average size of l to 2 µm radius (although extending to sizes greater than 10 µm) (Blanchard and Syzdek, 1988; Woolf *et al*., 1987). Small bubbles produce only jet drops and large bubbles produce only film drops.

These indirect processes contribute to the emission of sea salt in the PM-size ranges and have been addressed in laboratory settings as well as field experiments. These studies have yielded a number of empirical emission functions. For this study, a combination of two parameterisations were included into the LOTOS-EUROS model.

4.3 Particle size and density

Before we present the emission parameterisations used in LOTOS-EUROS, we present some assumptions on the particle size and density of sea salt particles. As the lifetime of the coarse mode, especially, is dependent on the actual size of the sea salt particles, the number of bins for the various sizes of sea salt in LOTOS-EUROS has been expanded. Previously, LOTOS-EUROS included only sea salt in the fine ($PM_{2.5}$) and coarse PM fraction ($PM_{2.5\text{-}10}$). In this study, we used four bins, three of which in the super-micron size range. For these bins, a fixed mass mean diameter is assumed (Table 4.1). This is a simplification, since the deposition processes will lower the mass mean diameter per bin as the deposition velocity increases with particle size and the largest particles within a bin, therefore, have the shortest life time.

All calculations of sea salt within LOTOS-EUROS are based on an ambient relative humidity (RH) of 80%. The diameter of the dry aerosol is about half that of the wet aerosol, at this humidity level. For the assessment of the sodium mass in each bin, the dry diameter was used. In reality, particles grow and shrink with increasing and decreasing RH. This effect affects the distribution of particles over the size classes as well as the deposition velocities (see Annex C). Above the sea, air is relatively moist and 80% RH seems a reasonable approximation. Above land, the air may become very dry (RH<50%) and the approximation is not valid anymore. For the Netherlands, such low RH is only encountered in periods of continental winds, which are associated with very little sea salt anyway.

For RH=80%, the radius of the dry aerosol is half of that of the wet aerosol and the volume is 1/8 of that of the wet aerosol. The particle density of the wet sea salt aerosol therefore equals 1/8 the density of sea salt (2170 kg/m³) plus 7/8 the density of water (1000 kg/m³) which leads to a density of 1146 kg/m³.

4.4 New emission algorithm

In general, the sea salt source formulation is an empirical relation between the whitecap cover, average decay time of a whitecap, the number of drops produced per square metre of whitecap. The resulting droplet flux dF/dr can be given:

$$\frac{dF}{dr_p} = W(U_{10}) \cdot \frac{1}{\tau} \cdot \frac{dE}{dr_p}$$

$$W = 3.84 \cdot 10^{-6} \cdot U_{10}^{3.41}$$

$$\tau = 3.53$$

dF/dr	source flux of salt particles per increment of drop radius ($\mu m^{-1} m^{-2} s^{-1}$)
r_p	wet droplet radius (µm)
U_{10}	wind speed at ten metres ($m\ s^{-1}$)
$W(U_{10})$	surface fraction covered by whitecap
dE/dr	droplet flux per increment of drop radius per unit of whitecap ($\mu m^{-1} m^{-2}$)

Mass flux in microgram per m² per second for U10 = 10 m/s Table 4.2

	Bin			
	Size 1	**Size 2**	**Size 3**	**Size 4**
Monahan	1.06e-3	7.26e-3	3.02e-2	5.88e-2
Mårtensson Tss=0 °C	1.35e-3	1.77e-3	5.10e-3	-
Mårtensson Tss=5 °C	1.61e-3	3.56e-3	1.46e-2	-
Mårtensson Tss=10 °C	1.87e-3	5.36e-3	2.41e-2	-
Mårtensson Tss=15 °C	2.13e-3	7.14e-3	3.36e-2	-
Mårtensson Tss=20 °C	2.40e-3	8.94e-3	4.31e-2	-

A large number of formulations for calculation of the white-cap ocean cover exist. The most widely used is the function by Monahan and O'Muircheartaigh (1980), which was also used in this study. For the droplet flux per unit of whitecap, a large number of formulations have been proposed. Here, we use a combination of two parameterisations: Monahan *et al.* (1986) for the coarse particles and Mårtensson (2003) for the fine fraction. Previous to the BOP project, Monahan was used for all size fractions. However, the Mårtensson *et al.* (2003) parameterisation is considered to be better for the fine aerosol mode, which is important when studying the contribution to $PM_{2.5}$. Both parameterisations depend on wind speed and are based on experimental fits. For a detailed description of the parameterisations we refer to Annex B. Parameterisations for coarser particles than those in PM_{10} were not used. The surf zone was not explicitly accounted for, since its effect on large-scale concentrations is supposed to be small.

To illustrate the behaviour of the emission parameterisations we calculated the emission flux for both the Mårtensson *et al.* (2003) and Monahan *et al.* (1986) methodologies for a wind speed of 10 m/s. The Monahan parameterisation is not dependent on sea surface temperature (SST) or yields, or increasing mass emission flux as a function of size. Mårtensson *et al.* (2003) does include a dependency on SST. The impact of the SST is large, as the emission flux is 2 to 6 times higher at an SST of 20 °C than at an SST of zero degrees. The Monahan function gives similar results for bin sizes 2 and 3 at a sea temperature of 15 degrees Celsius. For the sub-micrometre range, the Mårtensson parameterisation provides systematically higher emission fluxes. For particles larger than 5 µm, the parameterisation of Mårtensson is not valid, therefore no data are given in that column of Table 4.2.

In the model, sodium is used as a tracer, since its mass contribution to total sea salt is considerable and it remains in the PM fraction, unlike chloride, which may be converted to gas by chemical reactions. The latter is especially relevant when the modelled concentrations are validated with measurements. Hence, all mass fluxes were translated to equivalents of sodium.

4.5 Alternative scheme for dry deposition

The life time of coarse aerosol particles is largely dependent on the dry deposition velocity. Deposition velocity (Vd) is characterised by the gravitational settling velocity (Vg), which is mainly relevant for the larger particles, the aerodynamic resistance (Ra) and the surface resistance (Rs).

$$V_d = V_s + \frac{1}{R_a + R_s}$$

The formulation of Vg and Ra are well established and based on physical processes. The formulation of Rs is empirical with parameters that were based on a few field studies. Different formulations are in use for different land-use classes. In this study, the impact of the formulation by Zhang *et al.* (2001) was tested. The reason this scheme was chosen is that it has a uniform structure for all land-use classes, and it has an explicit dependence on aerosol size, which makes it flexible. Furthermore, it is well compared with other formulations, leading to reasonable agreement with the validity of the various formulations. The Zhang scheme is described in Annex C.

4.6 Run description

The LOTOS-EUROS model was used in three configurations for 2005. The first is the base case, in which the Monahan emission parameterisation was used for the fine and coarse aerosol mode. The second simulation incorporated the Mårtensson emission module for the sub-micrometre particles and the Monahan approach for the super micrometre size range. This simulation used 4 size classes as defined above. The third simulation aimed to investigate the sensitivity of the results to the dry deposition description of the particles. It used the Zhang dry deposition scheme in combination with the Mårtensson emission parameterisation.

4.7 Results

In this section, we show the modelled concentrations with attention to spatial and temporal variability. The concentration from three model runs will be compared to the available observations. Furthermore, the sensitivity of the model to the proposed model assumptions is discussed.

4.7.1 Distribution

Figure 4.2 shows the modelled annual mean concentrations of Na accross the European continent, with results from the basic model version and the newest version, including the Mårtensson function and the Zhang deposition scheme. The main difference was found in the absolute value of the concentrations, which was higher for the new model version. As expected, the concentrations were largest above the sea

LE Basic

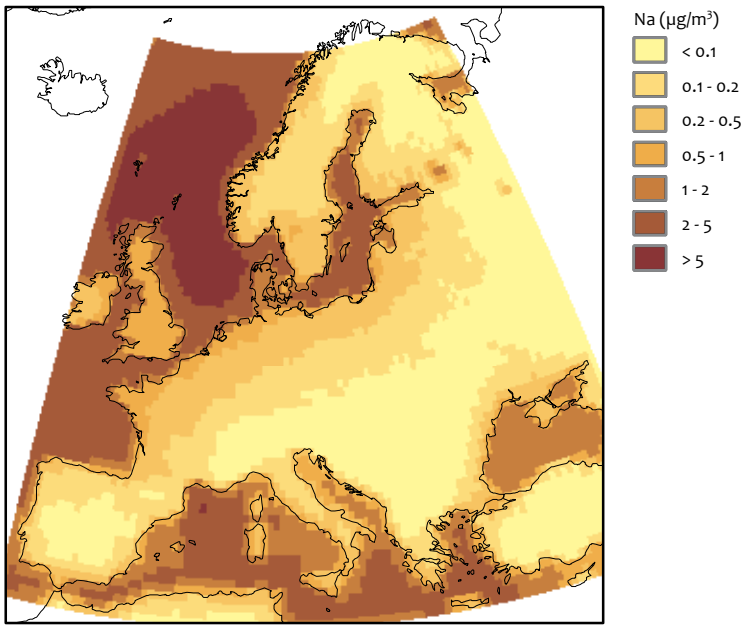

LE with Mårtensson source function and Zhang deposition scheme

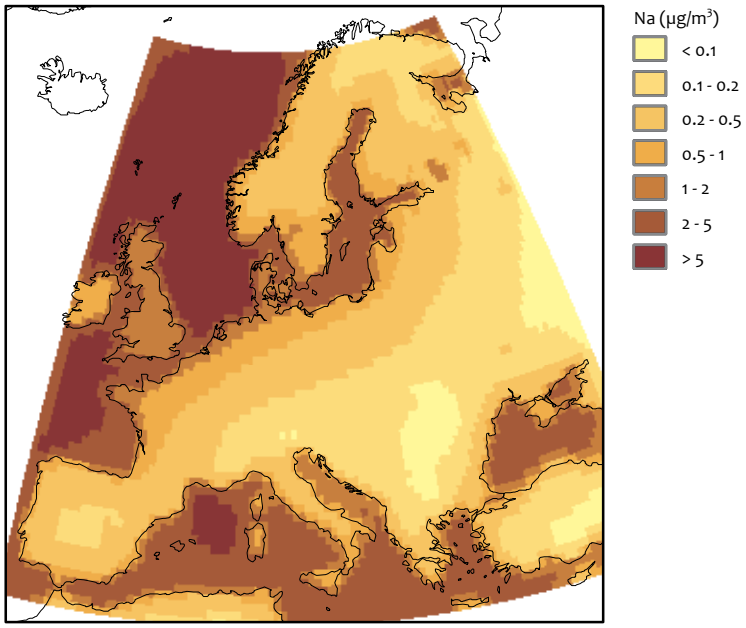

Annual mean Na concentration in 2005 in µg/m3. Left: LE basic version, right: LE with Mårtensson source function and Zhang deposition scheme. Note that the colour scale is not linear.

and decreased rapidly above land. Day-to-day variations could be large, as illustrated in Figure 4.3. Two snapshots are shown of daily average concentrations which indicated two different concentration regimes, depending on wind velocity and deposition characteristics. Hourly averaged concentrations (not shown) showed even larger variability. At the northern and eastern border of the domain, the effect of zero boundary conditions for sea salt was shown. Therefore, model results were only reliable at a certain distance from the model's border.

4.8 Verification

To assess the model performance for sea salt, a compilation was made of data from literature and EMEP. We have only compared with Na observations. For most locations, only

11 April 2005

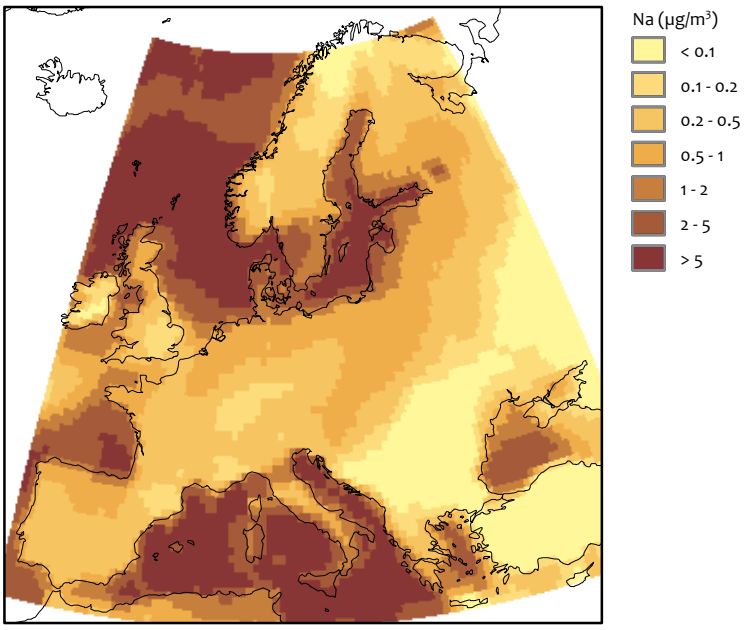

28 October 2005

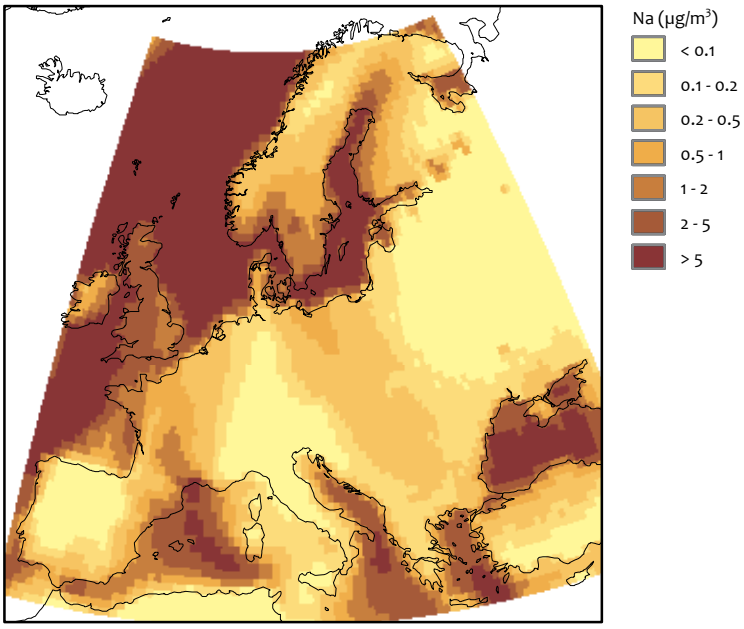

Daily mean Na concentration in µg/m³. Left: 11 April 2005, right 28 October 2005, with Mårtensson source function and Zhang deposition scheme.

annual mean values were available, for some locations daily observations could be used. For the Netherlands, in 2005, one month of Na observations were available.

4.8.2 Annual mean concentration

Table 4.3 shows the observed and modelled annual mean values. For nearly all stations, the modelled concentrations were up to twice as high as the observed concentrations. The stations close to the boundary of the domain were exceptions: Carnsore Point and Valentia Observatory (both in Ireland) and Campisalabos (Spain), the last of which is located further from the sea but the western boundary of LOTOS-EUROS is very close to land For these three stations, the model could not simulate the production and transport of enough sea salt since the fetch of the wind at sea is too small. Another exception was Rucava (Latvia), where LOTOS-EUROS significantly overestimated the concentration. This could be explained, at least partially, by the salinity of the Baltic Sea,

Comparison of the modelled and observed annual mean concentrations Table 4.3

Country	location	observed	LE (basic)	LE(Mart)	LE(Mart+Zhang)
AUT	Illmitz	0.07	0.09	0.10	0.15
DEU	Westerland	2.14	3.46	3.60	5.26
DEU	Langenbrugge	0.39	0.39	0.43	0.71
DEU	Schauinsland	0.14	0.12	0.14	0.23
DEU	Neuglobsow	0.41	0.37	0.41	0.71
DEU	Zingst	0.77	1.58	1.63	2.36
DEU	Melpitz	0.27	0.30	0.33	0.55
DNK	Keldsnor	1.07	1.68	1.73	2.43
DNK	Anholt	1.85	2.27	2.34	3.30
DNK	Ulborg	1.51	2.54	2.64	3.95
ESP	Campisalabos	0.50	0.07	0.08	0.19
ESP	Montseny	0.26	0.16	0.18	0.45
IRL	ValentiaObs	1.73	0.34	0.36	0.63
IRL	OakPark	0.71	0.53	0.55	0.88
IRL	MalinHead	2.44	3.30	3.39	4.56
IRL	CarnsorePoint	2.86	1.81	1.86	2.62
LVA	Rucava	0.22	2.69	2.76	3.91
NOR	Birkenes	0.46	0.49	0.66	1.23
NOR	Tustervatn	0.28	0.22	0.35	0.59
NOR	Kårvatn	0.18	0.24	0.29	0.49
SVN	Iskrba	0.07	0.06	0.07	0.16

Comparison of the modelled and observed annual mean concentrations (µg/m³) in 2005 for a number of stations in Europe.

Monthly mean concentration for the Netherlands, April 2005 in µg/m³ Table 4.4

station	observed	LE (basic)	LE(Mart)	LE(Mart+Zhang)
Biest-Houtakker	0.37	0.35	0.38	0.65
Vlaardingen	0.70	0.63	0.67	1.15
Bilthoven/Utrecht	0.50	0.47	0.50	0.83
Kollumerwaard	0.68	0.57	0.60	1.01

which is lower by a factor of 4 than that of the North Sea and the Atlantic Ocean. The salinity was assumed constant in LOTOS-EUROS and representative for open-sea conditions, which seemed correct for the Atlantic Ocean and the North Sea, but was clearly not valid for the Baltic Sea.

The amount of sea salt that is generated depends linearly on the source function. The effect of using the Mårtensson source function is the increase in the amounts of smallest particles. The effect on the total mass is relatively small, since the smallest particles do not contribute much to the total mass. Since smaller particles deposit slower than the larger particles, the relative effect on the total concentration tends to be larger for the more inland stations.

Figure 4.4 shows the scatter diagrams between observed and modelled annual mean values. The four problematic stations mentioned above, were left out. In the base case, the concentrations were overestimated by 43%. Note, that the smallest values are below the linear fit. With the Mårtensson source functions, the modelled concentrations increased slightly (overestimation by 49%). Although not expressed in the correlation coefficient, the fit improved for the low concentrations. The Zhang deposition scheme increased the residence time of the aerosol, which led to an increased overestimation (113%) of the observed concentrations. Again, the modelled low concentrations appeared to be positioned better with respect to the linear fit. Note that the spatial correlation values of all three model versions were very high (94, 95 and 93%) . Hence, based on this limited data set, the modelled spatial distribution appeared to be realistic.

Table 4.4 shows the mean concentrations for the Netherlands, for April, 2005. The comparison of the monthly mean data shows that the spatial gradients, even on this small scale, with higher concentrations close to the coast (Vlaardingen, Kollumerwaard) and lower concentrations inland, were in agreement with the observations. Concentrations were in the right magnitude for the basic version and with addition of the Mårtensson source function, with a slight underestimation for the coastal stations. The increase in concentrations when using the Zhang deposition scheme, caused an overestimation of the observed concentrations. The results are in line with the European results shown above.

4.8.3 Time series

Time series from the available stations were evaluated. Figures 4.5 and 4.6 show the daily average and monthly mean concentrations in Ulborg, a station in Denmark with moderate sea salt concentrations. LOTOS-EUROS correlated

Comparison between observed and modelled annual mean concentrations **Figure 4.4**

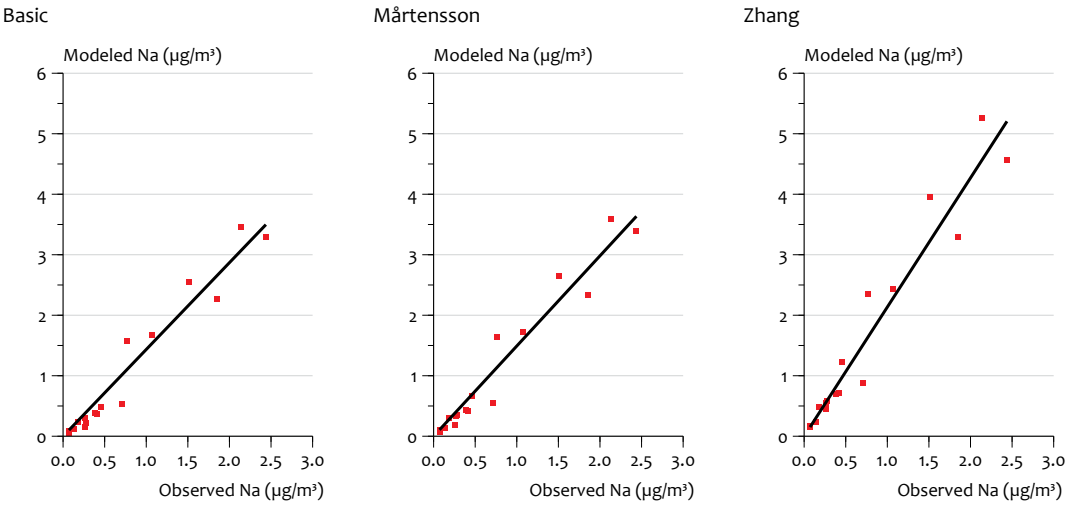

Comparison between observed and modelled annual mean concentrations at stations throughout Europe. Four problematic stations in Ireland, Spain and Latvia were left out (see text).

Comparison between the modelled and observed Na concentrations **Figure 4.5**

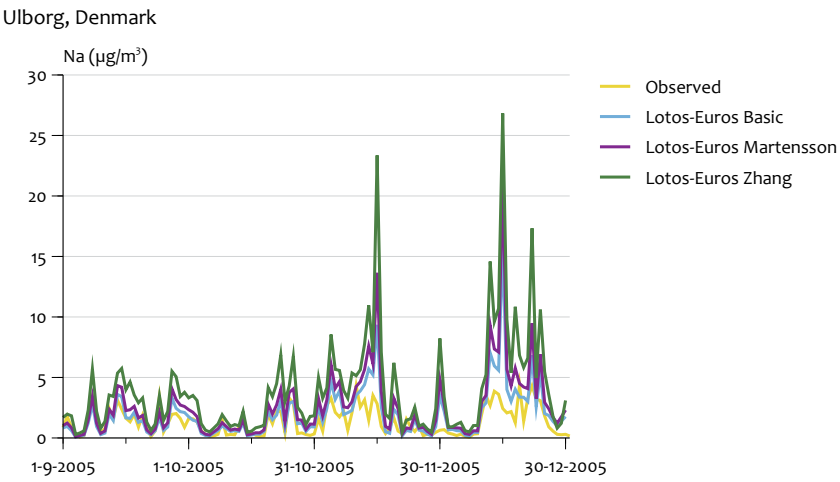

Comparison between the modelled and observed Na concentrations for Ulborg, Denmark.

well with the observations but overestimated the concentration. The simulation with the Zhang scheme for deposition showed general overestimations. The other simulations were quite close to the observed concentrations for most of the year, but a clear overestimation was observed during specific periods. The concentrations on around 15 November and during the last two weeks of December (and in January, but this is not shown) were seriously overestimated. These periods were characterised by (very) high wind speed conditions. These periods gave rise to the overestimation of the amplitude of the seasonal variability, which is generally well represented.

Table 4.5 gives the mean and the spread of the time series, both observed and modelled, and the correlation. The order of magnitude of both mean and spread were in agreement. Again the overestimation was evident, at most locations the spread was overestimated, but at Anholt it was underestimated, not only in absolute value but also relative to the mean value. This had clear impact on the correlation, which varied considerably from 0.2 in Ireland (which, in fact, is too close to the border of the model domain) to 0.7 for Ulborg.

4.9 Discussion

The main finding of this study was that the LOTOS-EUROS model overestimated the observed annual mean sea salt concentrations. The extent of the overestimation was dependent on the model configuration. The spatial and temporal variability of the sea salt concentrations were well represented. The variability was determined by meteorological conditions,

Comparison between the modelled and observed seasonal variation **Figure 4.6**

Na concentrations for Ulborg, Denmark

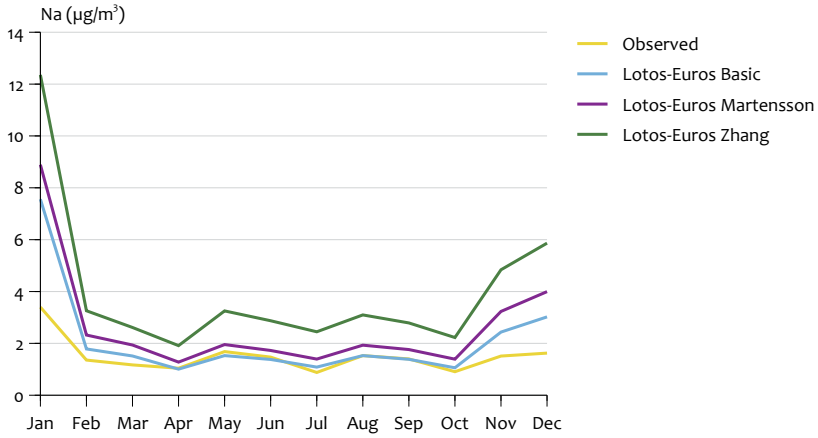

Comparison between the modelled and observed seasonal variation of Na concentrations for Ulborg, Denmark.

Statistical comparison between modelled and measured data for 2005. **Table 4.5**

		observed	LE (basic)	LE(Mart)	LE(Zhang)
Ulborg	mean	1.52	2.09	2.64	3.99
	stdev	1.33	2.80	3.46	4.94
	correlation		0.71	0.68	0.68
Anholt	mean	1.85	1.90	2.30	3.26
	stdev	3.28	1.86	2.14	2.78
	correlation		0.51	0.46	0.42
Langenbrugge	mean	0.39	0.25	0.38	0.70
	stdev	0.39	0.36	0.51	0.87
	correlation		0.67	0.63	0.60
Malin Head	mean	2.42	2.83	3.41	4.58
	stdev	2.15	4.47	5.40	6.54
	correlation		0.51	0.51	0.52
Oak Park	mean	0.71	0.42	0.55	0.88
	stdev	0.58	0.52	0.68	0.97
	correlation		0.30	0.27	0.23
Censore Point	mean	2.85	1.32	1.62	2.33
	stdev	2.44	1.46	1.83	2.55
	correlation		0.61	0.60	0.56

Statistical comparison between modelled and measured data for 2005. All data were based on daily samples. Langenbrugge was operated from June to December, Censore Point from May to December, and the other stations operated for the full year.

which affected the generation and transport, and deposition processes. The good spatial correlation of modelled and observed concentrations indicated that the net effect of these processes was modelled in a realistic way, but that the source function and deposition parameters were not fully known. Below, we discuss a number of issues related to the modelling of sea salt.

The choice of the source function has a linear influence on the concentrations. Thus, any uncertainty in the emission of sea salt had a direct influence on the concentration. Emission functions were highly uncertain since they were based on empirical fits to limited observations, both in the laboratory and at sea and these fits might not apply generally. A detailed and critical overview of emission functions is given in Lewis and Schwartz (2004), who estimate the uncertainty in the Monahan source function to be a factor 16 due to combined uncertainties, depending on the wind speed. However, the emission parameterisation used here is in the middle of most emission functions in literature and experts believe the uncertainty to be about 200-300% (G. de Leeuw, personal communication). This means that the modelled concentrations in LOTOS-EUROS were at least uncertain by a factor of 2 because of the uncertainties of the emission of sea salt aerosol. All CTMs suffer from this kind of uncertainty in the source function.

The effect of the Zhang deposition scheme is that concentrations become higher. The effect is larger for the largest particles. Not only because they contribute most to the total mass, but also because they are more sensitive to parameters in the deposition scheme, in particular to the gravitational settling velocity. In the basic version, one deposition velocity was used for the particles in the coarse size bin over the whole range from 2.5 to 10 μm. The deposition velocity is the sum of a land-use specific deposition velocity and a general settling velocity. The settling velocity of these large particles was set equal to the settling velocity of particles of 10 um, with the density of pure sea salt, whereas the aerosol would largely have consisted of associated water. Although the parameterisation was based on empirical data, the settling velocity and the combined deposition velocity could have been a maximum estimate leading to an efficient dry deposition of coarse mode particles. The sensitivity to the dry deposition velocity was evident as the inclusion of the Zhang scheme increased the sea salt concentrations by about 50%. As the uncertainty in the sea salt source strength (>200%) is larger than in the dry deposition (~50%), we could not draw conclusions on which description is best. Hence, the significant change in concentration with the Zhang deposition scheme was not unrealistic. An evaluation of the aerosol dry deposition velocity with recent experimental data is therefore recommended.

The ratio between fine and coarse mode sea salt may provide future opportunities to address the life time of the coarse aerosol mode. The model development influenced the ratio between Na in $PM_{2.5}$ and total PM_{10}. The basic version showed values of around 20% near the coast and 30% inland to up to 50% in the middle of the interior. When the Mårtensson function was included, more small particles were generated and the ratio increased by a few percent over the full domain. When the Zhang scheme was used, large particles were deposited less fast than in the original deposition scheme, leading to a serious decrease of the relative contribution of fine aerosol, with only 10 to 15% at the coast and 15 to 20% more inland. We expect data from the BOP measurement campaign to validate this ratio.

We observed an increased overestimation of the sea salt concentrations during high wind speed conditions. In the present parameterisations of sea salt emission, the surface conditions of the sea were taken into account via the whitecap ratio calculated from U10. Witek *et al*. (2007) propose the additional use of the orbital velocity of the wave field which can be obtained from a global wave model. For U10 in the range of 2 to 15 m/s, both approaches yield similar fluxes, although the approach by Witek *et al*. induced an additional spread in the flux by up to a factor of 10, which is within the range of uncertainties proposed by Lewis and Schwartz (2004). For U10>15 m/s, the present approach seems to overestimate the sea salt flux, for U10<2 m/s it underestimates the flux. This could partly explain the current overestimation, by LOTOS-EUROS, of the highest sea salt concentrations at high wind speeds.

Another issue that may have contributed to the overestimation during high wind speed conditions is (again) related to dry deposition. The roughness length above sea is assumed constant whereas in reality it depends on the wind speed and wave properties. The consequence is that for high wind speeds, the roughness length over sea is too short and the dry deposition is not effective enough, which leads to higher concentrations. Hence, this may also contribute to an overestimation of the concentrations during high wind speed conditions.

Sea salt generation in the surf zone was not taken into account, separately. In our simulation, sea salt was generated in the surf zone, but open-sea conditions were applied. Generally speaking, the surf zone will contribute locally to the additional generation of aerosol, depending on wind velocity and fetch (De Leeuw *et al.,* 2000). However, since this process is very local (an area of a few dozen metres width along the coast) its contribution to the total sea salt aerosol production is likely to be small and only noticeable in the immediate vicinity of the coast.

In the present model version, the salinity of the sea is not taken into account. The Monahan and Mårtensson source function assumed open-sea conditions with a salinity of 30-35 PSU. But, in some parts of the sea, the salinity may deviate substantially, for example in the Baltic Sea. Therefore, the salinity of the sea should be taken into account to avoid overestimations as observed in Latvia.

LOTOS-EUROS contained zero boundary conditions for sea salt. This is not realistic, since the western boundary is the Atlantic Ocean where sea salt aerosol is being generated. Stalpers (2003) has calculated the fetch of an equilibrium concentration (generation and deposition in balance) to build-up. For moderate winds (10 m/s) this would be about 1000 kilometres, and for very strong winds (30 m/s) up to 3000 kilometres. For the Netherlands, the western boundary of the LOTOS-EUROS domain is about 1200 kilometres away. At very strong winds, the concentration in the Netherlands could therefore be slightly underestimated, but no signs of such an underestimation were found in the validation. On the contrary, the concentrations at high wind speeds were overestimated (as discussed above). We can conclude that, for zoom regions of the Netherlands, boundary conditions must be used from a simulation on the full model domain.

Despite the large uncertainties in the modelled absolute concentrations, the spatial correlation between model and observations was good. The modelled absolute values were well within the range of the large uncertainties in the generation function and deposition. This would justify an approach in which model results are scaled to get the right order of magnitude with respect to the observations. When this problem with the scaling factor would be resolved through more observations and higher accuracy, LOTOS-EUROS could well be used for the assessment of sea salt concentrations. As the spatial correlation coefficients of the three simulations were practically the same, it was hard to choose the most suited simulation for such an experiment. From visual inspection, the linear fit in the low concentration range appeared to be slightly better in the simulation with the Zhang scheme.

4.10 Conclusions

The sea salt concentrations modelled by LOTOS-EUROS overestimated the observed concentrations by 43 to 113%.

The use of the Zhang deposition scheme for dry deposition increased the modelled sea salt concentrations by 50%.

For all three simulations the spatial correlation coefficient was very good.

The large uncertainty related to the emission strength (compared to the uncertainty in the dry deposition) prohibited the judgment of which model configuration was more sound.

The temporal correlation between modelled and measured concentrations is general reasonable.

During high wind speed conditions the difference between modelled and measured concentrations was especially large, which could indicate that the emission parameterisation is not valid at high wind speeds.

The application of the Mårtensson source function for the smallest particles and the implementation of the Zhang deposition scheme have brought the model more in accordance with current practice. The dry deposition parameterisations need to be evaluated.

The good spatial correlation could justify using a scaling factor to obtain an optimal estimate of the sea salt distribution over Europe. Similarly, the model results could be used to study the contribution of sea salt to exceedance days under conditions of low to moderate wind speeds.

The findings above should be validated with the BOP measurement data.

5 Modelling of crustal matter

Crustal material or soil particles typically contribute 5 to 20% to the ambient PM_{10} mass. In certain regions and/or under specific meteorological conditions, the contribution may be higher. This is illustrated in Table 5.1 with elevated contribution levels for northern EU and southern EU due to studded tire use and desert dust, respectively. Despite the importance of crustal material in total PM_{10} mass, the sources are still scarcely understood and not (well) represented in emission inventories or air quality models. Crustal material may originate from distinctly different sources, for instance, wind erosion of bare soils, agricultural land management, resuspension of road dust, road wear, driving on unpaved roads, handling of materials, and building and construction activities. In our study, we aimed to develop a methodology for checking first-order estimates of the various source strengths for Europe, and the Netherlands, in particular.

For this purpose, we implemented simple and therefore transparent emission functions in the LOTOS-EUROS model for wind erosion of bare soils, agricultural land management, resuspension of road dust and road wear as these are thought to contribute most for north-western Europe. Road wear is included in standard emission inventories and is much less important than direct resuspension (see below). Therefore, road wear is not separately discussed in this study. Furthermore, we included boundary conditions for desert dust from the global TM5 model. As the uncertainties concerning the dust emissions are very high, special attention was given to the identification of the controlling factors in the source estimates.

This chapter focuses on $PM_{10,}$ as crustal material is mainly found in the coarse PM fraction. The terms crustal material, soil dust, dust and mineral matter, used in this chapter, all indicate the same crustal material.

5.1 Emission module for windblown dust

In this section we present the emission description for windblown dust in LOTOS-EUROS. When the wind blows over a surface it exerts a certain force on it which may mobilise soil material. The transportation of soil material caused by wind stress on the surface occurs under three regimes: creep, saltation and suspension (See Figure 5.1). The (type of) mobilisation of a particle is controlled by the gravitational force, interparticle cohesion and wind-shear stress acting on the particle, all depending on the particle size.

Primary dust production by wind, that is, uplift and suspension of particles of a diameter smaller than 50um, is strongly limited by the cohesive forces that bind particles to the soil

Mean annual levels of PM_{10}, $PM_{2.5}$, crustal material **Table 5.1**

	Central EU			Northern EU			Southern EU		
	RB	UB	RS	RB	UB	RS	RB	UB	RS
PM_{10} (μgm^{-3})	14–24	24–38	30–53	8–16	17–23	26–51	14–21	31–42	45–55
Crustal material (μgm^{-3})	1–2	3–5	4–8	2–4	7–9	17–36	4–8	8–12	10–18
% Crustal material PM_{10}	5–10	10–15	12–15	20–30	35–45	65–70	12–40	25–30	25–37
$PM_{2.5}$ (μgm^{-3})	12–20	16–30	22–39	7–13	8–15	13–19	12–16	19–25	28–35
Crustal material (μgm^{-3})	0.5–2	0.4–2	1–2	1–3	2–4	4–6	1–3	2–5	4–6
% Crustal material $PM_{2.5}$	2–8	2–8	5	15–25	25–30	30–40	8–20	10–20	10–15

Source: Querol *et al.*(2004)

Mean annual levels (μgm^{-3}) of PM_{10}, $PM_{2.5}$, crustal material, and the equivalent contributions to bulk mass concentrations (% wt), recorded at regional backgrounds (RB), urban backgrounds (UB) and kerbside stations (RS) in central EU (examples from Austria, Berlin, Switzerland, The Netherlands, UK), northern EU (13 sites in Sweden) and southern EU (10 sites in Spain).

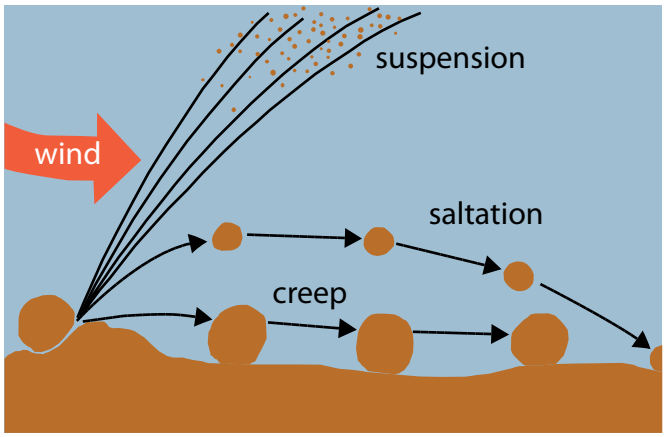

Schematic of soil movement processes

surface. Moreover, the smallest particles which are of interest for atmospheric PM_{10} typically occur within larger aggregates, in the size range of 30 µm to 1 cm. Hence, primary production can be neglected (see below) as a significant source of particles to the atmosphere. For particles with a particle size larger than 500µm, the vertical particle motion is suppressed as the upward force due to wind stress is dominated by the gravitational force. Hence, under normal conditions, these particles are too large to be lifted from the surface by wind drag. The particles roll or slide over the surface, a process which is called surface creep or surface traction. Thus, also the creep process does not cause a release of particles to the atmosphere.

Medium sized particles (D=50-500µm), however, are lifted from the surface and may reach a maximum height of one metre before falling back to the surface. This hopping movement, called saltation, occurs only if the wind friction velocity is above a certain threshold value, such that the gravitational force is partly overcome. When the saltating particles impact on the ground they can cause other, similar sized particles to eject and induce surface creep. More importantly, these particles can dislodge smaller particles (D < 20 µm) as they impact on the soil surface (particles either freed from the soil, or as fragments of the aggregate impacting particles themselves) and release them into suspension. This secondary process, also called 'sand blasting', is mainly responsible for wind-generated dust production.

Among others, Shao *et al.* (1993) found both the horizontal and vertical dust flux to be proportional to a power of 3 of the wind velocity in wind-tunnel experiments. These results indicate that the vertical suspension flux (F_v) is proportional to the saltation flux (F_h). Hence, the relation between the vertical and horizontal flux of dust particles is given by:

$$F_v = \alpha F_h$$

where α is a constant which varies widely over surface characteristics with values between 10^{-7} and 10^{-4} (Alfaro *et al.*, 1997, Alfaro *et al.*, 1998, Gomes *et al.*, 2003). In the literature, α has been chosen as a constant, or formulations based on surface parameters, such as surface texture, are used. Below, we describe our approach of the saltation flux, as well as the approach for determining α.

5.1.1 European soil texture map

The vulnerability of soil to wind erosion is dependent on its texture. In sedimentological studies, soil texture is generally classified on the basis of the textural triangle of clay, silt and sand, with respective particle sizes <4 µm, 4-80 µm and 80-2000 µm (see Figure 5.2). For a refined soil characterisation and susceptibility to wind erosion, Chatenet *et al.* (1996) defined four size populations that are related to specific mineralogical types: fine and coarse quartz sands, aluminosilicate silt and salty soil (Table 5.2). The authors suggested that the size distribution of any soil population could be described as a combination of these four mineralogical types. A lognormal representation of the size distribution of a soil type can therefore be written as

$$\frac{dm}{dD_p} = \frac{1}{D_p\sqrt{2\pi}} \sum_i \frac{f_i}{\ln\sigma_i} \exp\left(\frac{\left(\ln D_p - \ln \overline{D_{p,i}}\right)^2}{-2\ln^2\sigma_i} \right)$$

where f_i is the fraction of soil particles of mineralogical type i, with corresponding mass mean diameter $\overline{D_{p,i}}$ and geometric standard deviation σ_i.

A map of the soil-size distribution within the LOTOS-EUROS model domain was based on data on soil characteristics in the European Soil Database, a vector-based soil database provided by the Joint Research Centre (http://eusoils.jrc.it/ESDB_Archive/ESDB/index.htm). The geographical representation of the soil data information in this database corresponds to a resolution of 1:1,000,000. For the LOTOS-EUROS model calculations, the original vector data were aggregated on the model grid (0.50° longitude x 0.25° latitude) by means of interpolation (Figure 5.3). The soil texture in this database was classified according to the sand and clay fraction of the soil.

Texture classification of sediments **Figure 5.2**

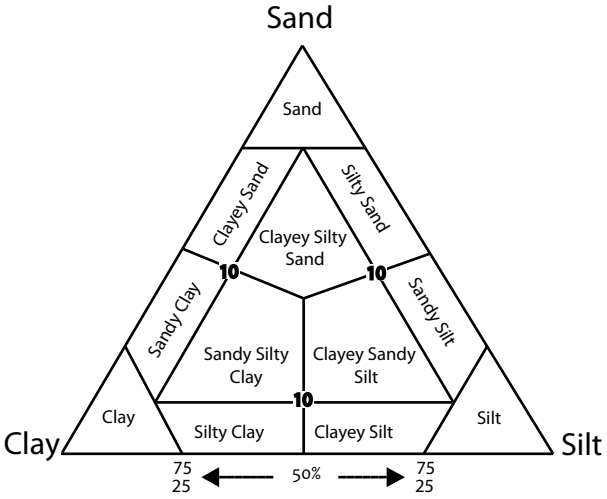

Texture classification of sediments (from Chamley, 1989).

Soil type classification by Chatenet et al. (1996). **Table 5.2**

Soil texture group			
Name	**Abbreviation**	$\overline{D_{p,i}}$ **(um)**	σ_i
Coarse dune sand	CS	690	1.6
Salty soil	MS	520	1.5
Fine quartz sand	FS	210	1.8
Aluminosilicate silt	FFS	125	1.6

Soil texture type and size classification **Table 5.3**

		Dominant soil texture[1]	**Fraction of particles per soil type**[1]			
Soil texture			CS	MS	FS	FFS
Coarse	18% < clay and > 65% sand	CS	0.8	0	0.1	0.1
Medium	18% < clay < 35% and >= 15% sand, or 18% < clay and 15% < sand < 65%	MS	0.1	0.4	0.25	0.25
Medium fine	< 35% clay and < 15% sand	FS	0.1	0.25	0.4	0.25
Fine	35% < clay < 60%	FS	0	0.1	0.4	0.5
Very fine	clay > 60 %	FFS	0	0	0.35	0.65
No texture[2] *or no information*	-	-	-	-	-	-

[1] the soil type abbreviations after Chatenet *et al*, (1996).
[2] because of rock outcrop, organic layer or other causes.

A translation of this classification to the mineralogical type as defined by Chatenet *et al*.(1996) was applied to calculate the soil size distributions according to Equation 5-2 and constitutes a soil size distribution class map for each mineralogical soil type (Figure 5.4). The soil texture classes as given by the dataset and the applied translation, are given in Table 5.3.

5.1.2 Saltation flux

Many researchers have studied wind generated abrasion initiated by saltation, also known as sandblasting. Dust production by saltation depends on the surface features and meteorological conditions. Bagnold (1941) suggested that the horizontal flux of saltating particles is a power function of the wind friction velocity, u^*, defined as $(\tau_0/\rho)^{1/2}$, where τ_0 is the shear stress on the surface and ρ is the fluid density. Saltation occurs only when a certain threshold value, $u^*_t(D_p)$, is reached, and depends on the soil particle size, D_p. The soil particle size, D_p, should not be mistaken for the size of suspended particles, which are much smaller. A variety of formulations for the horizontal saltation flux based on the definition given by Bagnold (1941) is used in literature.

The parameterisation for the horizontal and vertical dust flux utilised in this project is based on the work of Marticorena and Bergametti (1995, 1997), Gomes *et al*.(2003) and Alfaro *et al*.(2004). Marticorena and Bergametti (1995) defined the horizontal flux of saltating particles, F_h ($g.m^{-2}.s^{-1}$),as follows,

Dominant soil texture class **Figure 5.3**

As defined in the soil database by the Join Research Centre

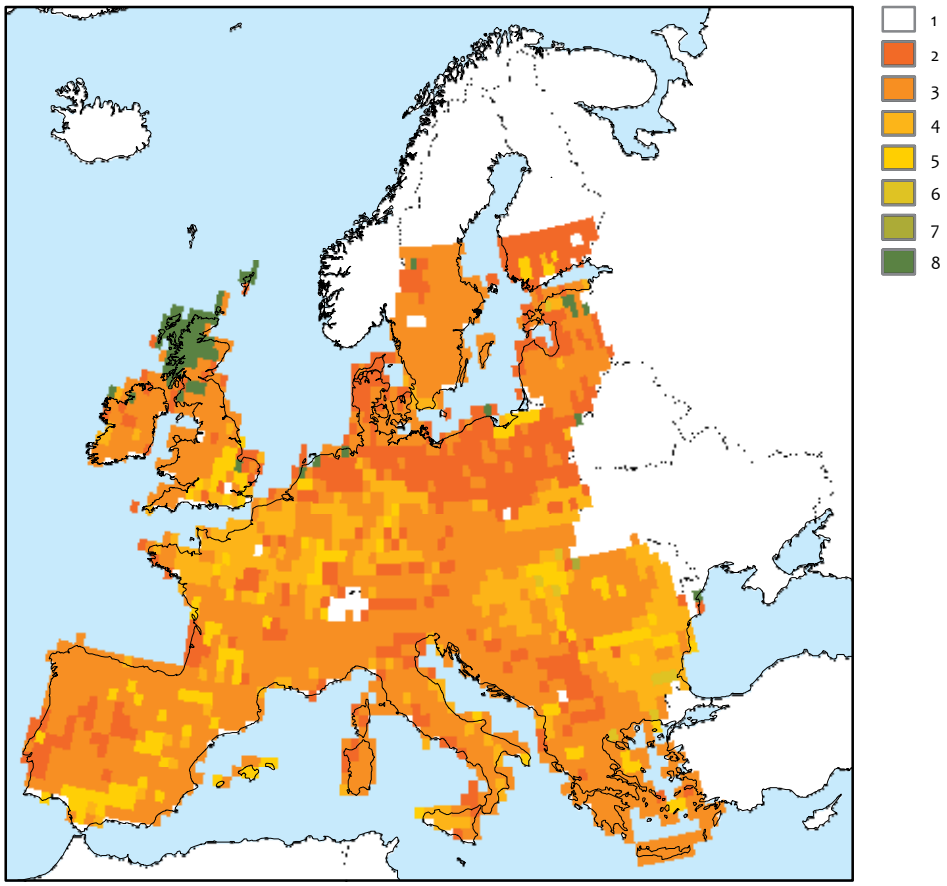

Dominant soil texture class as defined in the soil database by the Joint Research Centre, with 2=coarse, 3=medium, 4=medium fine, 5=fine, 6=very fine, and 1,7-9 are areas for which there is no soil texture information because of rock outcrop, organic layers or other causes.

$$F_h(D_p) = \frac{K_l \rho_{air}}{g} u^{*3} \left(1 - \frac{u^*_{th}(D_p)}{u^*}\right)\left(1 + \frac{u^*_{th}(D_p)}{u^*}\right)^2 \quad \text{for} \quad u^* > u^*_{th}$$

where the soil dust supply factor K_l and the threshold friction velocity $u^*_{th}(D_p)$ depend on several soil surface and surface geometry parameters. Below, we describe the soil dust reservoir and the methodology used for assessing the threshold friction velocity.

Soil dust reservoir

Factor K_l in equation 7-4, represents the presence of a limited reservoir of soil aggregates. More specifically, K_l covers the influence of land use on dust emission, including the limiting effect of vegetation cover, and the depletion of the soil dust reservoir. It is formulated such that K_l=1 represents the soil dust presence in desert areas. We apply K_l=0.02 for arable areas. Other bare surfaces (bare soils, dunes) are characterised by K_l=0.1, following Van Loon *et al.*(2003). It should be noted that with the present land use, classification does not distinguish between bare soil and bare rock. Therefore, we only assessed the emissions from arable land and disregarded other bare soils.

Threshold friction velocity

Following Marticorena and Bergametti (1995), the threshold friction velocity was modified by drag partitioning and moisture inhibition, as follows:

$$u^*_{th}(D_p, z_0, z_{0s}) = u^*_{th,u}(D_p) \frac{f_w}{f_{eff}(z_0, z_{0s})} \qquad (m.s^{-1}),$$

where $u^*_{th,u}$ is the threshold friction velocity uncorrected for soil moisture and effective wind shear over the soil surface.

Uncorrected threshold friction velocity

In theory, the threshold friction velocity, u^*_{th}, and the uncorrected threshold friction velocity, $u^*_{th,u}$, depend on the surface particle size and the turbulent flow characteristics. For natural conditions, there is insufficient accurate information available on the particle type and ,thus, also on the particle size, which can vary largely over time and space, especially in arid areas (Laurent *et al.*, 2006). The same is true for the natural turbulent flow characteristics close to the surface. These are determined by the local flow friction velocity, u*, and the local length scale, that is, the (smooth) surface roughness length. Marticorena and Bergametti (1995) assumed a mean

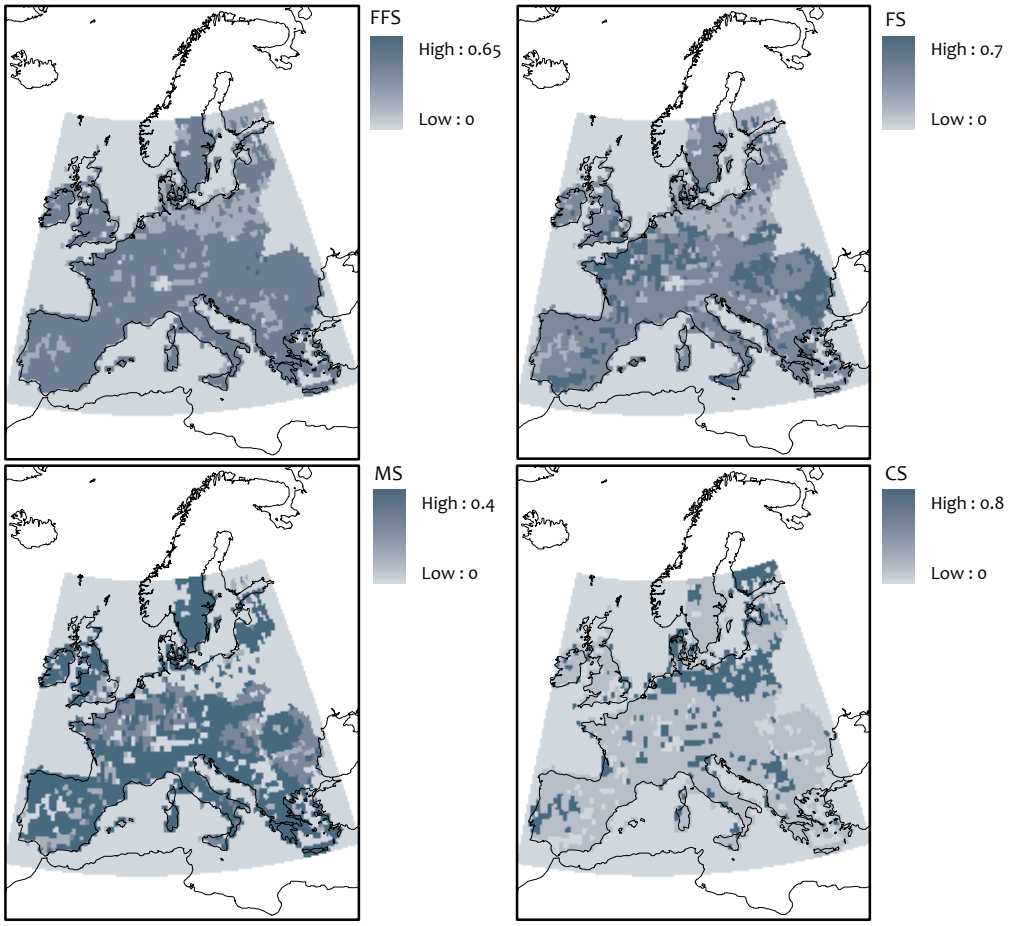

Mapped fraction of each mineralogical type (Chatenet, 1996): aluminosilicate silt (top left), fine quartz sand (top right), salty soil (bottom left), coarse dune sand (bottom right).

value for $u^*_{th,u}$ of 0.217 m.s^{-1}, corresponding to an average particle diameter, D_p=120 µm, which is the upper limit of the size range for which Iversen and White (1982) observed the minimum threshold friction velocity. However, Marticorena and Bergametti suggested that using a friction velocity with a size-dependent threshold for soil particles would be preferred. Hence, we applied their proposed approach to allow for such a dependency on soil-size diameter, as described below.Furthermore, we assumed a smooth roughness length, $z_{0s} \approx 4x10^{-6}$ m^{-1}, which corresponded to the chosen optimum value of D_p. The latter value was close to $z_{0s} \approx 1x10^{-5}$ m^{-1}, as was suggested by Marticorena and Bergametti (1995) for most natural surfaces.

In the current basic model set-up in LOTOS-EUROS of resuspension by wind, we applied an uncorrected threshold velocity, u^*_{th}, which did depend on soil particle size. We followed the formulations suggested by Marticorena and Bergametti (1995) to incorporate such dependence. They combined the formulations for u^*_{th}, including interparticle cohesion forces, as proposed by Iversen and White (1982) with a large data set of u^*_{th} obtained from wind tunnel experiments by Iversen (1976). The Reynolds number, reflecting the local turbulent flow characteristics, was given as Re= $u^*_{th}(D_p)D_p/\nu$, with ν being the kinematic viscosity of air. Marticorena and Bergametti (1995) approximated Re by the following analytical expression:

$$\mathrm{Re} = aD_p^x + b \quad \text{with} \quad a = 1331\,\mathrm{cm}^{-x}, b = 0.38, x = 1.56$$

where the values for the empirical constants a, b, and x were determined by the wind tunnel data, given an air density ρ_a of 0.00123 g.cm^{-3}and a particle density ρ_p of 2.65 g.cm^{-3}. This allowed a formulation for the uncorrected threshold friction velocity depending on particle size, as follows:

$$u^*_{th,u}(D_p) = \begin{cases} \dfrac{0.129\,C}{\left(1.928\,(aD_p^x + b)^{0.092} - 1\right)^{0.5}} & for \quad 0.03 < \mathrm{Re} < 10 \\ 0.12\,C\left[1 - 0.0858\exp\left(-0.0617\left((aD_p^x + b) - 10\right)\right)\right] & for \quad \mathrm{Re} > 10 \end{cases}$$

$$with \quad C = \left(\frac{\rho_p g D_p}{\rho_a}\right)^{0.5}\left(1 + \frac{0.006}{\rho_p g D_p^{2.5}}\right)^{0.5}.$$

Note that all length units in this formulation are in centimetres instead of in metres, and that the unit of factor 0.006 in the above equation is g.cm$^{0.5}$.s^{-2}. Furthermore, the above relations are valid for particle densities between 0.21 and

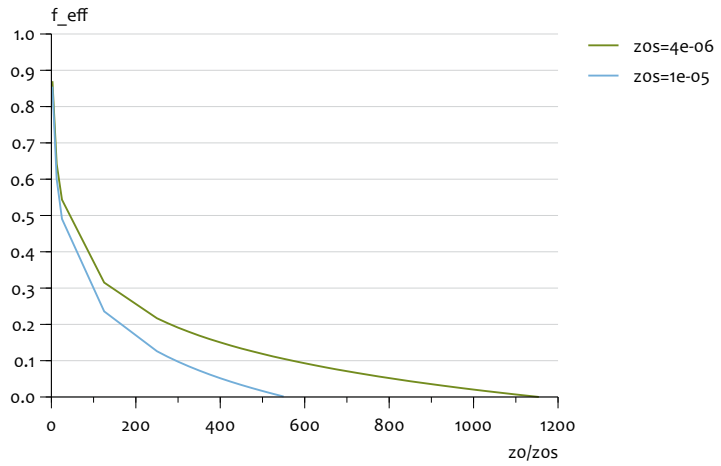

Drag partition, according to Marticorena and Bergmetti (1997), for various roughness lengths, z0.

11.35 g.cm^{-3} and particle diameters between 12 and 1290µm, and correspond to a minimum threshold friction velocity for particles with a diameter of ~60µm. Hence, the above formulations were considered to be valid for most natural soils and adapted for the calculation of the wind resuspended soil dust contribution to PM_{10}. For this study, this was done only in the areas for which soil texture was available and the wind-blown dust emission was set to zero in all other areas.

Drag partitioning

The efficiency with which wind shear is partitioned between the erodible soil surface and the non-erodible rough surfaces (e.g. rocks, vegetation), expressed by the semi-empirical factor f_{eff} is given by (Marticorena and Bergametti, 1997) as follows:

$$f_{eff} = 1 - \left(\frac{\ln\left(z_0 / z_{0s}\right)}{\ln\left(0.35\left(\frac{10}{z_{0s}}\right)^{0.8}\right)} \right).$$

In the above equation, z_0 represents the aerodynamic roughness length and z_{0s} represents the roughness length of the soil surface. The latter is also called smooth roughness length, relating to the soil particle diameter (Bagnold, 1941): $z_{0s} \approx D_p/30$. For smooth surfaces, however, z_{0s}, only slightly depends on particle size (Marticorena and Bergametti, 1995). Note that the above formulation is only valid for z_0 smaller than ~5 millimetres, where f_{eff} is nearly zero, and the threshold friction velocity is infinitely high. This effectively means that, for a surface with roughness elements larger than a few millimetres, there is no uplift of particles by saltation (see Figure 51). For z_0 larger than 5 millimetres, we assumed there to be no uplift of particles and set the vertical particle flux to zero. Hence, already at the stage of initial growth in the seeding season, saltation was strongly limited.

Our model calculations were done with z_0 = 0.25 metres in the growing season (April to September) and, equal to the assumed smooth surface roughness length, with $z_{0s} \approx 4 \times 10^{-6}$ metres outside the growing season, with intermediate values (z_0 = 0.125 m) in the months preceding and following the growing season. This means that there would be saltation and, thus, wind-blown dust emissions, only in autumn and winter.

Soil moisture inhibition

Moisture inhibition is represented by the soil moisture correction factor, f_w, (Fécan *et al.*, 1999) which by definition is a function of the soil gravimetric water content, w, and threshold soil moisture, w_t, below which the effect on u^* is negligible, as follows:

$$f_w = \begin{cases} 1 & for \quad w \le w_t \\ f_w = \sqrt{1 + 1.21(100(w - w_t))^{0.68}} & for \quad w > w_t \end{cases},$$

where both w and w_t are in kg.kg^{-1}. In principle, both w and w_t depend on the mixture of soil particle types. For the base model run, three-hourly ECMWF volumetric soil moisture data was used as input. The gravimetric soil moisture, w, was calculated from the volumetric soil moisture, w_v, as follows:

$$w = \frac{w_v \rho_w}{w_v \rho_w + (1 - w_v)\rho_{soil}}$$

Here, ρ_{soil}=1.3x10^{3}kg.m^{-3} is the soil density and ρ_w=999 kg.m^{-3} is the water density. The applied soil density corresponded to a soil size distribution with equal fractions of sand, silt and clay particles.

The sensitivity of f_w in relation to soil moisture and the soil moisture threshold, is illustrated by Figure 5.6.

For soil size distributions with a large fraction of clay particles, the threshold soil moisture tends to increase, and the soil moisture inhibition to slightly decrease. This means that for such soil, larger threshold friction velocities are necessary for the uplift of particles. Fécan *et al.*(1999) suggested a simple formulation for the dependence on soil moisture, by applying

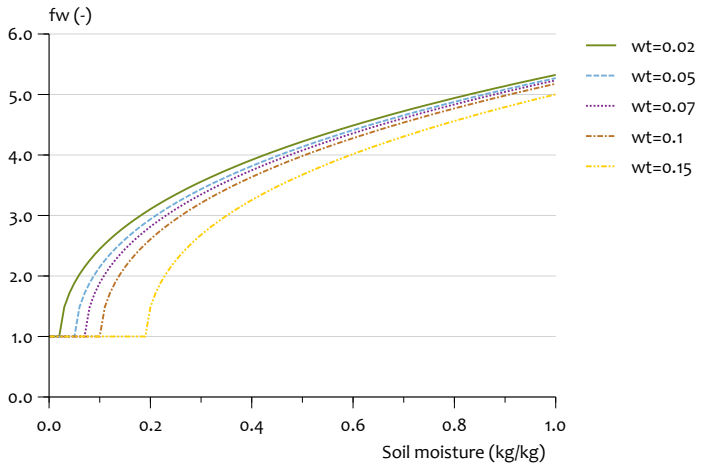

Soil moisture inhibition, according to Fécan et al.(1999), versus gravimetric soil moisture content, w, for various threshold values wt, which correspond to clay contents of 10, 25, 33, 43 and 59%.

the soil moisture threshold to be dependent on the clay fraction, c_f, which they formulated as follows:

$$w_t = 0.14c_f^{\,2} + 0.17c_f$$

where the unit of c_f is %. For a clay content of 33%, w_t would equal ~0.07 kg.kg^{-1}. In the current model set-up, the fraction of soil particles classified as the extra-fine size mode (FFS, see Tabel 7-3) was considered to represent the clay fraction, and applied to calculate the soil moisture threshold with the above equation.

Precipitation

In the present configuration of the LOTOS-EUROS model, the effect of precipitation (rain, snow) on dust emission is represented by assuming the dust flux to be zero during precipitation events up to 48 hours afterwards. In cases of snow cover the dust flux to also set to zero (ECMWF, three-hourly).

5.1.3 Vertical suspension flux

In reality, the relation between the horizontal flux of saltating soil aggregates and its induced vertical flux of aerosol particles, depends on the amount of aggregated soil, that of the released aerosol and the kinetic and binding energies involved. Alfaro *et al.* (1997, 1998) developed a sandblasting model which takes these dependencies into account. This sandblasting model was recently adapted for the calculation of wind-blown dust fluxes with the LOTOS-EUROS model.

Based on studies of wind tunnel experiments, Alfaro and Gomes (2001) distinguished three different log-normal modes for the aerosol particles released by sandblasting natural soils. The log-normal mass distribution of each aerosol size mode is formulated as follows:

$$\frac{dm_{a,i}}{dd_a} = \frac{1}{d_a\sqrt{2\pi}}\frac{1}{\ln\sigma_i}\exp\left(\frac{(\ln d_a - \ln d_i)^2}{-2\ln^2\sigma_i}\right)$$

where d_a is the aerosol diameter, d_i is the mass mean diameter of the ith mode and σ_i its geometric standard deviation. The size distribution characteristics and the corresponding binding energies (e_i) of all three modes are listed in Table 5.4.

The aerosol flux of the ith size mode suspended above soil with a soil size distribution described by log-normal distribution dm/dD_p (see Section 5.1.1) can be formulated as follows (Alfaro and Gomes, 2001):

$$F_{v,i} = \int_{D_p} F_h(D_p)\alpha_i(D_p)\frac{dm}{dD_p}dD_p$$

For a saltating soil particle of a given size D_p to be able to release an aerosol of size d_a, it needs a minimum kinetic energy to overcome the binding energy that keeps the aerosol bound to the saltating (or surface) soil aggregate. Given this as a fact, the sandblasting efficiency, α, for the production of aerosols with a characteristic size, d_i, can now be written as a function of the soil aggregate size, D_p, the fraction of kinetic energy, p_i, of the soil aggregate which is required for the release an aerosol particle of this characteristic size, and the binding energy of the aerosol particle, e_i. For the given classification of the aerosol size mode by Alfaro *et al.*(1997,1998), the sandblasting efficiency for the aerosol size of the ith mode can be written as follow:,

$$\alpha_i(D_p) = \frac{\pi}{6}\rho_{soil}B\frac{p_i d_i^3}{e_i}$$

where B=163m.s^{-2} is an empirical constant. The kinetic energy of saltating soil is formulated as:

$$e_c = \frac{100}{3}\pi\rho_{soil}D_p^{\,3}u^{*2}$$

The fraction, p_i, of the kinetic energy required for the release of aerosols with size d_i by an individual impacting soil aggregate, is given in Table 5.5. As can be seen in the table, the higher the kinetic energy of the impacting soil aggregate, the

Size distribution and binding energy characteristics Table 5.4

mode	d_i (µm)	σ_i (-)	e_i (kg.m^2.s^{-2})
1	1.5	1.7	$3.61.10^{-7}$
2	6.7	1.6	$3.52.10^{-7}$
3	14.2	1.5	$3.46.10^{-7}$

Size distribution and binding energy characteristics for the classification of aerosols released by sandblasting, according to Alfaro and Gomes (2001)

Fraction of kinetic energy of an individual saltating soil aggregate required Table 5.5

p_i (-)	e_c $e_c<e_3$ (kg.m^2.s^{-2})	$e_3< e_c< e_2$ (kg.m^2.s^{-2})	$e_2< e_c< e_1$ (kg.m^2.s^{-2})	$e_c> e_1$ (kg.m^2.s^{-2})
p_1	0	0	0	(ec-e1)/(ec-e3)
p_2	0	0	$(e_c- e_2)/(e_c- e_3)$	$(1-p1)(e_c- e_2)/(e_c- e_3)$
p3	0	1	$1- p_2$	$1- p_1- p_2$

Fraction of kinetic energy of an individual saltating soil aggregate required for the release of aerosols for all three aerosol modes by Alfaro and Gomes (2001).

larger the probability that finer mode particles, which have a higher binding energy, are released.

The above approach was used in the model calculations discussed in this report. It was applied solely in those areas for which soil texture information was available. Otherwise, wind blown dust emissions are set to zero.

To calculate the vertical dust flux as defined above (equation 7-11 and 7-12) at each time step and for each grid cell, is time consuming. The reason for this is that the kinetic energy of the soil aggregate is dependent on u*. To decrease the calculation time, a lookup table α_i as a function of u* was created. In this way, the integration over the soil size distribution has to be done only once.

After the calculation of $F_{v,i}$ for each aerosol mode, as defined by Alfaro and Gomes, we calculated the corresponding fine and coarse mode vertical dust fluxes as follows:

$$F_{v,j} = \int_{d_{a,j}} \sum_i F_{v,i} \frac{dm_{a,i}}{dd_a} dd_a$$

which is a summation of the contribution of each aerosol mode, as defined by Alfaro and Gomes (2001), to the fine ($d_a \leq 2.5\mu m$) or coarse ($2.5 < d_a \leq 10\mu m$) mode, as it is used in the LOTOS-EUROS model.

5.2 Saharan desert dust

Several times a year, during short periods of time with extremely high wind speeds, large amounts of dust are produced in desert areas and transported over great distances. These so-called dust events can lead to local concentrations of ambient soil dust exceeding 300 µg.m^{-3} at several hundreds of kilometres distance from the desert dust's source area.

The desert dust production outside the domain of LOTOS-EUROS is not described by its boundary conditions. However, it can contribute significantly to the mineral ambient PM_{10} within the model domain. Therefore, to include this contribution, we applied concentration data calculated by the TM5 global transport model (http://www.phys.uu.nl/~tm5/) as boundary condition at all boundaries of the LOTOS-EUROS model domain. The TM5 accumulation (0.1-1 µm) mode for dust was set to match the LOTOS-EUROS fine mode, and the TM5 coarse mode (1-20 µm) was set to match the coarse mode of the LOTOS-EUROS model. Through this assumption, some of the mass in the TM5 modes was incorrectly assigned to the respective LOTOS-EUROS modes. This will be adjusted in future model calculations. For a description of the boundary conditions obtained from TM5, we refer to Annex E.

5.3 Resuspension due to traffic

Traffic-generated fugitive dust is a predominant source of atmospheric particulate pollution at roadside locations (Thorpe *et al.*, 2007) and makes up a large part of the PM_{10} emission from traffic. Studies at traffic-influenced locations in Berlin (Lenschow *et al.*, 2001) and London (Harrison *et al.*, 2001) indicate that the resuspension of road dust is of the same order of magnitude as the primary emissions from traffic (e.g. vehicle exhaust and tyre abrasion, brake wear). Research on PM_{10} emissions from road traffic in Switzerland, by Gehrig *et al.* (2004), provided similar conclusions. For areas dryer than central Europe, resuspension is expected to dominate the exhaust emissions as observed in several studies in the United States (Abu-Allaban *et al.*, 2003; Gertler *et al.*, 2006). In this report, we present an approach to include resuspended emissions for regional scale modelling applications. The approach is based on an overview of available literature on the subject.

5.3.1 Conceptual framework

Road dust is mobilised in the turbulent wake of vehicles, and in the flow patterns of the turbulence generated by tyre rotation (Nicholson *et al*., 1989, Moosmüller *et al*., 1998). The amount of mobilised dust per vehicle kilometre travelled is a complex function which is not easily characterised. Before presenting literature data, we expand on the conceptual framework of the resuspension process.

The key parameter to address the emission per kilometre driven, is the amount of dust that is susceptible to mobilisation, the on-road dust or PM_{10} reservoir. Kuhns *et al*. (2003) suggested that the on-road PM_{10} matter exists at an equilibrium between emission and deposition processes, with short-term deviations lasting for several hours. The balance is straightforward, related to the amount of dust supply to the road surface. For paved roads, this supply is limited and includes material tracked in from unpaved areas (e.g. dirt roads, road shoulders, agricultural areas, construction sites), road sanding, spills from trucks and the deposit of ambient wind-blown material from nearby areas or of previously resuspended material. The amount of material lost is dependent on run-off by rain or road cleaning, as well as by resuspension caused by traffic. The difficulty is that none of these sources and sinks are well quantified (Kuhns *et al*., 2003). When interpreting and comparing literature data, it is important to keep these processes in mind.

As described above, the dust emission per vehicle kilometre is a loss term in the balance for the amount of available road dust. Hence, both properties are a function of the traffic properties, such as the aerodynamic properties of the vehicle, the vehicle speed and traffic volume. For example, a road with high traffic intensity has a large resuspension loss term, lowering the available dust load on the road, compared to a quiet road. The dust emissions per vehicle kilometre are, therefore, lower on busy roads than on quiet roads, although the total emissions are higher.

Below, we summarise the available literature and propose a simple methodology to account for resuspension emissions in a large-scale modelling application. Based on the principles described above, we distinguished two key factors: car type and road type. The first concerns the aerodynamic properties of the cars and we differentiated between HDV and LDV. The second factor concerns the dust reservoir dependent on traffic characteristics and road surrounding. Hence, we differentiated rural and urban roads, as well as motorways.

5.3.2 Literature data on emission factors of resuspension

There are several methodologies for estimating the emission strength from resuspension by cars. Most widely used is the so-called upwind-downwind method. In this method, PM_{10} concentrations are measured both upwind and downwind, which are then used in combination with dispersion models to determine emission factors (Claiborn *et al*., 1995, Gertler *et al*., 2006, Lohmeyer *et al*., 2000, Venkatram *et al*., 1999). Nevertheless, using the analysis of PM_{10} concentrations to infer emission potentials is not straightforward (Venkatram *et al*., 1999). It largely depends on the specific wind characteristics, the distance between measurement location and road, and the dispersion model characteristics. More recently, the linear relation between NO_x and PM_{10} has been used for inferring PM_{10} emissions from observed NO_x concentration differences (Gehrig *et al*., 2004, Thorpe *et al*., 2005). This method allows for a more precise estimation of PM emissions, than the direct extraction of PM emissions do from the observed upwind and downwind PM concentrations, since NO_x emission factors are rather well known. A similar approach is conducted with SF6 as a tracer by, for example, Claiborne *et al.* (1995).

Other researchers have developed techniques to also investigate the variability of road dust emissions. An example is the TRAKER method, an on-vehicle system for measuring PM_{10} emissions, which can be employed, by using dispersion models, to infer emission factors (Etyemezian *et al*., 2003). This method generally results in much larger emission factors for resuspended matter, than are measured in the upwind-downwind or tracer methods in which the measurements are taken at a larger distance from the emission source. The methodology is used for addressing spatial variability in emission potentials.

Separating emission from exhausts, direct wear (tire, brake, and road wear) and resuspension for real road conditions is not straightforward. Therefore, PM source estimates are often only separated in exhaust and non-exhaust components (e.g. Gehrig *et al.*, 2004). In the studies that do separate the different components of non-exhaust PM, a wide range of methods is applied. Abu-Allaban *et al.* (2003), for example, used CBM modelling in combination with measurements of PAH to calculate non-exhaust emission factors for LDV and HDV traffic, whereas Thorpe *et al.* (2007) applied a ratio of $PM_{10}/PM_{2.5}$ = 0.4, based on Harrison *et al*. (2001), assuming the $PM_{2.5-10}$ fraction to be equal to the non-exhaust PM, and using the EMEP/CORINAIR methodology (EEA, 2005) to separate tyre, brake and road surface wear. Often though, individual non-exhaust sources are not distinguished, as is done by Gehrig *et al*. (2004), who assumed the PM_{1-10} fraction of PM_{10} to be non-exhaust PM, and PM_1 equal to exhaust PM.

A summary of the emission factor estimates is listed in Table 5.6. Present knowledge on non-exhaust PM emissions is limited and observational studies are still rather incomplete. In other words, the emission estimates do not fully represent the wide range of conditions that are present within Europe. The provided estimates merely represent central en western Europe and the United States. Below, we first discuss the information presented in the overview and propose emission factors to be used for central European conditions. Next, we present an approach to account for potential regional differences in emission factors.

5.3.3 Selection of Emission factors for central Europe

Car type (LDV versus HDV)

Sehmel (1973) already observed that the resuspension caused by HDV traffic is roughly and order of magnitude larger than from LDV. Several recent studies confirm this finding. For London, Thorpe *et al.* (2007) found PM_{10} resuspension emission factors for LDV and HDV of 1.1-9.1 mg.vkt^{-1} and 139-183 mg.vkt^{-1}, respectively. Gehrig *et al.* (2004) determined emis-

An overview of European studies that include the estimation of the PM10 emission

Table 5.6

Europe

Reference	site type	Site type sub-category	Site name	Year	Method	PM instru-mentation	Included meteo obs.	Precipi-tation	Veh speed	Daily traffic number			PM10 Resuspension Emission Factors		
										LDV	HDV	LDV+HDV	LDV	HDV	LDV+HDV
									(m.s-1)	(-)	(-)	(-)	(mg.vkt-1)	(mg.vkt-1)	(mg.vkt-1)
Ketzel et al., 2007[1]	urb	kerb	Jagtvej, Copenha-gen, Denmark	2002-2004	CGA, KBg	TEOM	wind	mixed	45	-	-	25000	-	-	46
	urb	kerb	H.C. Andersens Blvd., Copenhagen, Denmark	2002-2004	CGA, KBg	TEOM	wind	mixed	55	-	-	60000	-	-	108
	urb	kerb	Hornsgatan, Stock-holm, Sweden	2002-2004	CGA, KBg	TEOM	wind	mixed	40	-	-	35000	-	-	198
	urb	kerb	Lutzerstrasse, Leip-zig, Germany	2003-2004	CGA, KBg	TEOM	wind	mixed	40	-	-	29000	-	-	67
	urb	kerb	Frankfurter Allee, Berlin, Germany	2004	CGA, KBg	Beta-ray abs.	wind	mixed	28	-	-	60000	-	-	57
	urb	kerb	Merseburger Strasse, Halle, Germany	2003-2004	CGA, KBg	TEOM	wind	mixed	50	-	-	35000	-	-	66
	urb	kerb	Runebergkatu, Hel-sinki, Finland	2003-2004	CGA, KBg	Beta-ray abs.	wind	mixed	39	-	-	17500	-	-	121
	rur		Volkermakrterstrasse, Klagenfurt, Germany	2004		HVS DIGI-TEL	wind	mixed	40	-	-	23000	-	-	109
Thorpe et al., 2007[2]	urb	kerb	Maryleborne (Bloomsbury), London, UK	2000	CGA, KBg	TEOM	wind, precip.	mixed	n/a	-	-	-	2.6	145	17.3
	urb	kerb	Maryleborne (Bloomsbury), London, UK	2001	CGA, KBg	TEOM	wind, precip.	mixed	n/a	-	-	-	0.3	139	15.4
	urb	kerb	Maryleborne (Bloomsbury), London, UK	2002	CGA, KBg	TEOM	wind, precip.	mixed	n/a	-	-	-	-0.5	139	14
	urb	kerb	Maryleborne (Bloomsbury), London, UK	2003	CGA, KBg	TEOM	wind, precip.	mixed	n/a	-	-	-	0	162	19.8
	urb	kerb	Maryleborne (Bex-ley), London, UK	2000	CGA, KBg	TEOM	wind, precip.	mixed	n/a	-	-	-	5.1	178	22.8
	urb	kerb	Maryleborne (Bex-ley), London, UK	2001	CGA, KBg	TEOM	wind, precip.	mixed	n/a	-	-	-	2.8	171	20.2
	urb	kerb	Maryleborne (Bex-ley), London, UK	2002	CGA, KBg	TEOM	wind, precip.	mixed	n/a	-	-	-	2.1	183	20.9
	urb	kerb	Maryleborne (Bex-ley), London, UK	2003	CGA, KBg	TEOM	wind, precip.	mixed	n/a	-	-	-	1.1	172	21.4
Gehrig et al., 2004[4]	rur		Aathal, Switzerland	2000	CGA, UD	Beta-ray abs.	wind	dry	50/50	1102	71	1173	33	207	-
	rur	hw	Birrhardl, Switzerland	2000	CGA, UD	Beta-ray abs.	wind	dry	120/85	2495	265	2760	47	74	-
	rur	hw, lower speed!	Humlikon (A4)l, Switzerland	2000	CGA, UD	Beta-ray abs.	wind	dry	88/76	1243	182	1425	22	144	-
	urb	kerb	Rosengartenstrasse, Zurich, Switzerland	2000	CGA, KBg	Beta-ray abs.	wind	dry	50/40	2730	168	2898	17	115	-
	urb	kerb/dist flow	Schimmelstrasse, Zu-rich, Switzerland	2000	CGA, KBg	Beta-ray abs.	wind	dry	0-50/0-50	1074	80	1154	92	819	-
	urb	kerb/dist flow	Weststrasse, Zu-rich, Switzerland	2000	CGA, KBg	Beta-ray abs.	wind	dry	0-50/0-50	1014	66	1080	39	383	-

Europe

Reference	site type	Site type sub-category	Site name	Year	Method	PM instrumentation	Included meteo obs.	Precipitation	Veh speed	Daily traffic number			PM10 Resuspension Emission Factors		
Lohmeyer et al., 2000[5]	urb	kerb	Schildhornstrasse, Berlin, Germany	2000	UD		wind, precip.	mixed	-	-	-	-	-	-	-
	urb	kerb	Lutzerstrasse, Leipzig, Germany	2000	UD		wind, precip.	mixed	-	-	-	-	-	-	-
Rauterberg-Wulff et al., 1999[4]	urb	kerb	Frankfurter Allee, Berlin, Germany	1999	UD		wind, precip.	mixed	-	-	-	-	-	-	-
Hueglin et al., 1998[4]	urb	kerb	Schimmelstrasse, Zurich, Switzerland	1998	UD		wind, precip.	mixed	-	-	-	-	-	-	-
Kupiainen et al., 2003	test facility	without traction sanding	-	2002			-	dry	15-25	-	-	-	-	-	10-20
	test facility	traction sanding; 900g/m2	-	2002			-	dry	15-25	-	-	-	-	-	30-50
	test facility	traction sanding; 900g/m2 <2mm sand grains	-	2002			-	dry	15-25	-	-	-	-	-	160
	test facility	traction sanding; 1800g/m2	-	2002			-	dry	15-25	-	-	-	-	-	70-160
Keuken et al., 1995[6]	rur	hw	N201, The Netherlands	1998					120	-	-	-	10	350	40

[1] *PM_{10} resuspension is assumed to be the difference between total PM_{10} and exhaust PM_{10}*

[2] *PM_{10} resuspension is assumed to be $PM_{2.5-10}$*

[3] *PM_{10} resuspension is assumed to be PM_{1-10}*

[4] *Data taken from Lohmeyer, A, and I. During, Validierung von PM_{10}-Immisionsberechnungen im Nahbereich von Strassen und Quantifizirung der Feinstaubbildung von Strassen, Karlsruhe/Dresden, 2001*

[5] *Data taken from Kupiainen et al., AE, 2003*

Observational methods:

CGA	NO_x dillution method based on the linear relation between NO_x and PM emissions (Tracer with NO_x)
UD	Upwind-Downwind measurements and dispersion model
Downwind or Upwind	Either Downwind or Upwind measurements only, combined with dispersion model
KBg	Kerbside measurements, background corrected
Tracer	Tracer technique by Claiborne *et al.*1995 (with SF6)
TRAKER	On-vehicle measurement of PM_{10}, measured behind front tyres (front bumper corrected), combined with dispersion assumptions in order to infer EFs.

An overview of European studies that include the estimation of the PM_{10} emission factor for resuspension.

An overview of US studies that include the estimation of the PM10 emission

Table 5.7

United States

Reference	site type	Site type subcategory	Site name	Year	Method	PM instrumentation	Included meteo obs.	Precipitation	Silt loading	Veh speed	Traffic number	PM2.5 Resuspension Emission Factors		PM10 Resuspension Emission Factors		
											LDV+HDV	LDV	HDV	LDV	HDV	LDV+HDV
									(g.m-1)	(m.s-1)	(veh.h-1)	(mg. vkt-1)	(mg. vkt-1)	(mg. vkt-1)	(mg. vkt-1)	(mg. vkt-1)
Abu-Allaban et al., 2003	rur	hw	Farrington Road, Durham/RTP,NC	jun 2000	Down-wind only	Teflon filter coll.	wind	-	-	82	-	8	-	110	-	-
-	urb	hdv	Highw 55, Durham/RTP,NC	jun 2000	Down-wind only	Teflon filter coll.	wind	-	-	-	-	5	35	230	1600	-
-	urb	hw exit	J. Motley exit, Durham/RTP,NC	jun 2000	Down-wind only	Teflon filter coll.	wind	-	-	-	-	26	300	320	2500	-
-	rur	hw	McCarran Blvd, Reno, NV	jan 2000	Down-wind only	Teflon filter coll.	wind	-	-	82	-	6	28	780	7800	-
-	urb	hw exit	Moana Lane exit, Reno, NV	jan 2000	Down-wind only	Teflon filter coll.	wind	-	-	-	-	2	17	63	-	-
-	urb	low speed	Revere Road, Durham/RTP,NC	jun 2000	Down-wind only	Teflon filter coll.	wind	-	-	57	-	2	-	150	750	-
-	urb	hdv	Sparks Blvd, Reno, NV	jan 2000	Down-wind only	Teflon filter coll.	wind	-	-	-	-	17	60	41	230	-
-	urb	low speed	Valley Road, Reno, NV	jan 2000	Down-wind only	Teflon filter coll.	wind	-	-	57	-	8	50	100	600	-
Venkatram et al.,1999	rur	hw	Motorway 215/60, Riverside, Cal.	1996	UD	Teflon filter coll.	wind, T, rh	-	-	-	8000	-	-	-	-	170
-	rur	near urban	Canyon Crest Dr., Riverside, Cal.		UD	Teflon filter coll.	wind, T, rh	-	0.075	-	990	-	-	-	-	680
-	rur	near urban	Iowa Avenue, Riverside, Cal.	1996	UD, Tracer	Teflon filter coll.	wind, T, rh	-	0.00016	-	1200	-	-	-	-	650
-	rur	near urban	Main Street, Riverside, Cal.	-	UD	Teflon filter coll.	wind, T, rh	-	0.006	-	875	-	-	-	-	3010
-	rur	near urban	Riverside Dr., Riverside, Cal.		UD	Teflon filter coll.	wind, T, rh	-	0.16	-	892	-	-	-	-	1080
-	rur	near urban	Fogg Street, Riverside, Cal.	1997	UD	Teflon filter coll.	wind, T, rh	-	0.22	-	42	-	-	-	-	220
-	rur	near urban	Unpaved road, Riverside, Cal.	1996	UD	Teflon filter coll.	wind, T, rh	-	-	-	66	-	-	-	-	790
Etyemezian et al., 2003	rur	-	Ada County, Treasure Valley, Idaho	jul2001	TRAKER	DustTrak monit.	-	-	-	-	-	-	-	-	-	3600
-	urb	-	Ada County, Treasure Valley, Idaho	jul2001	TRAKER	DustTrak monit.	-	-	-	-	-	-	-	-	-	4800
-	rur	-	Canyon County, Treasure Valley, Idaho	jul2001	TRAKER	DustTrak monit.	-	-	-	-	-	-	-	-	-	3700
-	urb	-	Canyon County, Treasure Valley, Idaho	jul2001	TRAKER	DustTrak monit.	-	-	-	-	-	-	-	-	-	5400
-	rur	-	Ada County, Treasure Valley, Idaho	feb/ mrt2001	TRAKER	DustTrak monit.	-	-	-	-	-	-	-	-	-	5500
-	urb	-	Ada County, Treasure Valley, Idaho	feb/ mrt2001	TRAKER	DustTrak monit.	-	-	-	-	-	-	-	-	-	8000
-	rur	-	Canyon County, Treasure Valley, Idaho	feb/ mrt2001	TRAKER	DustTrak monit.	-	-	-	-	-	-	-	-	-	4300
-	urb	-	Canyon County, Treasure Valley, Idaho	feb/ mrt2001	TRAKER	DustTrak monit.	-	-	-	-	-	-	-	-	-	6400

United States

Reference	site type	Site type subcategory	Site name	Year	Method	PM instrumentation	Included meteo obs.	Precipitation	Silt loading	Veh speed	Traffic number	PM2.5 Resuspension Emission Factors		PM10 Resuspension Emission Factors		
Claiborn et al., 1995	rur	hw	Motorway 395, Spokane, WA (collector street)	sep1992	UD,Tracer	TEOM	wind	-	-	-	529	-	-	-	-	3700
-	rur	unpaved road	55th Street, Spokane, WA	sep1992	UD,Tracer	TEOM	wind	-	-	-	47	-	-	-	-	140-360
-	rur	hw	Country Holmes Blvd, Spokane, WA	nov1993	UD,Tracer	TEOM	wind	-	-	-	2920	-	-	-	-	580
-	rur	hw	Division Street, Spokane, WA	feb-jun1994	KBg	TEOM	wind	-	-	-	1160	-	-	-	-	450-1220
-	rur	hw	Moscow-Pullman Motorway 270	sep1992	UD,Tracer	TEOM	wind	-	-	-	433	-	-	-	-	4200
-	rur	hw	Motorway 395, Spokane, WA (collector street)	sep1992	UD,Tracer	TEOM	wind	-	-	-	483	-	-	-	-	5100-9300
-	rur	hw	Motorway 12, Lewiston, WA	aug1992	UD,Tracer	TEOM	wind	-	-	-	1615	-	-	-	-	3200-34200
-	rur	unpaved road	Freya Street, Spokane, WA	sep1992	KBg	TEOM	wind	-	-	-	314	-	-	-	-	250-298
-	rur	unpaved road	Abbott Road, Spokane, WA	sep1992	KBg	TEOM	wind	-	-	-	18	-	-	-	-	75-3000
Gillies et al., 2005	rur	unpaved road	Ft. Bliss, TX	apr2002	UD	-	-	-	4-7%	-	-	-	-	48	2880	-
Kantamaneni et al., 1996	rur	traction sanding, a field study, four-lane road, sand (predominant 0.95 cm size distribution) dispersed 12 hrs prior to sampling	four-lane road in Spokane, Washington	1994	UD	DustTrak monit.	-	-	-	-	-	-	-	-	-	400-2000
-	rur	without traction sanding, a field study, four-lane road, sand (predominant 0.95 cm size distribution) dispersed 12 hrs prior to sampling	four-lane road in Spokane, Washington	1994	UD	DustTrak monit.	-	-	-	-	-	-	-	-	-	1000-2000
Gertler et al., 2006	rur/hw	-	several road/hw, baseline measurement	2003	UD	DustTrak monit.	wind	not during precip.	-	70-90	130-170	-	-	76	229	-
-	rur/hw	-	several road/hw, after salting	2003	UD	DustTrak monit.	wind	not during precip.	-	70-90	130-170	-	-	99	310	-
-	rur/hw	-	several road/hw, day1-2 after snow storm	2003	UD	DustTrak monit.	wind	not during precip.	-	70-90	130-170	-	-	112-133	610-660	-
-	rur/hw	-	several road/hw, after snow storms and subsequent road sweeping	2003	UD	DustTrak monit.	wind	not during precip.	-	70-90	130-170	-	-	211	735	-

Observational methods

CGA	NO_x dillution method based on the linear relation between NO_x and PM emissions (Tracer with NO_x)
DU	Upwind-Downwind measurements and dispersion model
Downwind or Upwind	Either Downwind or Upwind measurements only, combined with dispersion model
KBg	Kerbside measurements, background corrected
Tracer	Tracer technique by Claiborne *et al.*1995 (with SF6)
TRAKER	On-vehicle measurement of PM_{10}, measured behind front tyres (front bumper corrected), combined with dispersion assumptions in order to infer emission factors.

An overview of US studies that include the estimation of the PM_{10} emission factor for resuspension.

sion factors for city roads in Zürich and several motorways, obtaining emission factors varying between 17-92, 47-819 mg.vkt^{-1} for LDV and HDV, respectively. Although based on much larger absolute emission factors (41-320 mg.vkt^{-1} for LDV and 220-1600 mg.vkt^{-1} for HDV), Abu-Allaban (2003) found that the contribution of resuspended PM_{10} caused by HDV traffic was roughly eight times larger than that caused by LDV for rural and near-town roads in Nevada, United States. Based on these data, we assumed a PM_{10} emission factor ratio between heavy and light duty vehicles of 9, EF_{HDV}/EF_{LDV} = 9. Given the assumed constant ratio, only the LDV emission factors are discussed below.

Road type

The influence of road type on resuspension is rather complex and cannot easily be separated from the influence of the type of traffic flow, that is, vehicle speed, traffic intensity, and behaviour (Kupianen, 2005). The data presented in Tables 5.6 and 5.7 indicate that in the urban environment the resuspension per vehicle kilometre tends to be significantly higher than on motorways. The main differences are the higher average vehicle speeds and the higher traffic intensity on motorways, compared to urban roads, which both lead to a lower on-road dust reservoir. Also, disturbed traffic flow due to traffic lights or road exits, results in higher PM_{10} emissions (Lohmeyer *et al.*, 2004, Gehrig *et al.,* 2004, Thorpe *et al.,* 2007). Moreover, the supply of dust from the surroundings of an urban road is very likely to be significantly larger than from that of a motorway. Hence, motorway emission factors are assumed to be lower than those of the other road types, and in accordance with measurements (Etyemezian *et al.*, 2003, Gehrig *et al.*, 2003).

Reported emission factors for LDV on motorways ranged from 10 mg.vkt^{-1} (Keuken *et al.*, 1999) to 47 mg.vkt^{-1} (Gehrig *et al.*, 2003). The central value for motorways appeared to be about 22, close to values suggested by several authors (Gehrig *et al.*, 2004; Lohmeyer *et al.*, 2004) and equal to the description in the INFRAS emission factor handbook (UBA, 2004).

For urban roads, we applied an average of 48 mg.vkt^{-1} for LDV traffic, based on the emission factors for city road types in the INFRAS emission factor handbook (UBA, 2004). In comparison, Gehrig *et al.* (2004) observed an average emission factor of 17-92 mg.vkt^{-1} in an urban environment with some of the roads having disturbed flow situations.

The emission factor for rural roads poses a problem. There are nearly no data for this road type. Rural roads are generally defined as non-motorways and non-urban roads. This includes a wide range of roads, from important regional roads to small roads with very little traffic. Hence, in general, these road have less traffic driving at a lower speeds (up to 80km.h^{-1}) than on motorways. This implies that rural roads have a larger amount of on-road dust available for resuspension than motorways. Furthermore, rural roads receive material tracked in from unpaved areas and agricultural activities, motorways do not. Also, in the case of rural roads, traffic lanes are close to the road shoulder, which is also a road dust source. Finally, the road-surface condition of rural roads often is not as good as that of motorways. From this conceptual analysis, we expect the dust reservoir on rural roads and its associated emission factor to be significantly larger than on motorways. Consequently, we do not follow the approach by the INFRAS emission factor handbook (UBA, 2004) which assumes motorways and rural roads to have the same emission factor.

For resuspension emission factors, the comparison between rural and urban roads is more difficult. The lower traffic intensity combined with higher average speeds on rural roads, when compared to urban roads, would suggest somewhat similar emission factors for both road types. However, the question is if the amount of road dust is more important than traffic intensity or speed, and this question is not easy to answer. The dust on both road types may originate from very different sources. For example, a significant part of the urban road dust may consist of material coming from construction areas and parking lots, whereas the dust on rural roads may largely come from agricultural land. Moreover, the areas adjacent to a road generally vary considerably, and consequently, so do the dust sources. However, the quantity of the build-up material on roads could be of the same order. Furthermore, all of these factors depend strongly on the location. Etyemezian *et al.* (2003) provided slightly lower (~20%) estimates for the emission factors for rural roads. Ketzel *et al.* (2007) estimated a rural emission factor similar to that for urban roads. For rural roads, Gehrig *et al.* (2004) mentioned larger emission factors when compared to urban roads with undisturbed flow, but when compared to urban roads with disturbed traffic flow, the rural emission factors became smaller. Therefore, based on the above reasoning and suggestions and as a first best guess, we apply a rural road emission factor of 48 mg.vkt^{-1} for LDV traffic, which is equal to that for urban roads.

The suspension of dust from unpaved roads is nearly unlimited by an dust supply. For these roads, huge PM_{10} emission strengths have been observed (Gillies *et al.,* 2003, Claiborn *et al.,* 1995). The observed average emission factors are generally ~300 mg.vkt^{-1} at frequent road use (assuming that 90% of the traffic is LDV during the observations made by Gilles *et al.*, 2003). However, for little travelled roads, the observed emission factors can be higher by a factor of ten. In Europe, the amount of traffic on unpaved roads is very limited. Therefore, we neglected this source.

So far, we discussed the estimated emission factors under central European conditions. These values were taken as a starting point. However, emission factors are also a function of climatic conditions (aridity) and specific practices, such as road sanding. These issues are important to translate the emission factors mentioned above into a methodology which could also be used for southern Europe and for Scandinavia in winter.

A simple pragmatic approach was taken to calculate traffic related resuspension emission with the LOTOS-EUROS model. The method is based on a map of vehicle driven kilometres for Europe, specified into light and heavy traffic (LDV and HVD, respectively) and three road type classes (rural road, urban road and motorways), with corresponding emission factors.

PM2.5-10 emission factor (mg.vkt-1) for traffic related resuspension as a function **Table 5.8**

	Road type		
	HW	**RUR**	**URB**
HDV	198	432	432
LDV	22	48	48

$PM_{2.5-10}$ emission factor (mg.vkt^{-1}) for traffic related resuspension as a function of road type for light and heavy duty vehicles, applied in the LOTOS-EUROS model

The first order estimates for the applied emission factors for $PM_{2.5-10}$, as discussed in previous sections, are listed in Table 7.8. As a first approximation for the fine fraction emission factors, we assumed a ratio of $EF_{PM2.5}/EF_{PM2.5-10}=0.1$, following Thorpe *et al.* (2007), among others. The influence of precipitation on the resuspension flux was taken into account by setting the emissions to zero in case of rain and snow (ECMWF precipitation, three-hourly).

The model resuspension emission flux F_{trs} is defined as follows,

$$F_{trs} = c_{clim} c_{rs} \sum_{veh} \sum_{road} EF_{veh,road} D_{veh,road},$$

where $EF_{veh,road}$ is the emission factor and $D_{veh,road}$ is the total distance travelled in vehicle kilometres (VKT), as a function of road and vehicle type. C_{clim} and C_{rs} are factors to account for climate conditions and road sanding. Below, we elaborate on a possible strategy to account for these regional dependencies.

5.3.4 Regional variability in emission factors

The variation of ambient particulate-matter concentration due to traffic resuspension in Europe is presumably significant for several reasons. Here, we distinguish between two dominating factors that affect PM emissions on a regional level. First, we present a method for including the dependency on climatic conditions, most notably humidity and temperature. This methodology was used to capture the variability of the resuspension source strength between central and southern Europe. Secondly, we describe our approach of accounting for road sanding activity and studded-tyre use in winter, which are responsible for high peak PM emissions in springtime in Scandinavia and the elevated Alpine area.

Central and southern Europe

The observed emission factors for central Europe, by Thorpe *et al*. (2007), Gehrig *et al*. (2001) and others, are significantly smaller than the United States estimates. Moreover, the differences between estimated emission factors, for similar road types, by Gehrig *et al.* (2001) and Abu-Allaban *et al.* (2003), are a factor of 2 to 10, with the higher estimate for the United States. A more recent study by Gertler *et al.* (2006), does not indicate such high emissions, but there is still a discrepancy with the European estimates of up to a factor of 3. This may be largely attributed to differences in amount of dust sources on and near roads. Most of the United States studies, such as that of Abu-Allaban (2003), Claiborn *et al*. (1995), Venkatram *et al*. (1999), and Gillies *et al.* (1995), were conducted on rural sites or near cities, in dryer and therefore dustier areas, in the states California, Nevada, Idaho and Washington. These areas are not representative for central Europe, where most of the areas are vegetated and circumstances are more humid. However, they may be comparable to southern European countries, such as Spain. Sources apportionment studies (Putaud *et al*., 2004, Querol *et al*., 2004, Kuhlbush *et al*., 2000, Beekmann *et al.*, 2007) point out that for southern European countries (e.g. Spain) mineral ambient PM_{10} concentrations in city backgrounds and near busy roads are larger than at central European sites. Hence, there is a need to account for the increased resuspension flux as a function of the climatic conditions in southern Europe.

To account for climatic conditions one option would be to use the present United States estimates on traffic resuspension emission factors for southern European areas. This would mean that a similarity has to be assumed in regional conditions road, road condition and road adjacent area, and meteorological conditions between both regions. A number of arguments could be put forward against such an approach. First, using a discrete distribution of emission factors over Europe would lead to 'jumps'single in the modelled distribution and would pose the question of where to use which emission factor (central or southern Europe). Second, although the real emission factor for southern Europe probably would be within the range estimated for the United States, it was difficult to choose a central value due to the width of the range. Hence, we chose to follow a different approach.

An important pre-requisite for modelling the regional dependency on climate conditions is that it should yield a continuous relationship (without jumps) across Europe. One way to pursue this is to use a proxy map for Europe to which the emission potential is related. As the aridity of the soil plays an important role, we chose to use the annual average soil moisture map of Europe as a proxy field (see Figure 5.6). The next step was to relate the existing and poorly covered emission factor estimates to the soil moisture map. This posed a challenge as no emission factor estimates for southern Europe were available. Therefore, we based the emission sensitivity to soil moisture on the gradients in the more widely performed PM observations of (traffic) resuspended material. We assumed that traffic resuspension contributions to the total resuspension source strength within cities to be similar for both central and southern Europe. This approach is further justified by the observations studied by Querol *et al*. (2007). Querol *et al*. (2007) observed a higher concentration of certain crustal elements (e.g. Al, Ca, Fe, Ti, Li, Rb) at urban sites than at rural sites, indicating that their origin is mainly linked to road traffic. Hence, it can be assumed that the ratio in urban increment between southern and central Europe is

Observations of mineral PM_{10} and $PM_{2.5}$ throughout Europe Table 5.9

Reference	Country	Location	PM_{10} Rural bg ($\mu g.m^{-3}$)	PM_{10} Urban bg ($\mu g.m^{-3}$)	$PM_{2.5}$ Rural bg ($\mu g.m^{-3}$)	$PM_{2.5}$ Urban bg ($\mu g.m^{-3}$)
Putaud et al., 2004	Belgium (B)	Gent	-	3.5	-	1
	Switzerland (CH)	Chaumont	2	-	<0.5	-
		Zurich	-	2.5	-	1
		Basel	-	3	-	1.5
	Austria (A)	Illmitz	0.5	-	<0.5	-
	Spain (E)	Montenegra	4	-	-	-
	Italy (I)	Bologna	-	5	-	2.5
Querol et al., 2004	Sweden (S)		2-4	7-9	1-3	1-3
	The Netherlands (NL)		2	3	0.6	0.8
	Germany (D)		3	5	-	-
	Switzerland (CH)		2	2	1	1
	Spain (E)		6	10	2	3
Kuhlbush et al., 2000	Germany (D)	Spellen	3-5	-	1-3	-
		Oberhausen	-	10	-	13
Beekmann et al., 2007	Germany (D)	Berlin-Brandenburg	1.8-4.5*	-	-	-
		Berlin	-	2.5-7.4*	-	-

Regional differences between rural and urban background mineral PM_{10}, $PM_{2.5}$ Table 5.10

Regional grouping	PM_{10}		$PM_{2.5}$	
	Urb.-Rur. ($\mu g.m^{-3}$)	Urb./Rur. (-)	Urb.-Rur. ($\mu g.m^{-3}$)	Urb./Rur. (-)
Northern Europe (S)	3-7	1.8-4.5	0-2	1-3
Central Europe (NL, B, D)	2.1	1.6	2.9	2.2
Central Europe (CH, A)	1.0	1.7	0.4	1.8
Southern Europe (E)	5.0	2.0	1	1.5

a measure of the relative increase in the resuspension source strength.

Sources apportionment studies show that the rural background PM_{10} varies between 4 and 6 in Spain, and between 0.5 and 5 in the Netherlands, Belgium, Germany, Switzerland and Austria (Table 5.9). The ratio in urban over rural background PM_{10} increases only slightly from 1.6 in the Netherlands, Belgium and Germany to 2.0 in Spain. The last figure could indicate a possible large similarity in relative source contributions between rural and urban areas all over Europe. The absolute difference between observed urban background and rural background PM_{10} increased from central towards southern Europe, with more than twice the urban increase in Spain than in central Europe (see Table 5.10). The actual number used here was based on the urban increment for the non-mountainous countries of central Europe. The data for Switzerland and Austria were not taken into account, to exclude the possible influence of road sanding. The ratio of the urban increment between southern and central Europe then becomes 5.0/2.1 ~ 2.5.

The concentration of a primary pollutant in a source area is, besides the emission strength, also (linearly) dependent on the mixing layer height. Hence, we needed to account for the differences in mixing layer height (h_{mix}) to relate the urban increments to emission strengths. In the procedure, we have used the annual average mixing layer height from ECMWF for Spain (750 m) and central Europe (550m). To explain the observed Spanish urban increment, the emissions should have been about 2.5 * 1.4 = 3.7 higher than those in central Europe. Taking the average soil moisture content in Spain (0.225 $kg.kg^{-1}$) and central Europe (0.3 $kg.kg^{-1}$) a linear relation for regional multiplication factor for the emission factor as function of soil moisture can be constituted (Figure 5.8). For central European conditions the multiplication factor is obviously 1. We did not extrapolate outside the indicated range of soil moisture content. Hence, for LDV, maximum emission estimates of 3.7 * 22 = 80 $mg.vkt^{-1}$ for motorways and 3.7* 48 = 176 $mg.vkt^{-1}$ for urban and rural roads was used within the model domain.

The emission factors for Spain can be compared to estimates for the United States. Venkatram *et al.*(2004), Etyemezian *et al.*(2003b), Abu-Allaban (2003) and Claiborn *et al.*(1995), report emission factors between 170 and 9300 $mg.vkt^{-1}$. Our estimates fell into the lower range of these estimates. However, a part of the United States estimates (Venkatram *et al.*(2004), Etyemezian *et al.*(2003b)) were performed by measuring the PM_{10} emission from a vehicle itself, instead of inferring the emission factors from PM_{10} concentrations taken up and downwind of the road. The former approach, in general, led to a higher estimated emission factor than the latter. Considering only the more recent estimates, the majority of the values tended to concentrate around 100 to 220 $mg.vkt^{-1}$ for light traffic (Kupianen, 2005). Considering these numbers, our estimate for southern Europe fell within the range of the United States estimates.

Annual average volumetric soil moisture **Figure 5.7**

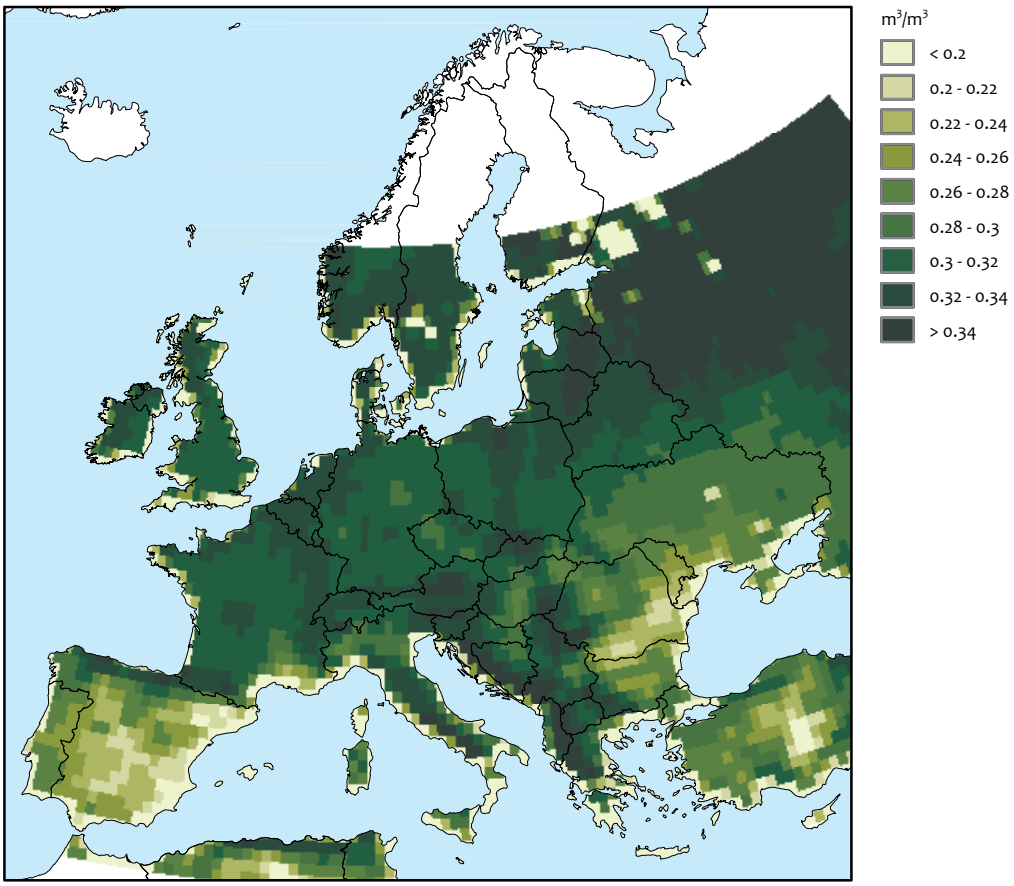

Annual average volumetric soil moisture for 2005 (ECMWF).

Mineral PM_{10} emission by traffic **Figure 5.8**

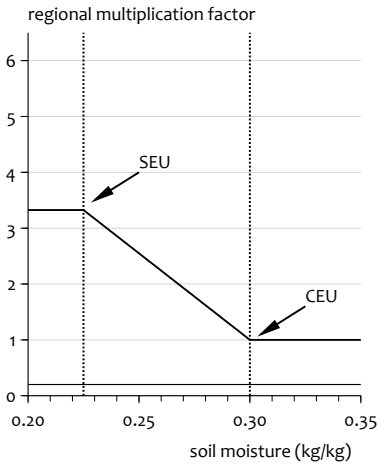

Regional multiplication factor for the mineral PM_{10} emission by traffic that corrects for climatic differences throughout Europe, based on observed PM, annual average soil moisture and mixing layer height at reference areas in central (CEU) and southern Europe (SEU).

The use of studded tyres and road sanding in winter, in Nordic and Alpine countries, caused additional, high springtime PM_{10} peaks with a contribution of non-exhaust mineral material up to 90% (Omstedt *et al.*, 2005, Kupiainen *et al.*, 2003). In United

Total PM_{10} and $PM_{2.5}$ emission factors for land preparation and harvesting activities **Table 5.11**

Reference	Location	Year	Method	Activity	Operation type	Emission factor $PM_{2.5}$ ($kg.ha^{-1}$)	Emission factor PM_{10} ($kg.ha^{-1}$)
Öttl et al.(2007)	Germany	2004	PM obs., disp. mod.	land preparation	harrowing	0.29	0.82
					discing	0.12	1.37
					cultivating	0.06	1.86
					ploughing (dry)	1.3	10.5
Funk et al.(2007)	Germany	2006	PM obs., disp. mod.	land preparation	ploughing (wet)	0.05	1.2
Gaffney et al. (2003)	California, US	1995-2003	Upwind-downwind	land preparation	root cutting		0.3
					discing, tilling, chiselling		1.3
					ripping, subsoiling		5.2
					land planing & floating		14.0
					weeding		0.9
				harvesting	almond		45.7
					corn		1.7
					cotton		3.8
					wheat		6.5

States studies by Gertler *et al.*(2006) and Wittorff *et al.* (1996), ~60% of the observed ambient PM_{10} could be attributed to road sanding, following winter storms. Furthermore, after the application of brine solution, once the road was dryed out, a ~30% increase of PM_{10}, and $PM_{2.5}$ was observed in the study by Gertler *et al.*(2006). Estimates of emission factors increased from 229 to 310-660 $mg.vkt^{-1}$ and 76 to 133 $mg.vkt^{-1}$ for PM_{10} and $PM_{2.5}$, respectively, between before and after a snow storm, during which time road abrasive was applied. Road sweeping after the snow storm only slightly raised PM_{10} emissions, but had a significant impact on $PM_{2.5}$ emissions. Kuhns *et al.*(2003) reported a short-term increase in PM_{10} up to ~75% due to the combined effect of winter sanding and road sweeping.

Omstedt *et al.* (2005) developed an empirical model for investigating the influence of road sanding and studded-tyre use on PM resuspension emission for Swedish roads. The model uses emission factors and traffic data, and takes into account the on-road dust layer thickness incorporating resuspension and run-off by precipitation or otherwise. This model was specifically and successfully applied to investigate the effect of road sanding and studded-tyre use in the Scandinavian winter on the fugitive PM_{10} concentration.

For the Scandinavian countries, based on the model study by Omstedt *et al.*(2005), a multiplication factor of 2 was applied during the spring months of March to May to the standard emission factors of PM_{10} and $PM_{2.5}$ for light and heavy traffic, to correct for the additional resuspension from road sanding and tyre use. For this study, we did not account for road sanding in the Alpine area.

5.4 Agricultural activities

Soil erosion resulting from land-management activities is receiving increased attention, mainly because of soil degradation. Presently, questions on its contribution to fugitive PM_{10} are raised. International scenarios for air pollution control strategies are being developed, for example, by the UNECE Convention on Long-Range Transboundary Air Pollution (LRTAP), which identifies the growing of plants and arable farming as considerable sources of PM emissions (Hinz *et al.*, 2007). However, dedicated research on emission factors of PM_{10} and the finer component $PM_{2.5}$ from a wide range of agricultural activities is still required, because of the lack of proper knowledge. This is mainly caused by an insufficient amount of reliable observations.

Currently, only a handful of studies are available that have estimated the emission potentials of several land-management activities. These studies have been summarised in Table 5.11. The range of reported estimates for emission factors of land preparation and harvesting is wide, and varies from 0.3 to14 $kg.ha^{-1}$ and from 3.8 to 45.7 $kg.ha^{-1}$, respectively. The uncertainty associated with these numbers is large. Most of the estimates presented in Table 5-11 were based on PM measurements taken close to the point of origin. The emission factor estimates were inferred from the PM observations by means of dispersion modelling. It has been discussed that these estimates may not reflect the particle emission on a larger scale (Hinz *et al.*, 2007). Nonetheless, it was the only information available and we tested whether these numbers were realistic or not.

Despite the little knowledge and scarce availability of observations, a first approach was made to calculate the resuspension emission related to agricultural activities with the LOTOS-EUROS model. The emission flux F_{ars} is defined as follows:

$$F_{ars} = \sum_{operation} C_{operation} EF_{operation} A$$

where $EF_{operation}$ ($mg.m^{-2}$) is the emission factor for a specific agricultural operation and A (m^2) is the surface area over which the emission occurs. $C_{operation}$ (h^{-1}) is a factor that accounts for the timing of each activity and its duration. Therefore, $C_{operation}$ depends on operation type. The surface area A is simply the arable land area within a model grid cell. The selected emission factors for the activities that we took

$PM_{2.5}$ and PM_{10} emission factors applied in the LOTOS-EUROS model Table 5.12

Reference	Location	Year	Method	Activity	Operation type	Emission Factor $PM_{2.5}$ ($mg.m^{-2}$)	PM_{10} ($mg.m^{-2}$)
Öttl et al. (2007)	Germany	2004	PM obs., disp. mod.	land prep.	harrowing	29	82
					discing	12	137
					cultivating	6	186
					ploughing (dry)	13	1005
Gaffney *et al.* (2003)	California, US	1995-2003	Upwind-downwind	harvest	corn	21*	191

*on basis of a ratio of emission factors for $PM_{2.5}$ and $PM_{10-2.5}$ of 0.1

Calendar of agricultural activities Table 5.13

Jan	Feb	Mar	Apr	May	Jun	Jul	Aug	Sep	Oct	Nov	Dec
winter		land preparation. & seeding		growing season			harvest			winter preparation	

into account are given in Table 5.12. In our model set-up, we assumed the land preparation activities to consist of harrowing, discing, cultivating and ploughing and we applied the respective emission factor estimates by Öttl *et al.* (2007). For harvesting, we applied the corn harvesting emission factor estimate by Gaffney *et al.* (2003). The emission factor estimates are total emissions per activity. Therefore, the emission from each activity is spread over the period of occurrence.

In comparison to resuspension by traffic, soil dust production by land-management operations is characterised by high emission intensities occurring in relatively short periods of time. In addition, the timing of all operations varies widely and is locally dependent on the growing season, local weather conditions and the crops grown. We followed the seasonal calendar in agricultural practices shown in Table 5-13. During winter, the activities on the fields were not present and neglected. Land preparation emissions are characteristically emitted in spring and late autumn, whereas those from harvesting are emitted only between August and October. We neglected the emissions from during the growing season, because agricultural land-management activities are minimal at that time. The land-management activities and associated emission factors in Table 5-12 are assigned to this calendar. We distinguished two different periods for land-preparation activities. During the land preparation for the seeding periods we assumed harrowing, discing, and ploughing activities, whereas during the winter preparation we considered only cultivation activity. The apportionment of the emission from each activity to an emission flux per hour, covered by the factor $C_{operation}$, is the inverse of the total period of activity on the calendar. Hence, we assumed that all fields would be managed distributed evenly over the period, which is an obvious simplification. To avoid strong night-time emissions, we only considered the hours between 07.00 and 17.00, using an hourly emission profile which was set to 0 for the hours outside this time frame and up to 2.5 for the daytime hours during the week. For the weekends, a slightly different daily profile was applied, with a smaller intensity than that applied on a weekday.

The emission estimates were based on observations of the total in PM emissions. Aside from the mineral source contribution, all emission factor estimates contained a significant but unknown contribution of organic matter. The fraction of organic matter was expected to depend largely on the type of operation and soil properties. For instance, the organic matter fraction was expected to be large in the case of harvesting activities, in contrast to that of land preparation activities.

The emission factors for ploughing dry and wet soil (Öttl *et al.*, 2007) indicate that there is a large dependency on the state of the soil. However, there was no information available on the soil conditions for any of the other activities, therefore, we were not able to separate between soil conditions and neglected this in our model description. The only exception was that we neglected emissions during rain events.

We did not take regional dependency into account in our model set-up. Moreover, we assumed the calendar of agricultural activity to have been constant for the entire LOTOS-EUROS model domain, and defined it as shown in Table 5-13.

5.5 Results

5.5.1 Modelled distribution

The modelled annual average concentrations of mineral PM_{10} was about 2 $\mu g.m^{-3}$ across Europe (Figure 5.9). Concentrations exceeding 3 $\mu g.m^{-3}$ were modelled in densely populated areas and in relatively dry and arid environments. Lower values of 0.2 $\mu g.m^{-3}$ were simulated for large forest, where no sources were located.

The modelled annual average distribution of wind-blown dust showed that the dust from wind erosion of European soils generally contributed less than 0.1 $\mu g.m^{-3}$. The importance of this source with respect to the other modelled mineral dust sources, although uncertain, appeared to be low. It was lower than the annual contribution from traffic, which in general was less than 0.3 $\mu g.m^{-3}$ in rural areas, but varied up to 5 $\mu g.m^{-3}$, or more, in densely populated regions. Furthermore, the model results indicated that both contributions seemed to be smaller than the calculated estimate of the annual contribution from agricultural management activity, with an annual

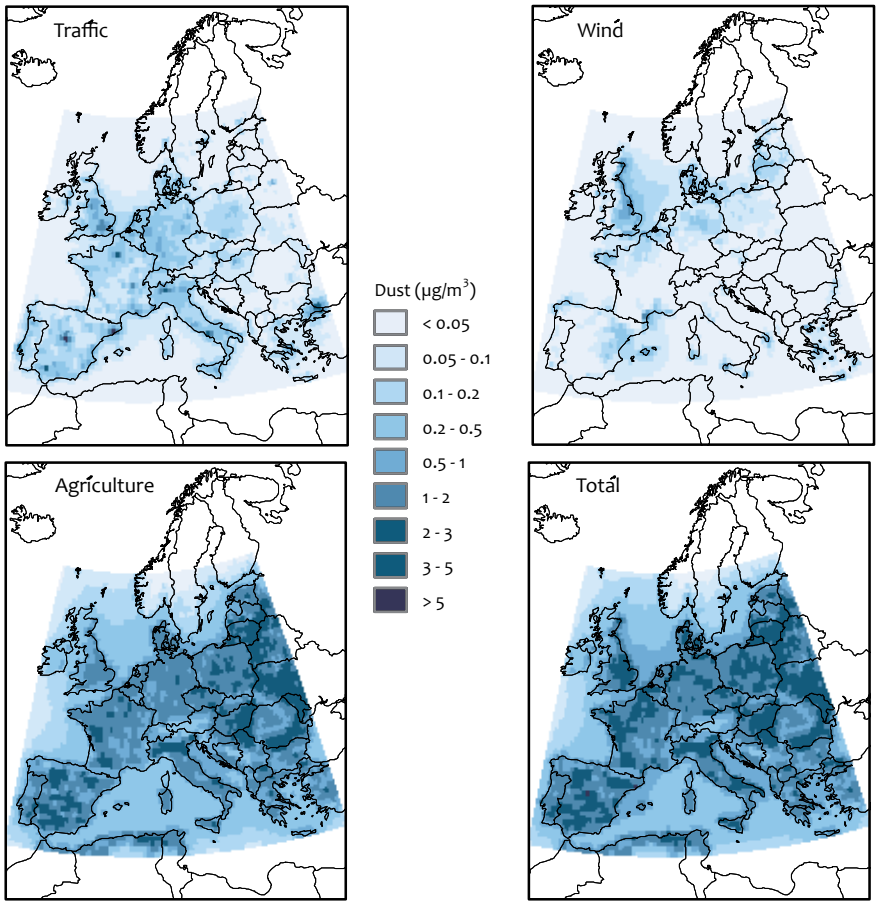

Modelled mineral dust contributions to PM_{10} as a result of resuspension from traffic (top left), from wind (top right), and from agriculture (bottom left), and the total modelled resuspension of mineral dust contributing to PM10 (bottom right), for 2005.

average slightly lower than 2 µg.m^{-3} but with contributions exceeding 3 µg.m^{-3} for the arable areas. This is in line with the current understanding that dust from arable land management is a, by far, larger source of dust than that from wind erosion.

The wind-blown dust contribution was largest in areas with high annual average wind speeds, and it reflected the areas with relatively high amounts of soil dust of the type occurring in resuspension. The distribution due to traffic resuspension was largest over densely populated areas. In main cities, such as London, Paris, Madrid and Milan, this leds to high peaks in resuspended soil dust compared to nearby rural areas (Figure 5.9). It is only around cities that the contribution from traffic resuspension exceeds that from agriculture. The distribution by agricultural land-management activities of ambient mineral matter is very different from that of wind-blown dust or from traffic. Compared to traffic resuspension, the distribution by agricultural land-management acitivities showed a more regional dependence. Within the agricultural areas, the highest concentrations were found in regions with low amounts of precipitation.

The contribution of desert dust is only important in the Mediterranean at latitudes below 44°N (Figure 5.10). In Spain, southern Italy, Greece and Turkey, the annual average inflow of desert dust contributed an additional 0.2-1 µg.m^{-3} and, in some locations, up to 2 µg.m^{-3} to the total ambient mineral dust concentration. On occasion, significant amounts of African desert dust reached higher latitudes. In most of these cases, the desert-dust enriched air masses were first being transported over part of the Atlantic Ocean before reaching central Europe. Sporadically, there was inflow of desert enriched air mass at the south-eastern boundary of the model domain, with dust originating from south-eastern and Asian desert areas, rather than from the Sahara. In the Netherlands, in 2005, the level of desert dust only once reached a concentration of 2.5 µg.m^{-3} (see Annex E).

5.5.2 Seasonal variation

Figures 5.11 to 5.14 depict the seasonal variation of the different sources of resuspension of mineral dust at selected locations in Europe, which are listed in Table 5-14. These locations were chosen for several reasons. Firstly, for these sites some data sets of continuous observations were available, which could be used as indicators of ambient mineral matter

Modelled mineral dust contribution to PM_{10} of desert sources

Figure 5.10

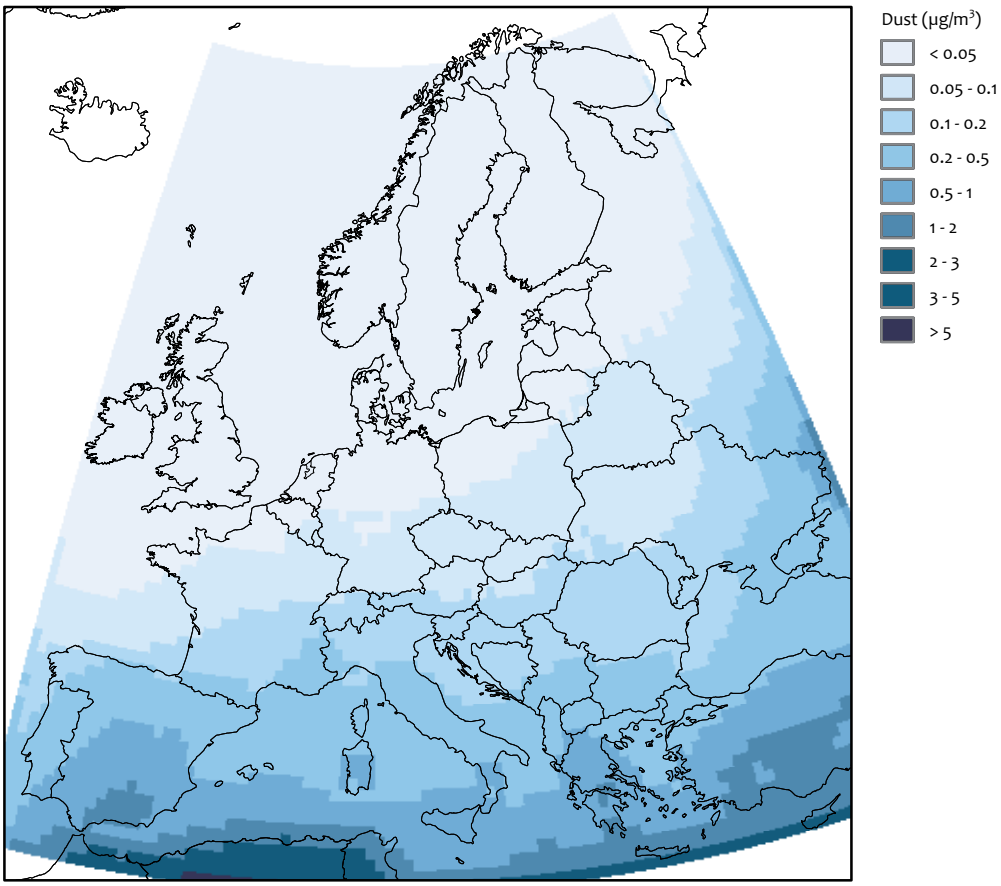

Modelled mineral dust contribution to PM_{10} from desert sources outside the LOTOS-EUROS model domain (input at domain boundaries from TM5 transport model).

Annual average mineral dust contribution to PM10 for selected sites within Europe

Table 5.14

				Annual average mineral dust contribution to PM_{10}					
				Model				Observations[1]	
Site name	Longitude	Latitude	Site type	Traffic	Wind	Agriculture	Total	Ca	Total
	(deg E)	(deg N)		(µg.m^{-3})	(µg.m^{-3})	(µg.m^{-3})	(µg.m^{-3})	(µg.m^{-3})	(µg.m^{-3})
Kollumerwaard (NL)	6.28	53.33	rural	0.27	0.06	0.86	1.19	0.09	0.71[2]
Illmitz (A)	16.36	48.23	rural	0.11	0.07	1.64	1.82	0.19	1.39[2]
Langenbrügge (D)	10.76	52.8	rural	0.19	0.13	1.47	1.79	0.14	1.07[2]
Melpitz (D)	12.93	52.53	rural	0.23	0.09	1.28	1.60	0.14	1.03[2]
Montseny (ES)	2.38	41.78	rural	2.55	0.07	1.02	3.64	0.38	3.57
Onda (ES)	-0.25	39.96	suburban-industrial	0.14	0.16	0.93	1.23	1.22	9.46
Birkenes (N)	8.25	58.38	rural	0.03	0.01	0.12	0.17	0.06	0.46[2]
Iskrba (SI)	14.57	45.57	rural	0.04	0.00	0.38	0.43	0.13	0.97[2]

[1]the observations are taken from the EMEP database (http://emep.int), with the exception of the observations in Montseny and Onda in Spain, which were obtained from Querol *et al.*(personal comm.) and correspond to the observations discussed in Querol *et al.*(2007).
[2]total PM_{10} concentration inferred from the elemental Ca concentration by assuming a ratio of 7.5 between the Ca and the mineral dust concentration for PM_{10}.

Annual average mineral dust contribution to PM_{10} for selected sites within Europe, as calculated with the LOTOS-EUROS model and found on the basis of observations

to verify the model results. Secondly, these locations are regional backgroud sites for which the LOTOS-EUROS model is representative.

Traffic resuspended mineral dust **Figure 5.11**

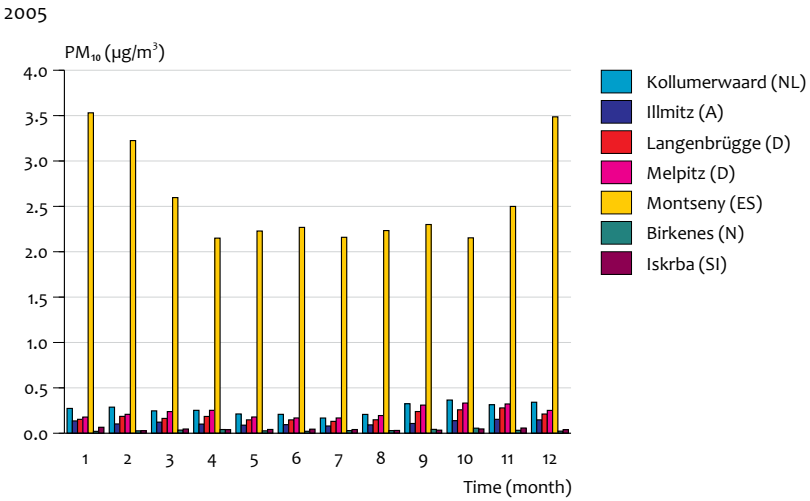

Seasonal variation, for 2005, of the modelled contribution from traffic resuspension to mineral PM_{10} in Kollumerwaard (The Netherlands), Illmitz (Austria), Langenbrügge (Germany), Melpitz (Germany), Montseny (Spain), Birkenes (Norway), and Iskrba (Slovenia).

Windblown mineral dust **Figure 5.12**

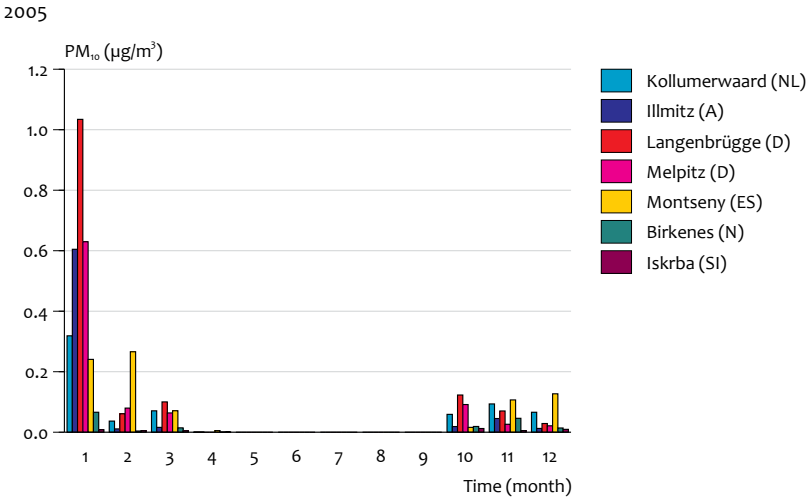

Seasonal variation, for 2005, of the modelled contribution from resuspension by wind to mineral PM_{10} in Kollumerwaard (The Netherlands), Illmitz (Austria), Langenbrügge (Germany), Melpitz (Germany), Montseny (Spain), Birkenes (Norway), and Iskrba (Slovenia).

The seasonal variation in the resuspension emissions and the resulting ambient concentrations were specific to each source. The concentration of resuspended material from traffic was relatively constant throughout the year, with <0.4 µg.m^{-3} at rural locations and between 2.5 and 3.5 µg.m^{-3} at Montseny in Spain. It should be mentioned that, despite Montseny being classified as a rural observation site, it is located close to Barcelona. Due to the coarse model grid resolution, the modelled, atmospheric mineral matter concentration was strongly influenced by the traffic emissions in Barcelona, which is expected not to be the case in reality. The seasonal variation in the traffic induced mineral dust concentration was mainly due to a variation in meteorological parameters (e.g. precipitation, boundary layer height, horizontal advection). The effect of the variation in mixing layer height seemed to be most important. In summer, the dust concentration was lower than in winter when the mixing layer was relatively shallow, despite the fact that in autumn and early winter increased precipitation limited the dust production and increased the removal of ambient particles. The seasonal dependence of traffic induced resuspension was less pronounced than that induced by wind or agricultural activities, which also showed a different timing of enhanced dust concentration.

Agricultural dust

Figure 5.13

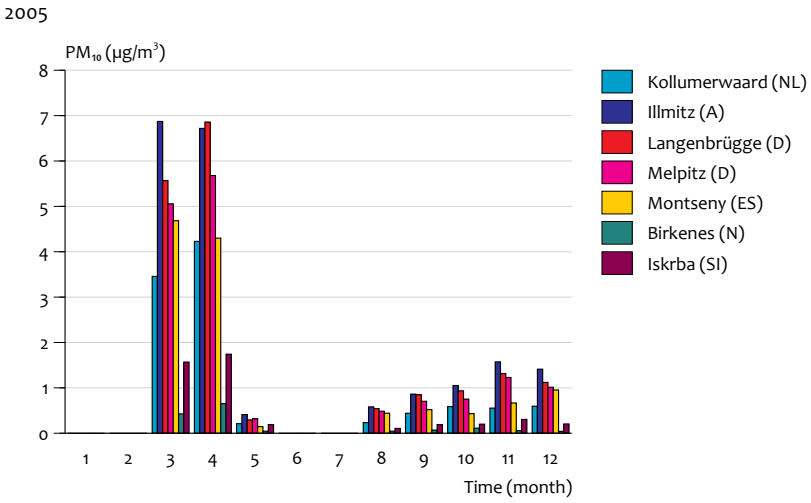

Seasonal variation, for 2005, of the modelled contribution from resuspension by agricultural activity to mineral PM_{10} in Kollumerwaard (The Netherlands), Illmitz (Austria), Langenbrügge (Germany), Melpitz (Germany), Montseny (Spain), Birkenes (Norway), and Iskrba (Slovenia).

Total modelled mineral dust

Figure 5.14

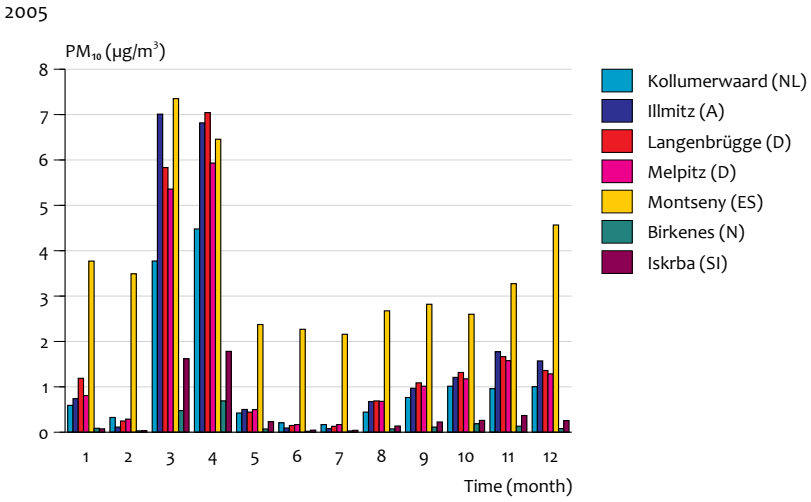

Seasonal variation, for 2005, of the total modelled contribution from resuspension sources to mineral PM_{10} in Kollumerwaard (The Netherlands), Illmitz (Austria), Langenbrügge (Germany), Melpitz (Germany), Montseny (Spain), Birkenes (Norway) , and Iskrba (Slovenia).

The modelled concentration of soil dust resuspension by wind (Figure 5.12) revealed the timing of high average wind speeds (for 2005 in January) which caused an increase in the annual average dust production by a factor of 10 or more. Also, the seasonal variation revealed the timing of the growing season when most of the arable land is covered by vegetation and resuspension was neglected in our model set-up. Hence, the modelled ambient soil dust concentrations dropped to zero in spring and remain there throughout the summer.

For land-management induced resuspension, the timing of the emissions and associated periods with high concentrations was linked to the activity calendar (Table 5-13) applied for the agricultural emissions. Concentrations peaked in the spring months, to values of up to 7 $\mu g.m^{-3}$ in the German and Austrian locations (see Figure 5.13). Significant concentrations, varying between 0.5-1.5 $\mu g.m^{-3}$ at the listed locations, were modelled for autumn and early winter The concentrations drop to zero during the growing season and in the middle of winter, because then there is no land- management activity.

Mineral dust Montseny 2005 **Figure 5.15**

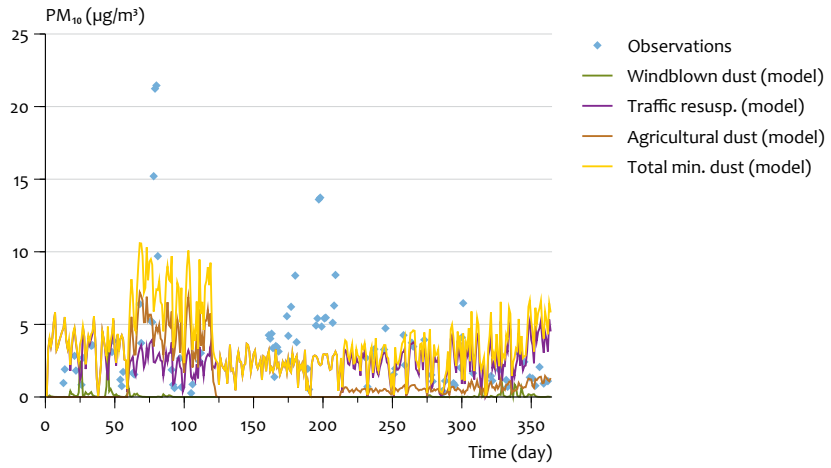

Time series of the observed and modelled contribution of mineral matter to PM_{10} in Montseny (Spain) in 2005.

Desert dust Montseny 2005 **Figure 5.16**

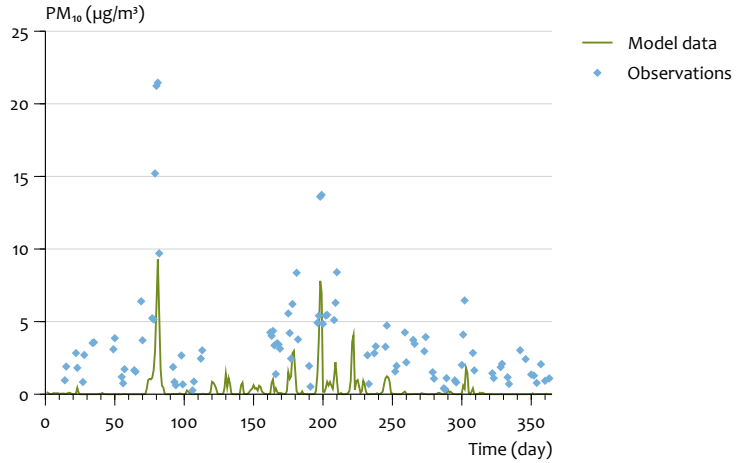

Time series of the observed contribution of mineral matter to PM_{10} (blue) and the desert dust as modelled (red) by the LOTOS-EUROS model with TM5 boundary conditions in Montseny (Spain) in 2005.

5.6 Verification

The model calculations were compared with observed mineral PM_{10} concentrations. Unfortunately, there is only a small number of data sets available of observed ambient mineral PM_{10}, which limited the possibilities for comparison. We used mineral dust concentrations as reported for Spain. We also compared the model calculations with observations of one of the tracer compounds, calcium (Ca), which is an indicator for mineral dust. As a tracer, Elemental Ca may not be as strongly correlated with mineral dust as aluminium (Al) or silicium (Si), but the number of time series of observations available for the year 2005 is relatively large. For this reason, we chose to compare our model results with the observations for Ca., The observed time series of seven different sites were taken into account for the verification discussed in this report.

One of the existing data sets of time series available for mineral dust, includes data observed at a few locations within Spain (Querol *et al.*, 2007). Below, the comparison between observed mineral dust and the amount calculated with the LOTOS-EUROS model is shown for the location of the rural site Montseny, which is close to Barcelona (Figures 5.15, 5.16). The reported mineral dust concentrations were calculated by the authors, based on the elemental composition of PM_{10}.

In Montseny, the model concentrations were of the same order of magnitude as the observed mineral dust concentration. The annual average concentrations for both the model and the observations was ~3.6 µg.m^{-3} (see Table 5-14). Furthermore, the values and the timing of the variation in the modelled concentration were in agreement with the observed concentration for the months of February and September to November. From December to January, the modelled concentration was overestimated by the model, which

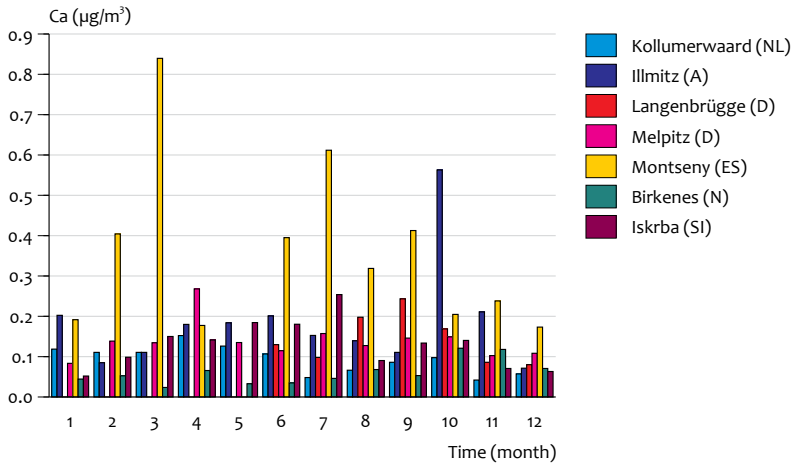

Seasonal variation of observed ambient Ca concentration (PM_{10}) in 2005 at Kollumerwaard (The Netherlands), Illmitz (Austria), Langenbrügge (Germany), Melpitz (Germany), Montseny (Spain), Birkenes (Norway) and Iskrba (Slovenia).

was mainly due to an overestimation of the resuspension by traffic (see Figure 5.15). However, this may be explained by the fact that Montseny is very close to Barcelona and the relatively coarse model grid cell resolution (approximately 30x30 km at this latitude). The concentrations modelled for Montseny might have been too heavily influenced by the (traffic) resuspension emissions from Barcelona. In addition, in March and towards the end of June, as well as at the start of July, very high concentrations were observed which were not captured by the model calculations. These so-called dust events corresponded to an inflow of desert dust originating from the Sahara, the timing of which was evidenced by the model calculations, solely carried out with the boundary input of mineral dust from the TM5 model (Figure 5.16). Furthermore, the contribution of agricultural emissions in the spring was likely to be overestimated in the model calculations, since such a strong increase was not observed in the measurements.

The abovementioned measurement data were based on mineral dust concentrations derived from a full elemental composition of PM_{10}. Below, we concentrate on information derived from calcium data. In Figure 5.17, the seasonal variation of the observed elemental Ca concentration is shown. The time correlation between the modelled mineral PM_{10} concentration and the observed Ca concentration time series was less than 0.2, which indicated that the modelled time dependent variation was not in close agreement with the observational data. This is partly explained by the fact that Ca is a relatively poor indicator of mineral dust. Both model and observations seemed to show a comparable seasonal dependency with enhanced spring, late summer and autumn concentrations. However, the seasonal dependency of the modelled mineral dust concentration was much stronger than that of the Ca observations and, especially, the modelled high spring peak concentrations were not observed in reality. Since the used model calculations were dominated by agricultural land management emissions, this clearly implies that the agricultural land management emission factors used for the spring season activities were too high. Considering the fact that the spring emissions were predominately from ploughing, the applied emission factor for ploughing could be lower. However, a more thorough study of the timing of agricultural emission from the different land management operations and associated emissions would be required to improve the present model approach.

Figure 5.18 shows the time series of the modelled mineral dust concentration at Kollumerwaard (the Netherlands) versus the mineral dust concentration inferred from Ca observations applying a ratio of 7.5 for the relation between ambient concentrations of mineral dust and elemental Ca. This number was based on observations of both concentrations at De Zilk (the Netherlands) for 1998 and 1999. We assumed the annual average ratio between ambient Ca and mineral PM concentrations at Kollumerwaard to be the same as at De Zilk. The mineral PM_{10} time series, obtained from applying this multiplication factor to the Ca observations, again showed an overestimation by the model. This could be mainly attributed to the modelled contribution from agricultural land management, that is, the modelled agricultural dust related spring peak was not seen in the observations and, although with a smaller overestimation, the modelled contrations in autumn and early winter were lower than those observed.

For 2005, the ratio between the annual average mineral PM_{10} concentration and that of Ca was 9.4 in Montseny and 7.8 in Onda, as is shown in Table 5-14. These ratios are close to the ratio that was suggested for De Zilk, mentioned above. For simplicity, to retrieve a first-order estimate for the magnitude of mineral PM_{10}, we assumed a 7.5 ratio at all selected locations for which there are no observations of mineral PM_{10} concentrations. The obtained annual average mineral PM_{10} con-

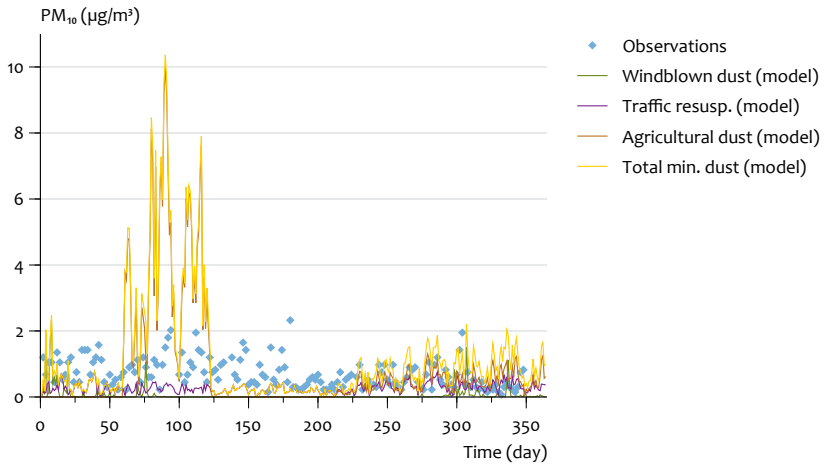

*Time series of the mineral dust contribution to PM_{10} in 2005, inferred from Ca observations by assuming a PM_{10}_CM=7.5*PM_{10}_Ca at Kollumerwaard (The Netherlands).*

centrations show us that the agreement between model and observations varies per location. The model overestimated the mineral dust concentration at the locations in agricultural areas (e.g. in Illmitz, Langenbrügge and Kollumerwaard), but underestimated the mineral dust concentration by a factor of 2 at sites which were under less influence of agriculture, such as in Birkenes and Iskrba. The same would apply for stations in agricultural areas if the ploughing emission factor would be 10 times lower.

5.7 Discussion

This report describes the model set-up and mainly discusses the technical details of the chosen approaches for the different source contributions to ambient PM. Thorough verification of these model approaches by comparing them with observations would require the availability of a large and continuous set of observations. However, such a data set of extensive observations is unfortunately not available. From the BOP programme, data are expected soon to become available for several locations within the Netherlands, for the period between 1 August 2007 and 1 August 2008. A small additional data set of available observations at locations throughout Europe is presently being constituted. Hence, in this report robust conclusions could only be drawn based on a limited comparison with observational data. Note that the BOP data may allow addressing mineral dust in the $PM_{2.5}$ fraction, but this has not been focused on in our report.

The modelled contributions to mineral PM_{10} from the different resuspension sources are a crude approximation of reality. In general, the emission factors were based on a limited data set, not representative of the full range of European conditions. For this reason, the range of uncertainty associated with the modelled concentrations is relatively large.

The modelled concentrations from traffic resuspension are expected to be closest to reality, since the introduced emission factors were based on relatively well-known emission factor estimates, compared to those from agriculturally induced resuspension. Furthermore, the implemented parameterisation is simple and coupled to a relatively accurate map of vehicle driven kilometres. Part of the uncertainty in the modelled concentrations is determined by the uncertainty in the emission factor estimates and by the implemented regional correction factor. We feel that the overall uncertainty in the modelled traffic resuspension can be multiplied by about a factor of 2 to 3. The uncertainty could very well be dominated by the linear relation between soil moisture and emission strength assumed in this study.

The uncertainties in the modelled calculations of the contribution of ambient mineral dust, generated by wind induced abrasion, is fairly large because of the uncertainty in the soil type dependent dust loading factor K and the uncertainty in the erodibility factor α. The dust loading factor K ranges between 0.01 and 1, whereas α, depending on the soil type, ranges between 10^{-4} and 10^{-6} m^{-1}. Given the range in the parameters and the large impact of slightly different numbers, the uncertainty is difficult to quantify correctly. The report's calculated wind-blown dust contribution to mineral PM_{10} is (very) small, compared to that from traffic resuspension or agricultural activity. The contribution could be larger in reality, and could be detectable because of the strong episodic character of these emissions. Hence, for this purpose, a well-characterised dust storm would be needed within the European domain.

Compared with resuspension from traffic or wind, the modelled mineral dust induced by agricultural activities is the most uncertain. There are three studies on these emission factors for European (read German) conditions. These studies are by no means complete and do not contain important explanatory variables, such as soil humidity, equipment, etc. Thus, the uncertainty in the selected emission factors is large. The emission factors for each activity are determined in terms of $kg.ha^{-1}$ for the application of a single activity. Hence, the

translation required to calculated the contribution of the agriculturally as a function of time, includes a proper knowledge of timing and duration of each type of operation, which is not available. Thus, a simple calendar of agricultural land management operations was applied. A more thorough study of the observations should point out whether such a simple approach is possible for the calculation of the agricultural contribution to mineral dust resuspension.

Our model set-up for the contribution from agricultural land management operations was rather an upper limit for several reasons. The available estimates were estimates of total PM. Consequently, they included an unknown but significant part of organic material. In addition, these estimates were machinery bound primary emissions measured close to their point of origin. Therefore, it is questionable whether they would be representative of the larger and regional scale (Funk *et al.*, 2007). We assumed that the effect on a regional scale would be less strong than these estimates indicate. Currently, a range of measures are being applied to reduce soil erosion. The absolute effect of such measures, although unknown, may be large. For example, only allowing ploughing to take place under relatively humid conditions, would certainly affect the mineral dust production per unit area. The currently applied agricultural emission figures are a clear overestimation of reality. The large overestimation for the spring could mainly be attributed to emissions from ploughing operations. For this land management operation, we applied an emission factor estimate which was obtained from ploughing operations under dry conditions which would be nearly 10 times higher than the estimate for under moist soil conditions. To produce more realistic results from future calculations, we suggest that an intermediate valued emission factor would be used as a first-order estimate for ploughing emissions under all weather conditions.

An additional uncertainty is associated with the dry deposition scheme for coarse particles. The sea salt calculations, as described in Chapter 5 with the dry deposition scheme as proposed by Zhang *et al.* (2001), yields a 50% higher coarse particle concentration than the base case scheme applied here. Although the uncertainty associated with the dry deposition velocity may be smaller than that associated with the source strengths, it should be addressed for mineral dust as well.

5.8 Conclusions

We have implemented source descriptions of wind-blown dust, traffic resuspension and agricultural land management activities, which is novel in Europe.

The emissions from agricultural land management contribute most to the total modelled mineral dust concentration, followed by those from traffic resuspension and wind erosion.

The limited set of observations available hampers a thorough evaluation of the model performance.

The verification of the modelled seasonal variation in the mineral PM_{10} concentration indicates that the model overestimates the impact of agricultural activities. This is caused by the high emission factors for ploughing.

The comparison between modelled concentrations and these observations (after accounting for the overestimation in agricultural mineral dust production) indicates that the total mineral dust contribution is being underestimated in our model approaches. This underestimation is thought to be mostly caused by the large uncertainties in the present the source descriptions and the fact that not all mineral dust sources have been taken into account. Construction activities, material handling, other diffusive sources and part of the primary PM_{10} production may be of significant importance to the total mineral PM_{10}.

We now have a tool for investigating the contributions from various sources. We expect to gain further understanding, on basis of the specific timing and spatial distribution of each source category. The temporal and spatial patterns of observations and model predictions will give important clues to whether the balance between sources and the timing of their emissions is correct in our appraoch. Within the uncertainties surrounding this exploratory approach, the balance in source contributions can be optimised to fit the observations, in terms of absolute annual concentrations as well as in the temporal patterns over the year. The result is a constraint on the total source strength of crustal material and an indicative ranking of the importance of contributing sources, for various European areas.

6 Carbonaceous aerosol

Chemistry transport models underestimate the concentrations of carbonaceous material. Previous studies have concluded that the emissions of EC and OC are probably underestimated (Schaap et al., 2004 and others). In addition to primary EC and OC, secondary organic aerosol may contribute significantly to the observed OC levels. The formation of secondary organic aerosol (SOA) is not represented in LOTOS-EUROS and may also partly explain the inability of the model to close the gap between modelled and observed OC levels. These issues call for a representation of VOCs and the SOA formation pathways in current modelling tools.

VOCs derive from anthropogenic sources, as well as biogenic sources. Whereas the biogenic emissions dominate those of anthropogenic origin on a global scale, the anthropogenic emissions in Europe outweigh those of biogenic origin. However, the mayor anthropogenic emissions are concentrated in several areas/countries, and in large areas within Europe the biogenic emissions dominate over anthropogenic emissions. Moreover, even in the most polluted areas within Europe, the biogenic sources may periodically exceed those of anthropogenic emissions because of their strong sensitivity to meteorological conditions. Furthermore, current knowledge indicates that biogenic VOCs are more efficient at forming secondary organic aerosol than those of anthropogenic origin. Hence, state-of-the-art biogenic emission parameterisations need to be included in a model for assessing their influence on SOA and O3 formation.

During this study, we have expanded the model formulation for biogenic emissions and we have incorporated a chemical formation scheme for SOA. As the formation of SOA is very uncertain and subject to a large scientific effort, we have chosen to implement a scheme from Carnegie Mellon University (Pittsburg; Pun *et al.*, 2003) that appears to be most promising to use in the ongoing updates of model formulations. Because of the large uncertainties, we did not improve on this formulation but tested the impact of this scheme for northwestern Europe.

Below, we document the model formulation now used in LOTOS-EUROS. First, the land-use database is described. Next, the emission routine for the biogenic precursors and the expansion of the chemical scheme are documented. Finally, the aerosol chemistry is described. In Section 2, the first results with this model formulation are presented and briefly discussed.

6.1 Model development

6.1.1 Land-use data

The starting point in this study was the official Corine/Phare Land Cover Data from the EEA, which was completed for the full European domain by Smiatek (FI-Garmisch Partenkirchen) using (mainly) the Pelinda database. The database has a resolution of 0.0166x0.0166 degrees which is aggregated to the required resolution during the start-up of a model simulation. The land-use database has the following categories:

1 Urban areas
2 Agriculture
3 Grassland
4 Deciduous forest
5 Coniferous forest
6 Mixed forest
7 Water
8 Marsh or wetland
9 Sand, bare rocks
10 Tundra
11 Permanent ice
12 Tropical forest
13 Woodland scrub

In Figure 6.1, the land-use data are shown for the Netherlands and for Europe as a whole.

The Corine/Smiatek database has been enhanced by using the tree species map for Europe. made by Koeble and Seufert (2001), who also used Corine/Smiatek as a basis. This database contains 115 tree species, on a grid of 1 x 1 km^2, with coverage per grid. In parts of the LOTOS-EUROS modelling domain, especially for Russia, the Koeble tree map provides no information. In coupling the Corine/Smiatek land-use database with the database on tree species, the land-use database was leading, meaning that tree species were only appointed to forest areas. In case no tree species information was available for a forest area, the three Corine forest categories were maintained. So, the full tree database contains 115 + 3 categories. The combined database has a resolution of 0.0166x0.0166 degrees which is aggregated to the required resolution during the start-up of a model simulation.

6.1.2 Isoprene and monoterpene emissions

In LOTOS-EUROS we need both the isoprene as the monoterpene emissions.

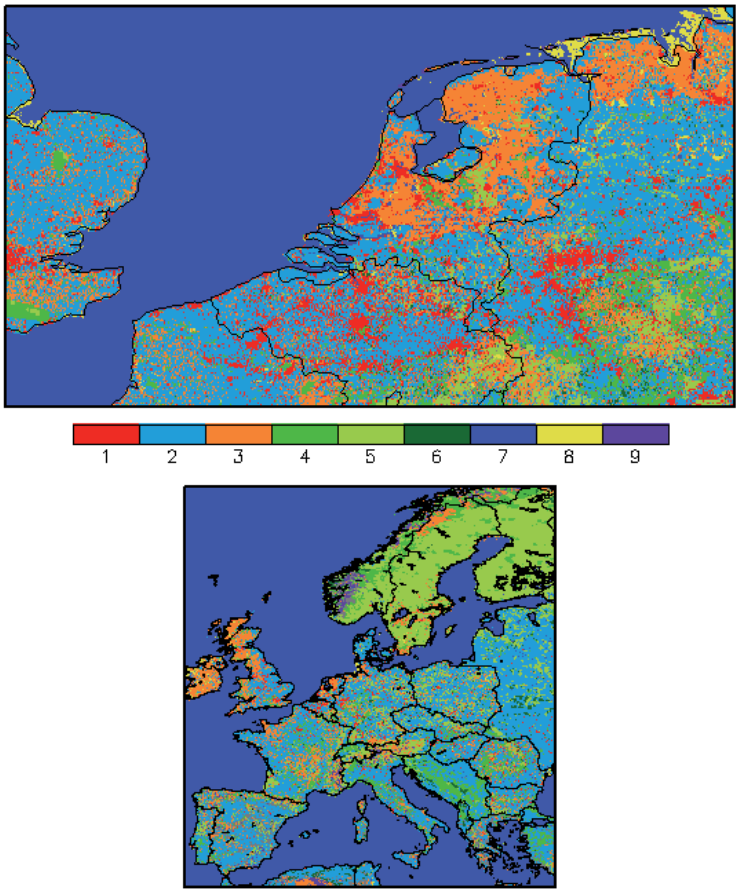

High resolution land-use database for Europe. Categories are listed in the main text.

Isoprene
All studies on the emission of isoprene and monoterpenes show clear temperature dependence. In addition, isoprene emissions have been shown to be triggered by light, as a result of the link between isoprene emission and synthesis from photosynthetic products. As no large isoprene pool exists, synthesis and, hence, emission will cease within minutes under dark conditions (e.g. Guenther *et al.*, 1991).

For a mathematical description of the temperature and light dependence of the isoprene emissions, empirically designed algorithms are used. One of the commonest algorithms is the formula

*E =F A * D * ES * γ(iso)*

proposed by Guenther *et al.* (1991, 1993), where *E* is the actual emission, A is the area (m²), D is the biomass density (g/m²) and *ES (g/g)* is the standard emission factor (at a standard temperature *Ts* of 30 °C and a standard 1000 *μ*mol m⁻² s⁻¹ photosynthetically active radiation (PAR)). *γ(iso) is a* function of temperature and light.

$$\gamma(iso) = \frac{\alpha C_{L1} Q}{\sqrt{1+\alpha^2 Q^2}} * \frac{\exp\frac{C_{T1}(T-T_s)}{RT_sT}}{1+\exp\frac{C_{T2}(T-T_M)}{RT_sT}}$$

With:
Q =F PAR [μmol(photons)/(m² s)]
T =F ambient temperature [K]
T_s =F leaf temperature at standard [K] (=F 303K)
R =F 8.314 J*K^{-1}*mol^{-1}
α =F 0.0027
C_{L1} =F 1.066
C_{T1} =F 95000 J*mol^{-1}
C_{T2} =F 230000 J*mol^{-1}
T_m =F 314K
C_{T3} =F 0.961

C_{T2}, T_m, α and C_{L1} are empirically defined parameters, derived from measurements on four isoprene-emitting temperate plant species.

Monoterpenes
Monoterpene emissions are generally regarded as light-independent, because they are compounds stored after synthesis in special organs, such as resin ducts or glands, exhibiting quite large storage pools compared to the emission rates (Lerdau *et al.*, 1994; 1997). Hence, their emission, which is temperature-dependent and related to the vapour pressure and to the transport resistance along the diffusion path, is regarded to be a volatilisation out of storage organs (Guenther *et al.*, 1991). The emission response to tempera-

Isoprene emissions over Europe for 2005

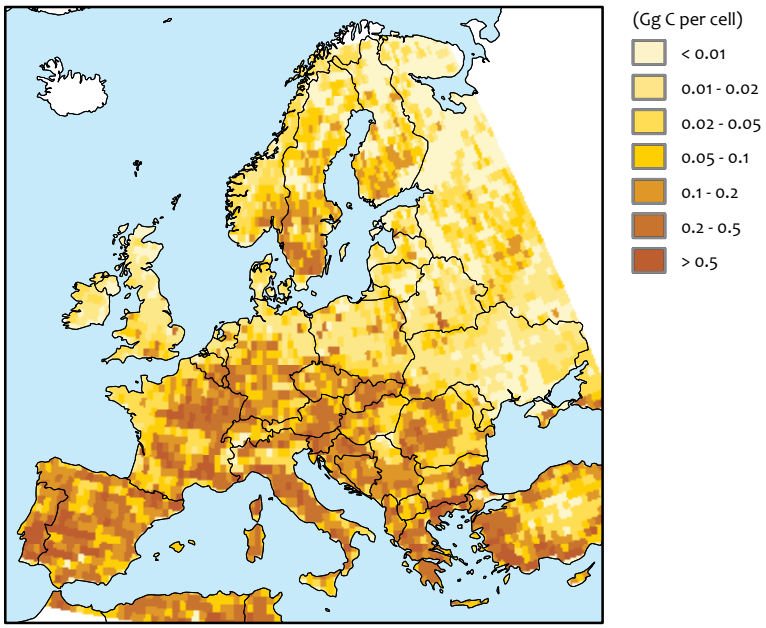

Monoterpene emissions over Europe for 2005

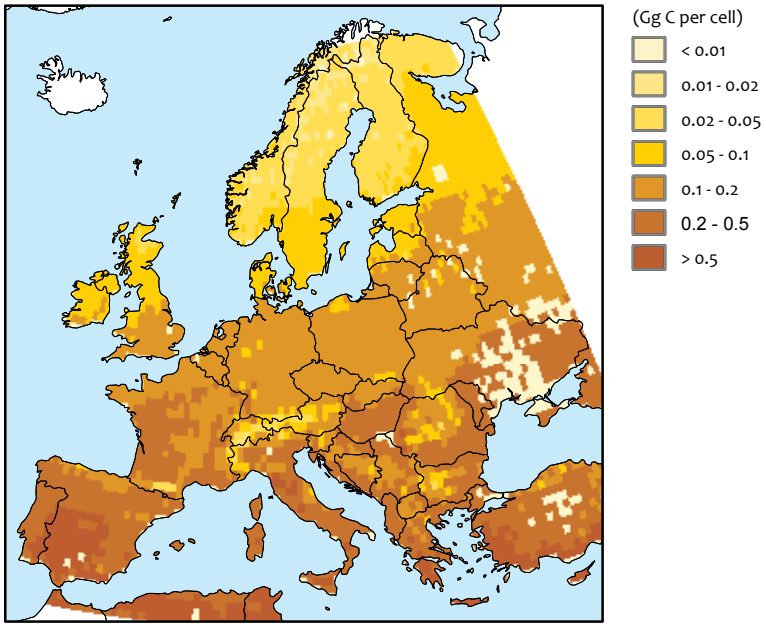

Distribution of isoprene (left) and monoterpene (right) emissions (Gg C per cell) over Europe, for 2005.

ture shows an exponential increase with temperature and is usually described using the formula by Tingey *et al.* (1980):

$$E = F\ A*D*ES * \exp[\beta*(T-T_s)]$$

where E is the emission at temperature T , A is the area (m^2), D is the biomass density (g/m^2), β is the slope $d\ln E/dT$, and ES is the emission at a standard temperature, T_s. Values for β found in the literature range between 0.057 and 0.144 K^{-1}. As a generally accepted mean value, 0.09 K^{-1} is used (Fehsenfeld *et al.*, 1992; Guenther *et al.*, 1993).

Some species do not store monoterpenes. For these species the temporal evolution of the emissions is modelled following the abovementioned formulas for isoprene.

All land use and tree species specific emission parameters are listed in Annex C.

Annual emission estimates

The annual emission distribution for both isoprene and monoterpenes is shown in Figure 6.2. The annual emission total for isoprene is 1.07 Tg a^{-1}. The isoprene emissions show a general

decline from south to north, due to the gradient in radiation and temperature favouring emissions in southern Europe. On top of this gradient, the forest areas with species that are strong emitters are also visible. For monoterpenes, the emission total is 1.8 Tg a^{-1}. Inspection of the distribution over Europe learns that there is a clear south to north gradient in the emission strength and that the distribution is much smoother than for isoprene. The latter can be explained by the high importance of grassland for monoterpene emissions and the lower variability of the emission potential per species.

6.1.3 Gas phase chemistry

Above, we have expanded the model formulation for the emissions of biogenic emissions. Here, we describe the implementation of the chemical formation scheme for SOA. As the formation of SOA is very uncertain and subject to a large scientific effort, we have chosen to implement a scheme from Carnegie Mellon (CMU) (Pun *et al*., 2003; Strader *et al*., 1999) that appears to be most promising to be used in the ongoing updates of model formulations. Because of the large uncertainties, we did not improve on this formulation but made the scheme ready for operational use.

The CMU module is formulated on the basis of empirical SOA formation data from smog chambers. In Strader *et al*. (*1999*), SOA formation from alkanes, alkenes, aromatics, secondary aromatic products (such as phenol, cresol, and nitrophenol) and terpenes, is represented. Since CBM-IV does not explicitly treat alkane and alkene species, it was necessary to map individual species to the CBM-IV functional groups. We followed the approach by Pun *et al*. (2003). The formation of condensable compounds from alkanes and alkenes was represented in the reactions of paraffins (PAR) with OH and olefins (OLE) with OH, O_3, and O, respectively. In these reactions, the yields of the condensables take into account the fraction of PAR and OLE that represent higher alkanes and alkenes (since short-chained alkanes and alkenes do not form SOA), based on the composition of ambient VOC in the Nashville area and the SOA yields of higher alkanes and alkenes. Condensable products were included in the toluene (TOL), xylene (XYL), and cresol (CRES) reactions. New reactions include those of benzaldehyde (BZA) and radicals derived from it and the reactions of phenol (PHEN) and nitrophenol (NPHN). Note that radicals and O_3 are regenerated in these new reactions, so that they do not affect O_3 chemistry. Terpenes are represented by one model class (TERP), which forms two condensable products. In total, six condensable products are used to represent SOA formation. The following SOA reactions to form condensable gases have been implemented in the CBM-IV mechanism:

Production of condensable gases from existing reactions:

PAR + OH ⟶ 0.87 XO2 + 0.13 XO2N + 0.16 HO2 + 0.11 ALD2 + 0.76 ROR + (- 0.11) PAR + 3.4e-4 CG4

OLE + OH ⟶ FORM + ALD2 + XO2 + HO2 + (-1) PAR + 5.6e-4 CG4

OLE + O3 ⟶ 0.5 ALD2 + 0.74 FORM + 0.33 CO + 0.44 HO2 + 0.22 XO2 +0.1 OH + (-1) PAR + 5.6e-4 CG4

OLE + O ⟶ 0.63 ALD2 + 0.38 HO2 + 0.28 XO2 + 0.3 CO + 0.2 FORM + 0.02 XO2N + 0.22 PAR + 0.2 OH + 5.6e-4 CG4

OLE + NO3 ⟶ 0.91 XO2 + 0.02 XO2N + ALD2 + FORM + (-1) PAR + NO2 + 5.6e-4 CG4

TOL + OH ⟶ 0.08 XO2 + 0.36 CRES + 0.44 HO2 + 0.56 TO2 + 0.044 CG1 + 0.092 CG2

XYL + OH ⟶ 0.7 HO2 + 0.5 XO2 + 0.2 CRES + 0.8 MGLY + 1.1 PAR + 0.3 TO2 + 0.030 CG1 + 0.12 CG3 + 0.1 BZA

CRES + OH ⟶ 0.4 CRO + 0.6 XO2 + 0.6 HO2 + 0.3 OPEN + 0.029 CG4

CRES + NO3 ⟶ CRO + HNO3 + 0.029 CG4

CRO + NO2 ⟶ NTR + NPHN

Production of condensable gases from new reactions:

Terpene:

TERP + OH ⟶ OH + 0.075 CG5 + 1.0e-5 CG6

TERP + NO3 ⟶ NO3 + 0.075 CG5 + 1.0e-5 CG6

TERP + O3 ⟶ O3 + 0.075 CG5 + 1.0e-5 CG6

Benzaldehyde:

BZA + OH ⟶ 6.5e-4 CG4 + BZO2 + OH

BZA + NO3 ⟶ 6.5e-4 CG4 + BZO2+ NO3

Peroxybenzyl radical:

BZO2 + NO ⟶ PHO + NO

BZO2 + HO2 ⟶ PHEN + HO2

BZO2 + C2O3 ⟶ PHEN + C2O3

BZO2 + XO2 ⟶ PHEN + XO2

Phenoxy radical:

PHO + HO2 ⟶ PHEN + HO2

PHO ⟶ PHEN

PHO + NO2 ⟶ NPHN + NO2

Phenol:

PHEN + OH ⟶ 0.022 CG4 + OH

PHEN + NO3 ⟶ 0.022 CG4 + NO3

Nitrophenol:

NPHN + NO3 ⟶ 0.049 CG4 + NO3

The production of the 6 condensable gases was calculated in the chemistry routine. The partitioning between the gas and aerosol phase was calculated in the SOA module.

6.1.4 Aerosol chemistry

For the gas/particle partitioning of condensable products, an absorption module was used. A pseudo-ideal solution and Raoult's law were assumed for the organic particulate phase. Therefore, the partition relationships were defined based on the saturation vapour pressure of the condensable substances, and the gas-phase concentration was defined to be equal to the product of the substance mole fraction in the liquid phase and the pure liquid saturation vapour pressure:

$$G_i = \frac{A_i / MW_i}{\sum_{j=1}^{n} A_j / MW_j} c_i^0 = X_i c_i^0$$

where G*i* is the concentration in air (in µg/m³), MW*i* is the molecular weight of substance *i*, *Xi* is the mole fraction of *i* in the liquid phase, and c_i^0 is the pure liquid saturation vapour concentration (in µg/m³) (Table 6.1). Mole fractions were

Characteristics of the condensable gases in the SOA routine Table 6.1

Condensable Gas	Product	MW	c_i^0 (µg/m³)
CG1	SOA1	150	18.9
CG2	SOA2	140	470.0
CG3	SOA3	163	640.0
CG4	SOA4	140	5.7
CG5	SOA5	180	6.6
CG6	SOA6	180	6.6

Modelled monthly mean SOA concentration for January and July Figure 6.3

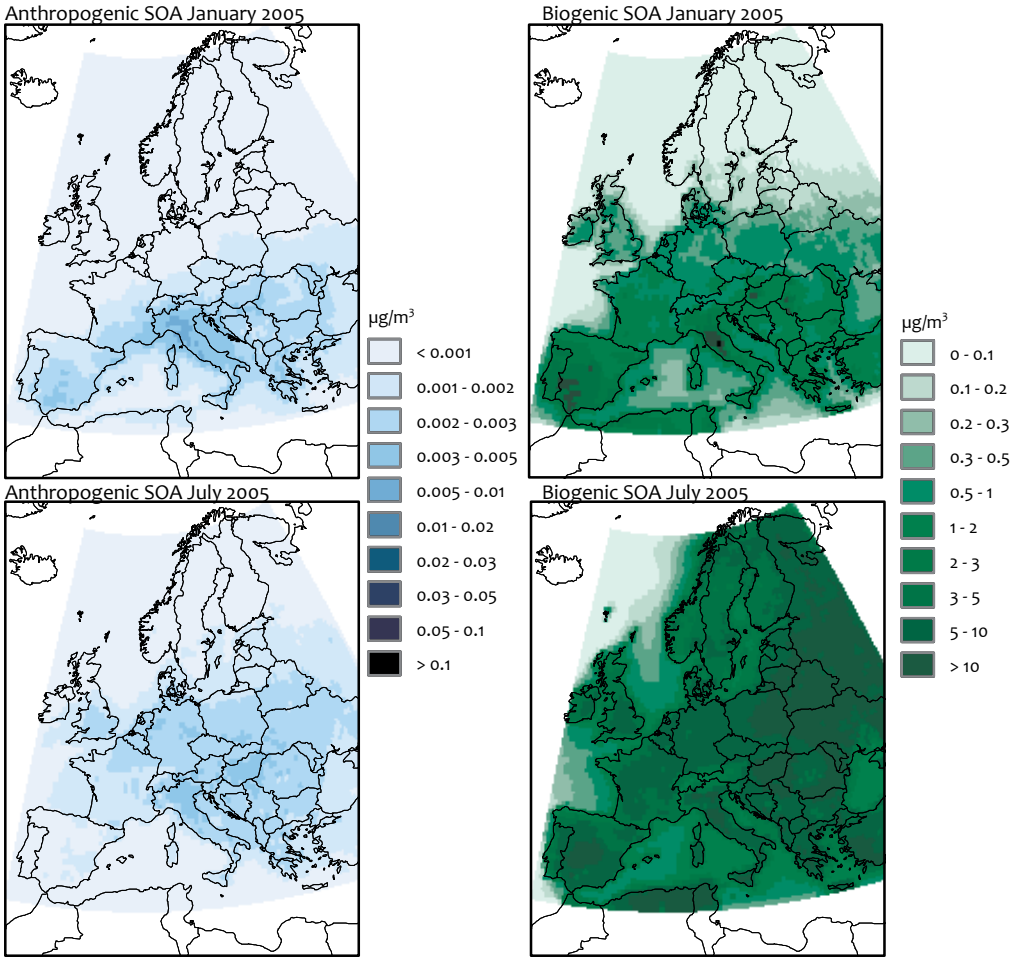

Modelled monthly mean SOA concentrations for January (top) and July (Bottom) Derived from anthropogenic VOC (left) and biogenic VOC (right).

defined based on condensable compounds and primary (non-volatile) OC and SOA dissolved in a solution of primary and secondary compounds. The saturation vapour pressure c_i^0 is a function of temperature according to the Clausius-Clapeyron equation, with ΔHvap =F 70 kJ mol^{-1}. Within the implementation, the denominator was treated as constant for a given time step in the partition calculation. Hence, it was assumed that the total condensed organic material is not significantly altered during a time step.

6.2 Results and discussion

The results of the implementation of the SOA scheme into LOTOS-EUROS are shown in Figure 6.3. The anthropogenic contribution to SOA was modelled to be very small, and negligible, compared to biogenic SOA. Biogenic SOA showed a maximum in summer, when the emissions of terpenes maximised. During July SOA concentrations in the model were 2-5 µg/m³ over most of Europe, with a maximum over Russia and in areas where the terpene emission maximised. In winter, the modelled SOA concentrations were lower and significant amounts were only modelled for southern Europe

where the emissions are still considerable and photo-chemistry is still active.

The modelled concentration distribution in summer showed little gradients across Europe. The concentrations were on the high side, compared to OC measurements (Yttri *et al.*, 2008). Furthermore, the measurement data did show a considerable gradient in OC levels with low values outside the industrialised parts of Europe, such as Scandinavia. Hence, from that perspective the SOA formation in the module was probably too high.

The results presented here are associated with a very high uncertainty. The parameterisations are highly simplified and may not reflect the actual processes that occur in ambient air. Note that the module reflects the state-of-the-art of 2003. Nowadays, theories differentiate between degrees of volatility and assume ageing processes in which the volatility of the organic substances is lowered in time. Also, in these approaches, the anthropogenic emissions may be much more important than in our scheme. The implementation of a new parameterisation can be easily accommodated by our set-up of the SOA module. However, there is still no conceptual framework that could be trusted to provide a reasonable guess on the formation of SOA. Insights are changing fast and it is difficult to keep up to date without constant attention and involvement in the research. Hence, a large effort on SOA formation appears not to be valuable for policy support applications, as long as there is no scientific consensus. The SOA formation process is and will be under large discussion in the scientific arena for the coming years.

7 Model Intercomparison: LOTOS-EUROS, EMEP and OPS

7.1 Introduction

A study was performed, comparing the model outcome of LOTOS-EUROS (Schaap et al., 2008), EMEP Unified version 2.8 (Simpson, 2003; Fagerli, 2004) and OPS (Van Jaarsveld, 2004) for particulate matter (PM) in the Netherlands. The comparison was based on calculated average concentrations of different PM components and on the results of linear source-receptor matrices (SRMs), which were derived from the model results. OPS is a long-term Lagrangian transport and deposition model, contrary to LOTOS-EUROS and EMEP, which are hourly Eulerian chemistry-transport models. All computations for this study were performed with emission data obtained from EMEP (WebDab, 2007) and meteorological data from ECMWF (ECMWF 2005), for the year 2005. The results from the EMEP model were obtained from the EMEP status report (Tarrasón, Jonson et al., 2007) and the EMEP online database (WebDab, 2008).

Since air pollution is a trans-boundary issue, it does not only depend on a country's domestic emissions, but also on foreign contributions. SRMs, or so called "blame" matrices, provide information on the origin of air pollution. Policymakers use these data, together with other data (e.g., economic factors), in their discussions on the revision of the National Emission Ceilings directive (NEC) of the European Commission (EP, 2001). Discussions are ongoing on emission reductions in NO_x, SO_2, $PM_{2.5}$, NH_3, and VOCs, for individual countries, by 2020.

To support this policy process it is essential to have a good view of the variability of SRM data from different models. The variability between models reflects an overall uncertainty margin. Recent publications on particulate matter, which resulted from the Eurodelta project (JRC 2008), specifically address the performance of different models and the effect of emission reductions in Europe (Thunis et al., 2008; Vautard et al., 2009, Schaap et al., submitted for publication).

In the exercise reported here, we focused on the Netherlands with models used for the support of national policy issues on air quality.

- Firstly, average concentrations of different particulate components are shown as they were computed by LOTOS-EUROS, EMEP and OPS: primary particles ($PPM_{2.5}$ and PM_{coarse}) and secondary inorganic aerosols (SIA). The calculated contribution of sea salt is also shown. In the Netherlands, sea salt is an important component of particulate matter. Secondary organic aerosols (SOA), which are chemical products from VOCs, were not considered here.
- Secondly, the results of SRMs from the three models were treated to investigate the modelled reaction of PM concentrations to emission reductions. Emission densities of NO_x, SO_2, NH_3, VOCs, and primary particles in the Netherlands are among the highest in Europe. The reaction of primary and secondary particulate components was computed by imposing a 15% emission reduction in primary $PM_{2.5}$ and the SIA precursor gases NO_x, SO_2 and NH_3.

7.2 Concentrations in the Netherlands

Average concentrations for the base situation in 2005, in the Netherlands, according to all models[1], are given in Figure 7.1. Note that PM_{10} and $PM_{2.5}$ are totals of calculated concentrations. Several relevant components of PM, such as mineral dust, were not included in this comparison. The calculated PM_{10} and $PM_{2.5}$ concentrations (Figure 7.1), therefore, could not be compared directly to the measured PM_{10} and $PM_{2.5}$ which, naturally, include all components. Next to anthropogenic emissions of primary PM_{10} and $PM_{2.5}$ particles, SO_2, NO_x, and NH_3, model calculations included emission estimates of sea salt particles, both in the fine and coarse modes. The EMEP results (Tarrasón, Jonson et al., 2007), however, did not include results for sea salt.

The emission and dispersion of sea salt particles are processes which carry many uncertainties. The model results for the sea salt fraction in PM_{10} and $PM_{2.5}$ are, therefore, also very uncertain. Manders et al. (2009) elaborate on the contribution of sea salt to PM_{10} and $PM_{2.5}$ in the Netherlands, based on

1 Computations with the various models were performed with the same emission totals per sector and country, although small differences in spatial distribution of emissions existed between the models.

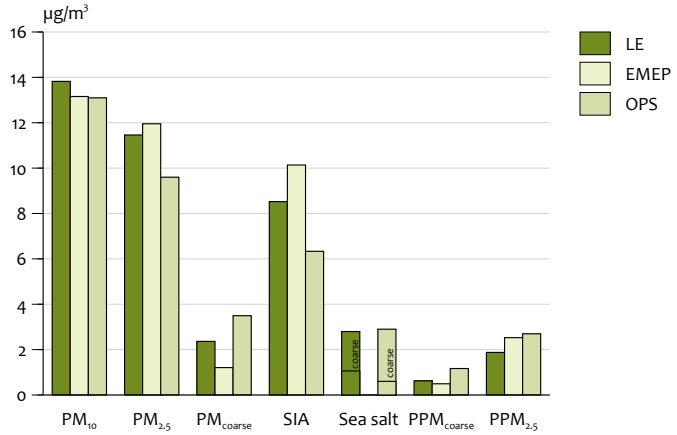

$PPM_{2.5}$	primary particles in the $PM_{2.5}$ size range
PPM_{coarse}	primary particles in the size range between $PM_{2.5}$ and PM_{10}
Sea salt	$SS_{2.5}$, sea salt in the $PM_{2.5}$ size range (fine)+ SS_{coarse}, sea salt in the size range between $PM_{2.5}$ and PM_{10} (coarse)
SIA [b]	$NO_3^- + SO_4^{2-} + NH_4^+$
PM_{coarse} [b]	$PPM_{coarse} + SS_{coarse}$ [a]
$PM_{2.5}$	SIA [b] + $PPM_{2.5}$ + $SS_{2.5}$ [a]
PM_{10}	SIA + $PPM_{2.5}$ + PM_{coarse} + $SS_{2.5}$ [a] + SS_{coarse} [a]

[a] particulate fractions from EMEP model do not include sea salt
[b] the EMEP model promotes part of the nitrate fraction to PM_{coarse}

Calculated average concentrations of different fractions of PM_{10} and $PM_{2.5}$ for the Netherlands, in 2005, with LOTOS-EUROS, EMEP and OPS

sodium measurements and model calculations with LOTOS-EUROS and the short-term version of the OPS model (OPS-ST), see also Chapter 4. The emission of sea salt is strongly dependent on the wind velocity and, therefore, has an episodic nature. The annual-average approach of the standard OPS model cannot handle these processes. The 'OPS' sea salt concentrations in Figure 7.1 were computed with this OPS-ST version (Van Jaarsveld and Klimov, 2008).

Sea salt

The results for PM_{coarse} from EMEP were lower than from LOTOS-EUROS and OPS, because, unlike the other two models, EMEP status report (Tarrasón, Jonson et al., 2007) did not include data on sea salt. The PM_{coarse} fraction shown by EMEP contained only coarse nitrate and coarse primary particles (PPM_{coarse}). The same applies to results for PM_{10} and $PM_{2.5}$. Nevertheless, EMEP's $PM_{2.5}$ concentrations were higher than those from the other two models. Therefore, these EMEP PM_{10} and $PM_{2.5}$ levels would be even higher if sea salt were to be included. OPS and LOTOS-EUROS computed almost identical average sea salt contributions to PM_{10}. However, the distribution of fine and coarse sea salt fractions differed considerably between them (Table 7.1). The fine-to-coarse fraction ratio from LOTOS-EUROS was 0.61 while for OPS, this was 0.24.

Primary particles

The primary particle concentrations from OPS were higher (3 to 40%) than those computed by EMEP and LOTOS-EUROS.

SIA

Figure 7.1 shows that secondary inorganic aerosol was estimated to be higher by EMEP than by the other models: 9% higher than LOTOS-EUROS, and 23% higher than OPS. The differences were larger between the model results for the individual SIA components (-17% to 33%). For SIA and individual components, the results from both the Eulerian chemical transport models EMEP and LOTOS-EUROS, were in better agreement than when compared with the results from the Lagrangian model OPS which carried a limited description of the SIA chemistry. The results for ammonium concentration from OPS were about 30% lower than those from EMEP and LOTOS-EUROS. This also applies to nitrate levels; according to OPS these were 15 to 20% lower than according to EMEP and LOTOS-EUROS.

The results for relative contribution of the individual SIA components: nitrate, sulphate, and ammonium, to the total SIA were very similar for all three models (Figure 7.2), in spite of the fact that the concentration differences within the individual SIA components varied considerably between the models (from -17% to 33%).

Recently, (Tarrasón, Fagerli et al., 2008) reported a bug in the EMEP model version 2.8 with regard to the formation of nitrate. This bug has several consequences for the results reported here:

- EMEP overestimated the night-time production of HNO_3 and, consequently, of ammonium nitrate.
- The SIA level from EMEP as reported here is believed also to have been overestimated.

Range [µg/m³] and bias [%] per PM component from modelled average concentrations Table 7.1

Substance	Range	LE - EMEP	LE – OPS	EMEP - OPS
PM_{10}	13.1 - 13.8	-	3	-
$PM_{2.5}$	9.6 - 12.0	-	9	-
SO_4^{2-}	1.2 - 3.5	-	4	-
SIA	6.3 - 10.1	-9	15	23
NO_3^-	1.5 - 2.2	-7	4	21
NH_4^+	1.1 - 2.3	-	27	-
NO_3^-	3.7 - 5.7	-	14	-
Sea salt (SS)	2.8 - 2.9	-	-2	-
$SS_{2.5}$	0.6 - 1.1-	-	30	-
SS_{coarse}	1.7 – 2.3	-	-15	-
$PPM_{2.5}$	1.9 – 2.7	-15	-32	-3
PPM_{coarse}	0.5 – 1.2	12	-18	-41

Range [µg/m³] per PM component from modelled average concentrations and relative bias [%] between the modelled average concentrations for the Netherlands, in 2005. Note that bias were left out in the cases where modelled PM components were not completely comparable because some components were missing.

- The relative contribution of individual SIA components according EMEP, as shown in Figure 7.2, may alter in subsequent model versions of EMEP.
- The exercises investigating the effect of emission reductions, reported on in the next section, rendered rather uncertain results for the SRMs derived from EMEP version 2.8, especially for nitrate.

In this section, we describe a comparison between average concentrations for the Netherlands from LOTOS-EUROS and those from the EMEP and the OPS model, for the base situation in 2005. Per component, each model calculated a specific spatial distribution over the Netherlands. Annex F shows the annual average spatial distributions of the components NH_4^+, SO_4^{2-}, NO_3^- and primary PM_{10}, which resulted from LOTOS-EUROS and OPS,.

The results from OPS, on a resolution of 5 x 5 km², were compared to results from LOTOS-EUROS, on a resolution of about 7 x 7 km². The LOTOS-EUROS concentrations were calculated on a zoomed resolution, 0.125° x 0.063° longitude-latitude (i.e. higher than the default, see also Chapter 3).

The comparison in Annex F shows that the agreement between the spatial distributions calculated with LOTOS-EUROS differed per component from those calculated with OPS. The best agreement was found between the calculated spatial distributions for the primary fraction of PM_{10}. The spatial patterns of the two models were in reasonable agreement for the components SO_4^{2-} and NO_3^-, although the absolute values differed according to the results in Table 7.1. The agreement between the spatial distributions for NH_4^+ was poor.

The main reason for the discrepancy between the results from OPS and LOTOS-EUROS for the spatial distribution of the secondary components was found in the differences in the descriptions of the SIA formation. In LOTOS-EUROS, the formation pathways of NH_4^+, SO_4^{2-}, and NO_3^-, were coupled in the parameterisation. OPS is not a dynamical chemistry model, such as LOTOS-EUROS and EMEP. The dependencies of the chemical formation rates of NH_4^+, SO_4^{2-}, and NO_3^-, on other substances are parameterised in the model by using prescribed background concentration maps of SO_2, NO_x, and NH_3, based on historical concentrations and future projections, see Van Jaarsveld (2004) for more details. The parameterisation can be characterised as a practical fit to the specific circumstances in the Netherlands. Therefore, it is expected that OPS is not suitable for emission scenario studies of SO_2, NO_x and NH_3 when the ratios between the emissions deviate substantially from the regular emission situation in the Netherlands. See also the discussion about NH_3 emission reductions as part of the source receptor matrices discussion

The spatial distribution of primary PM_{10} calculated with OPS showed more spatial detail than when calculated with LOTOS-EUROS. The OPS approach (Lagrangian) is specifically appropriate for describing the dispersion of primary pollutant emissions. LOTOS-EUROS is a Eulerian chemistry-transport model with a limited vertical resolution (4 layers) and, therefore, more suitable to describe secondary components which have maximal concentrations after several hours of transport, dilution, and chemical transformation.

7.3 Source Receptor Matrices and 15% emission reductions

Data from source receptor matrices (SRMs) provide information on the origins of air pollution, for instance, on a country-to-country basis. SRMs are frequently used for supporting policy-making on air quality and climate change issues (e.g. IIASA's RAINS/GAINS model; see also text box GAINS source receptor matrices).

LOTOS-EUROS was used for making SRMs for PM for five emitting countries: the Netherlands, Belgium, Germany, France, and Great Britain. The impact of emissions from these countries on the anthropogenic part of particulate matter within the Netherlands is dominant (> 70%).

Relative composition of individual components to secondary inorganic aerosol **Figure 7.2**

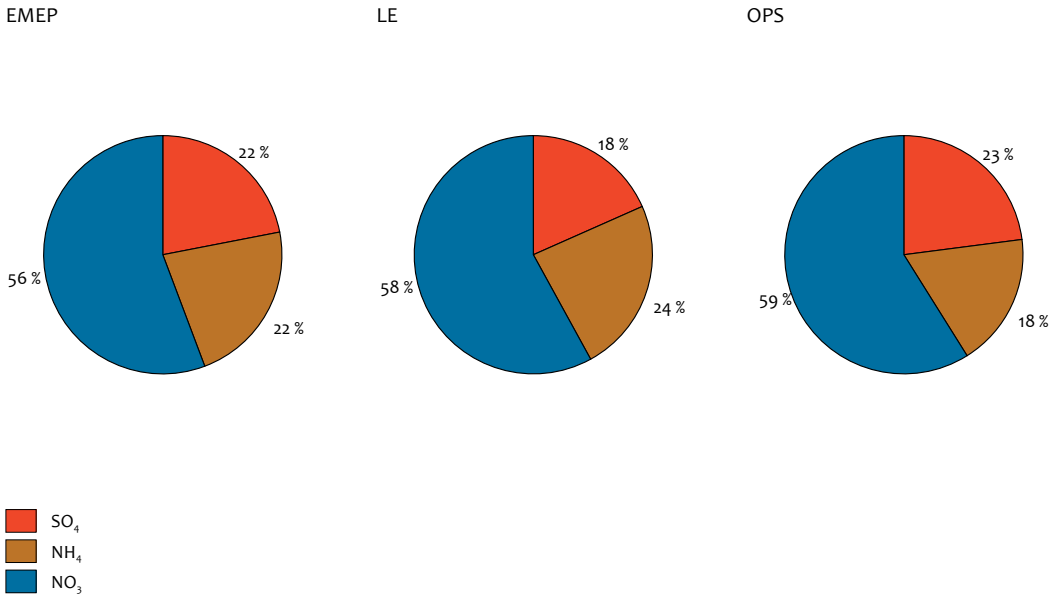

Relative composition of individual components to secondary inorganic aerosol (SIA) for all models in percentage of mass.

How were the SRMs derived? At first, a base computation was established for the situation in 2005 (referred to as 'CLE', Current legislation). Then the emissions of a particular pollutant relevant to PM were reduced by 15% for each emitting country separately. Table 7.2 shows the equivalent emission reductions in kiloton of a 15% reduction for the countries considered and for all pollutants. The difference in average annual PM concentrations between the base and the reduction computation yielded the perturbation in PM concentrations caused by the emission reduction considered. The average perturbation in a country is a measure of the contribution to PM concentration from outside that country.

The results of the SRMs are presented in three different ways:

1. The absolute reaction of PM concentrations (ng/m³) in the Netherlands to a 15% emission reduction in primary PM and PM precursor.
2. The relative reaction of PM concentrations in the Netherlands, in percentage of concentration change, per 15% emission reduction in PM or PM precursors.
3. The relative reaction of PM (ng/m³) in the Netherlands per kiloton emission reduction in PM or PM precursors. This shows the effectiveness of emission reductions.

The SRMs derived from LOTOS-EUROS were compared with the SRMs computed with EMEP version 2.8, as given in (Tarrasón, Jonson et al., 2007), and with OPS, from which only data for the Netherlands as receptor were available. The average relative bias for each SRM including its range (difference between lowest and highest relative bias) is given in Table 7.3. The SRMs from LOTOS-EUROS and EMEP overall showed good agreement with the average relative bias between the two models, ranging from -1% to -10%. This also shows that LOTOS-EUROS estimated the contribution of emissions from the five countries to PM concentrations within the Netherlands to be lower than EMEP. EMEP (Tarrasón, Jonson et al., 2007) only provided SRM data on $PM_{2.5}$, not on PM_{10}.

The difference between LOTOS-EUROS and OPS was larger, judging the average relative bias that ranged from -2 to 51%. The overall range was somewhat lower than between LOTOS-EUROS and EMEP.

7.3.1 Reduction in NO_x emissions

The average relative bias between LOTOS-EUROS and EMEP was relatively small with -7%, but the range was much larger with 50%, see Table 7.3. This means that, for one country, both models yielded rather different contributions to the air pollution in the Netherlands. This is illustrated by Figure 7.3, showing the contribution of NO_x emissions to PM concentrations in the Netherlands: there was a large discrepancy between the model results for contributions from Germany. Preliminary results with a later version of EMEP, however, showed this discrepancy to be eliminated. This is an ongoing research and will be the subject of forthcoming publications. Nevertheless, both LOTOS-EUROS and EMEP estimated the German NO_x emission contribution to the Dutch PM concentrations to be higher than that from other countries, including the Netherlands itself.

There was also a reasonable agreement between LOTOS-EUROS and OPS with an average relative bias of -2% and a range of 60%. This large range was mainly due to the contributions from within the Netherlands itself, which was much

Equivalent emission reductions [kiloton] of a 15% reduction for all countries Table 7.2

Pollutant	BEL	DEU	FRA	GBR	NLD
NO_x	40.1	217	182	244	51.6
NH_3	11.1	92.9	110	47.6	20.3
SO_2	21.7	84.1	74.5	106	9.3
$PPM_{2.5}$	4.4	16.6	49.7	14.5	3.4

Average and range of the relative bias between SRMs calculated by LOTOS-EUROS Table 7.3

	LE - EMEP		LE - OPS		EMEP - OPS	
SRM	Average	Range	Average	Range	Average	Range
NO_x	-7	50	-2	60	5	85
NH_3	-1	63	51	42	53	32
SO_2	-10	32	2	25	12	50
$PPM_{2.5}$	-9	76	-15	17	-5	83

Average and range of the relative bias between SRMs calculated by LOTOS-EUROS and EMEP for contributions to PM concentrations in the Netherlands [%] (All five countries included).

higher in OPS than in LOTOS-EUROS. It is noted that, for OPS, the change in PM was caused solely by a change in nitrate (NO_3^-), due to the linearity of the model. A reduction in NO_x emissions in LOTOS-EUROS and EMEP, however, also resulted in a change in the other SIA components ammonium (NH_4^+) and sulphate (SO_4^{2-}). This is illustrated for LOTOS-EUROS in Figure 7.5, showing both the absolute and the relative composition of the change in SIA. Note that sulphate concentrations increased slightly, due to the NO_x emission reduction.

7.3.2 Reduction in NH_3 emissions

The SRMs for NH_3 derived from LOTOS-EUROS and EMEP, had an average relative bias of only 1%, but a range of 63%. From Figure 7.4 can be concluded that the large range was caused by contributions from Germany and from within the Netherlands itself. When the contribution from Germany and the Netherlands were added, the results from the LOTOS-EUROS model and the EMEP model appeared the same, but the models disagree about whether the origin of the contribution is predominantly German or Dutch.

OPS showed much lower results than the other models. This was caused by the linearity of the OPS model approach, due to which only ammonium (NH_4^+) concentrations changed as a result of NH_3 emission reduction. OPS is not a suitable model for scenario studies which investigate the reaction of PM to reduction of only one SIA precursor gas. Source-receptor data, generated with OPS, are reliable when NO_x, SO_2, and NH_3 emissions are reduced proportionally and at the same time. Although PM concentrations are sensitive to the emission of SIA precursor gases, in particular, to the ratio of NH_3 and NO_x emissions, changes in historical emissions ratios have been limited. For instance, over the last 15 years the emission ratio of NH_3 and NO_x has been more or less constant in the Netherlands and neighbouring countries (Webdab, 2007). Moreover, the OPS model approach includes the effect of long term changes of NO_x, SO_2, and NH_3 concentrations on the formation rates of the secondary inorganic components on a year by year basis. The OPS model is currently used to describe the effect of the emission changes of NO_x, SO_2, and NH_3 on average PM concentrations over the last decades and also for the future. The OPS model approach is reliable to assess future concentration levels provided that concentrations of of NO_x, SO_2, and NH_3 will not deviate much from the current projections included in the OPS model. Secondary inorganic aerosol concentration levels, calculated with the OPS model, are in line with measured concentrations over the last decades (Hoogerbrugge et al., 2009). However, as a result of the measurements in the BOP project, it appears that the historical measurement series of secondary inorganic aerosol are considerable underestimates of the actual concentrations, up to 40% (Weijers et al., 2009). These findings are to be integrated in future model improvements.

In the non-linear chemistry models LOTOS-EUROS and EMEP, a reduction in NH_3 emissions automatically resulted in changes in nitrate (NO_3^-) concentrations. Figure 7.5 shows that nitrate formed the largest part (almost 80%) of the total

GAINS source receptor matrices

The GAINS approach (IIASA, 2007) is based on the modelling of economic activity, such as transport, industry, power generation, etc., and yields present and future emission levels. For the latter, different sets of cost-effective emission control strategies can be explored to find an optimal combination to reduce air pollutants and greenhouse gases. The GAINS model has been used to investigate and establish emission ceilings in preparation of the National Emissions Ceilings directive (NEC) of the European Commission (EP, 2001). The SRMs presently used in the GAINS model are calculated by the EMEP model. Few model intercomparison studies are performed for source receptor matrices; a recent study on SRMs for different economic activity sectors is performed in the Eurodelta II project (Thunis et al., 2008).

Foreign contributions to PM in the Netherlands by 15% emission perturbations of NO_x **Figure 7.3**

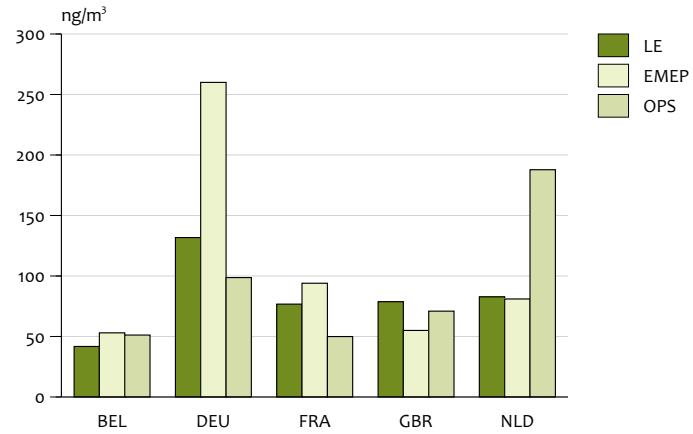

Reaction of PM in the Netherlands to a 15% reduction in NOx emissions in Belgium (BEL), Germany (DEU), France (FRA), Great Britain (GBR) and the Netherlands (NLD).

Foreign contributions to PM in the Netherlands by 15% emission perturbations of NH_3 **Figure 7.4**

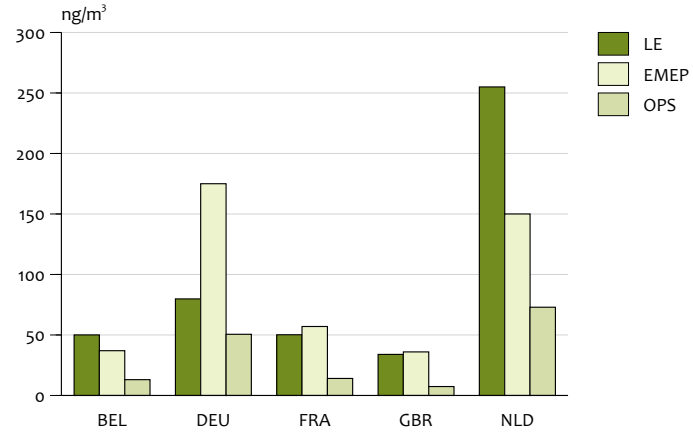

Reaction of PM in the Netherlands to a 15% reduction in NH_3 emissions in Belgium (BEL), Germany (DEU), France (FRA), Great Britain (GBR) and the Netherlands (NLD).

change in SIA, due to a reduction in NH_3. It also shows that the amount of ammonium change was about 60 ng/m3, which is close to the 70 ng/m3 from OPS, given in Figure 7.4. The high contribution of nitrate to the change in SIA concentrations, due to NH_3 emission reduction, emphasises the importance of including non-linear SIA chemistry in the generation of SRMs for specific emission scenario studies.

In Table 7.2 can be seen that, mass-wise, the NO_x reduction was the largest of all the pollutant reductions in all countries. Nevertheless, Figure 7.4 and 7.5 suggest that, in the Netherlands, abatement is more effective for NH_3 emissions than for NO_x emissions, in order to reduce nitrate, and, therefore, PM mass concentrations.

7.3.3 Reduction in SO_2 emissions

The average relative bias between LOTOS-EUROS and EMEP was the largest for SO_2 with -10%, but the range was the smallest with 32%, see Table 7.3. Figure 7.5 shows that a change in SO_2 emissions mainly effected the sulphate concentration. Since the relative contribution of sulphate to the composition of SIA was largest in EMEP, see Figure 7.2, it explained the higher change in PM concentrations for SO_2 emission in this model, see Figure 7.6.

Figure 7.6 shows the contribution of SO_2 emissions to PM concentrations in the Netherlands, from all countries. This shows that all models estimated the German contribution to be the largest. Similar to the effect of NO_x and NH_3 emissions on PM concentrations, see Figures 7.3 and 7.4, the German contribution to Dutch PM concentrations was much larger in EMEP than according to the other models. A similar model

Composition of SIA change in the Netherlands as computed by Lotos-Euros **Figure 7.5**

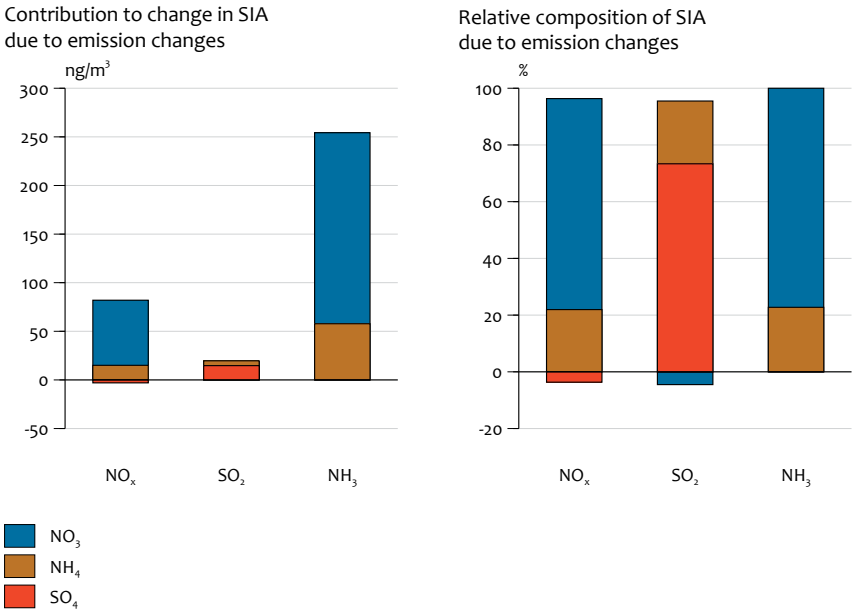

Composition of SIA change due to emission reductions in the Netherlands, as computed by the LOTOS-EUROS model.

behaviour was found for NO_x and NH_3, see Figures 7.3 and 7.4. No particular reason for this phenomenon could be found. Preliminary results from a newer version of the EMEP model, however, showed the German contribution to drop, thus, getting closer to the results from LOTOS-EUROS and OPS.

Note that foreign SO_2 emissions contributed more to Dutch PM concentrations than the domestic SO_2 emissions. However, OPS estimated Dutch contributions to be slightly larger than those from Belgium or France.

7.3.4 Reduction in primary $PM_{2.5}$ emissions

For the SRM of primary $PM_{2.5}$ ($PPM_{2.5}$) emissions, differences between LOTOS-EUROS and the other two models were of acceptable magnitude, with an average relative bias of -9 and -15% for EMEP and OPS, respectively. The range of 76% between LOTOS-EUROS and EMEP was large, however, and similar to the SRM for NH_3 in Figure 7.4, caused by German and Dutch contributions, see Figure 7.7. LOTOS-EUROS estimated the domestic contribution to be much larger than that from Germany; in EMEP this was the other way around. The lowest range found was 17%, between LOTOS-EUROS and OPS: OPS estimated a larger domestic contribution of about 70 ng/m³.

Looking at the total amount, in tons of $PPM_{2.5}$ reduction in Table 7.2, and the high change in PM concentrations from $PPM_{2.5}$ emission reduction in Figure 7.7, it can be concluded that a reduction in $PPM_{2.5}$ is an effective way of reducing PM concentrations in the Netherlands. This contrasts with NO_x and SO_2 emission reductions, which seem to be less effective

7.4 Relative reaction of PM to emission reductions

As is the case in the EMEP status report (Tarrasón, Jonson et al., 2007), the SRMs presented here are given in absolute values (ng/m³), with emissions reductions fixed at 15% of the country's total emissions. Since SIA levels under Current legislation (CLE) and primary $PM_{2.5}$ differed between the models (see Figure 7.1), an other comparison was made when the SRMs were expressed relatively, with respect to the CLE concentration level. This is shown in Figure 7.8 for SIA, for perturbations of NO_x, NH_3 and SO_2.

The models were in overall reasonable agreement, but also showed large differences in a few particular cases: for all pollutants, the EMEP model estimated the German contribution to Dutch PM to be the largest – higher than in LOTOS-EUROS or OPS. These differences are comparable with the differences found in the absolute SRMs shown in the previous sections.

According to Figure 7.8, a 15% reduction in SIA-related pollutant emissions, in any of the five countries, resulted in a relative small reduction in Dutch SIA concentrations, compared to 15% emission reduction. A reduction of as much as 15% in domestic emissions resulted in a reduction of no more than 3% in Dutch SIA concentrations. For primary $PM_{2.5}$, larger reductions in concentrations were found at a 15% emission reduction in primary $PM_{2.5}$: more than 7% in domestic emissions, according to LOTOS-EUROS and OPS. EMEP estimated the domestic contribution to be about half that of the other models. The differences between EMEP and LOTOS-EUROS could have been caused by differences in emission distributi-

Foreign contributions to PM in the Netherlands by 15% emission perturbations of SO_2 **Figure 7.6**

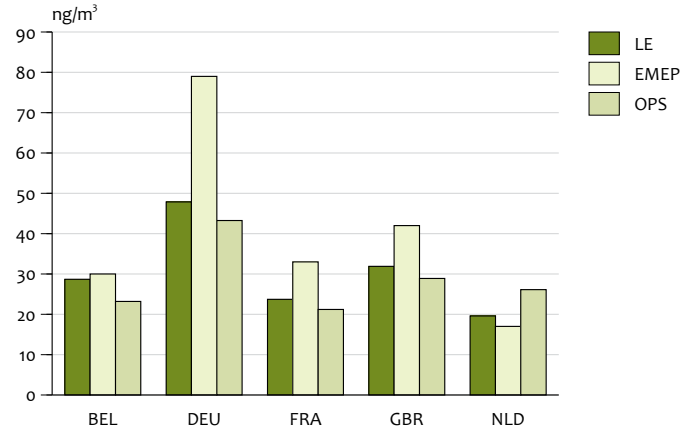

The reaction of PM in the Netherlands to a 15% reduction in SO_2 emissions in Belgium (BEL), Germany (DEU), France (FRA), Great Britain (GBR) and the Netherlands (NLD).

Foreign contributions to PM in the Netherlands by 15% emission perturbations of $PPM_{2.5}$ **Figure 7.7**

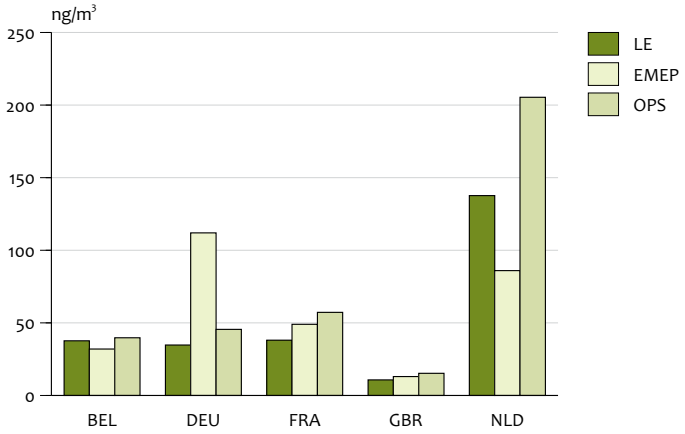

Reaction of PM in the Netherlands to a 15% reduction in primary $PM_{2.5}$ emissions in Belgium (BEL), Germany (DEU), France (FRA), Great Britain (GBR) and the Netherlands (NLD).

ons and grid resolution. The total emissions per country, for both models, were the same.

The effectiveness of emission abatement policies to reduce PM concentrations is expressed in terms of concentration change per kiloton emission reduction. This is shown in the right histograms in Figure 7.8 and shows that reducing PM emissions per kiloton through the abatement of domestic $PPM_{2.5}$ emissions, naturally, would be more effective than through the abatement of NO_x, SO_2 or NH_3. Abatement of NH_3 emissions per kiloton is more effective for reducing PM than abatement of NO_x and SO_2 emissions. While German contributions to PM in the Netherlands were high, as shown in the histograms on the left in Figure 7.8, abatement per kiloton of these German emissions had less impact on PM concentrations in the Netherlands than the size of the contribution would suggest. From all five foreign contributors, is a reduction in Belgian emissions the most effective for reducing PM in the Netherlands, followed by those from Germany, France and Great Britain.

7.5 Conclusions

Overall, the results from the LOTOS-EUROS model were in better agreement with the results from the EMEP model version 2.8, than with those from the OPS model. Primary particulate matter (PM) concentrations using Current legislation emissions for 2005 showed the highest difference between LOTOS-EUROS and OPS for $PPM_{2.5}$ of 0.8 µg/m³, and between EMEP and OPS for PPM_{coarse} of 0.7 µg/m³. All models found large differences in total SIA, especially between EMEP and OPS, where the difference was 3.8 µg/m³. In EMEP, no sea salt data were available, but the total sea salt levels from

Relative change in SIA and $PPM_{2.5}$ in NLD at 15% emission reduction

Figuure 7.8

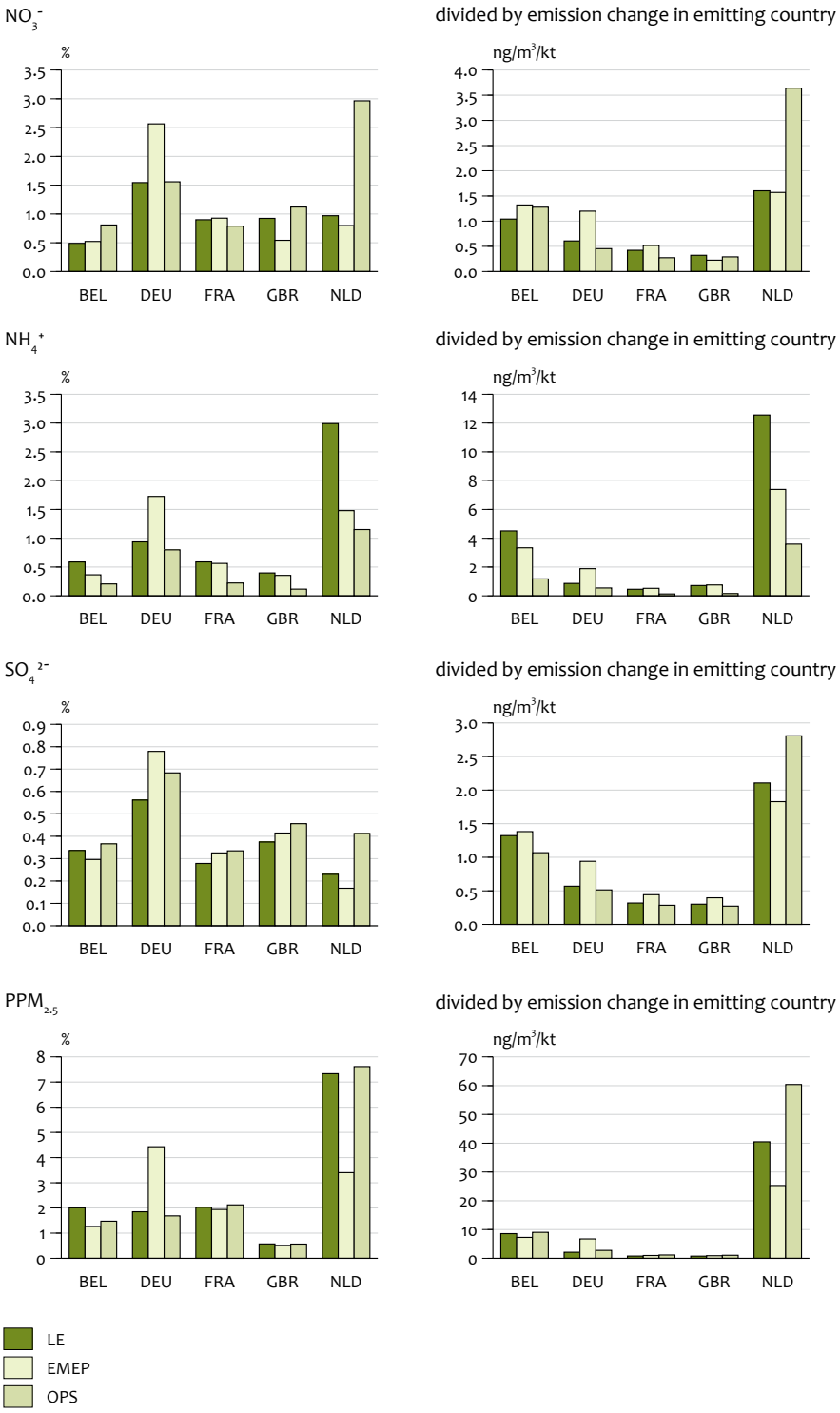

The histograms on the left show relative reactions of SIA and $PPM_{2.5}$ concentrations, in the Netherlands, to 15% reductions in NO_x, NH_3, SO_2 and $PPM_{2.5}$, for the Dutch CLE levels of SIA and $PPM_{2.5}$ [%]. The histograms on the right show the reaction of PM, in the Netherlands, per kiloton emission reduction in the indicated countries. BEL=Belgium, DEU=Germany, FRA=France, GBR=Great Britain, NLD=The Netherlands.

LOTOS-EUROS and OPS were very close together. However, the results for coarse and fine fractions of sea salt from LOTOS-EUROS and OPS showed large differences, with a fine-to-coarse fraction ratio of 0.61 for LOTOS-EUROS and 0.24 for OPS.

The OPS model is currently used for calculating average annual concentrations of primary particulate matter (PPM) and the secondary inorganic aerosol (SIA) for the specific air quality situation in the Netherlands. OPS is not always suitable for scenarios studies on the effect of emission reductions of SO_2, NO_x and NH_3, due to the absence of non-linear chemistry modelling. This is confirmed in this report by the SRM results, in particular, by those for NH_3. The accuracy of the spatial distribution of ammonium with OPS on a 1x1 km2 grid is limited due to the linear approach. Source-receptor data, generated with OPS, are reliable when NO_x, SO_2, and NH_3 emissions are reduced proportionally and simultaneously.

Overall, the models showed reasonable agreement. However, LOTOS-EUROS and EMEP showed large differences for SRMs of NO_x, NH_3 and $PPM_{2.5}$ for Germany and the Netherlands. This might have been caused by differences in emission distributions and grid resolution, since the countries' total emissions were the same in both models. An emission reduction of 15% showed the German contribution to the Dutch PM concentrations to be the largest for NO_x and SO_2.

The relative reaction of the average particulate matter concentration in the Netherlands to 15% reduction in $PPM_{2.5}$, NH_3 and NO_x was about the same for all three (several percents reduction). 15% emission reductions of SO_2 lead to less than 1% reduction of PM. The reaction per kiloton emission change gave an impression of the effectiveness of emission changes. Reducing $PPM_{2.5}$ was most effective, naturally, followed by NH_3, NO_x and SO_2. The reaction per kiloton of emission reduction, for all pollutants considered, was largest in the Netherlands, followed by Belgium, Germany and France, and was the smallest in Great Britain.

8

Outlook

In this report, we presented a number of model developments to reduce the uncertainties related to the modelling of PM_{10} and its composition. As such, this report provides a technical background document for the modelling work that is to be performed within the BOP project. The model with the current description of sea salt and mineral dust can be used as a tool for addressing policy relevant questions. The LOTOS-EUROS model will be used to help the interpretation of the experimental data obtained within the programme. In addition, the experimental data will provide a valuable data set to perform a validation for the Netherlands. Based on this model, through measurement comparison, a further iteration through the model code is expected and updates will be reported on in the thematic reports. These include the thematic reports on sea salt, secondary inorganic aerosol, and crustal matter. Finally, a number of scenario simulations will be performed to assess the contribution from the major source categories within the Netherlands. These data will be compared to statistical source apportionment techniques, based on source-specific tracers measured from the PM_{10} samples.

Annex A New meteorological input

For this study, a number of model developments were incorporated in the LOTOS-EUROS model. For these new parameterisations, we obtained a number of additional meteorological parameters from ECMWF that were not included in the operational LOTOS-EUROS data set downloaded from the ECMWF data centre..The parameters and their ECMWF codes are listed in the table below.

The soil water content is used for the new dust emission module. Snow cover prohibits dust suspension and affects the deposition velocity of most gases. In the sea salt emission routine, sea ice cover and sea water temperature are used, as they respectively prohibit and impact the emission of sea water droplets. Photosynthetic active radiation on the surface causes the emission of volatile organic compounds from vegetation. All parameters were incorporated in the meteorological module of LOTOS-EUROS and are made available for the model domain.

Additional meteorological parameters made available from ECMWF **Table A.1**

Meteorological parameter	Code	Unit	Nr
Cloud liquid water content	CLWC	kg kg^{-1}	246
Volumetric soil water layer 1	SWVL1	m^3 m^{-3}	39
Sea ice cover	CI	(0 - 1)	31
Sea surface temperature	SSTK	K	34
Snow depth	SD	m of water equivalent	141
Photosynthetic active radiation at the surface	PAR	W m^{-2}	58
Net solar radiation at the surface	SSR	W m^{-2}	176
Surface solar radiation downwards	SSRD	W m^{-2}	169

Annex B Sea salt emission

In this annex, the Mårtensson and Monahan emission modules are described in detail. In general, the sea salt source formulation is an empirical relation between the whitecap cover, average decay time of a whitecap, and the number of drops produced per square metre of whitecap. The resulting droplet flux dF/dr can be given as follows:

$$\frac{dF}{dr_p} = W(U_{10}) \cdot \frac{1}{\tau} \cdot \frac{dE}{dr_p}$$

$$W = 3.84 \cdot 10^{-6} \cdot U_{10}^{3.41}$$

$$\tau = 3.53$$

dF/dr	source flux of salt particles per increment of drop radius ($\mu m^{-1} m^{-2} s^{-1}$)
r_p	wet droplet radius (µm)
U_{10}	wind speed at ten metre ($m\ s^{-1}$)
$W(U_{10})$	surface fraction covered with whitecap
dE/dr	droplet flux per increment of drop radius per unit whitecap ($\mu m^{-1} m^{-2}$)

A large number of formulations for the whitecap coverage exist. The most widely used is the function by Monahan and O'Muircheartaigh (1980), which was also used here. For the droplet flux per unit of whitecap, a large number of formulations have been proposed. Here, we used a combination of two parameterisations: Monahan *et al.* (1986) for the coarse particles and Mårtensson (2003) for the fine fraction. Previous to the BOP project, Monahan was used for all size fractions. However, the Mårtensson *et al.* (2003) parameterisation is considered to be better for the fine aerosol mode, which is important when studying the contribution to $PM_{2.5}$.

Both parameterisations depend on wind speed and are based on experimental fits. Below, a detailed description of the parameterisations is given.

B.1.1 Mårtensson

For fine mode sea salt particles the Mårtensson *et al.* (2003) formulation can be used. It describes the dry particle flux as a function of the sea water temperature T (in K) and the size-dependent (k) coefficients *a* and *b*. These coefficients were deduced from fits through experimental data and are presented in Tables B.1 and B.2. This formulation was used in LOTOS-EUROS for particles D_p <1 µm (dry diameter D_d <0.5 µm).

$$\frac{ar_0}{d\log D_d} = W(A_k T_w + B_k)$$

$$W = 3.84 \cdot 10^{-6} \cdot U_{10}^{3.41}$$

$$A_k = a_0 + a_1 D_d + a_2 D_d^{\ 2} + a_3 D_d^{\ 3} + a_4 D_d^{\ 4}$$

$$B_k = b_0 + b_1 D_d + b_1 D_d^{\ 2} + b_3 D_d^{\ 3} + b_4 D_d^{\ 4}$$

B.1.2 Monahan

For larger particles (1<D_p<10 µm), the Monahan *et al.* (1986) formulation is used. They use the following formula for the droplet flux per unit of whitecap:

$$\frac{dE}{dr_n} = (1 + 0.057 r^{1.05}) \cdot 10^{1.19 \exp(-B^2)}, B = \frac{0.38 - {}^{10}\log(r_p)}{0.65}$$

Combining this equation with the whitecap cover function yields:

Coefficients for the polynomial Ak in the Mårtensson parameterisation for the three size ranges (k) **Table B.1**

Interval, µm	a_0	a_1	a_2	a_3	a_4
0.020 – 0.145	-2.881 × 10^6	-3.003 × 10^{13}	-2.867 × 10^{21}	5.932 × 10^{28}	-2.576 × 10^{35}
0.145 – 0.419	-6.743 × 10^6	1.183 × 10^{14}	-8.148 × 10^{20}	2.404 × 10^{27}	-2.452 × 10^{33}
0.419 – 2.800	2.181 × 10^6	-4.165 × 10^{12}	3.132 × 10^{18}	-9.841 × 10^{23}	1.085 × 10^{29}

Coefficients for the polynomial Bk in the Mårtensson parameterisation for the three size ranges (k) **Table B.2**

Range, µm	b_0	b_1	b_2	b_3	b_4
0.020 – 0.145	7.609 × 10^8	1.829 × 10^{16}	6.791 × 10^{23}	-1.616 × 10^{31}	7.188 × 10^{37}
0.145 – 0.419	2.279 × 10^9	-3.787 × 10^{16}	2.528 × 10^{23}	-7.310 × 10^{29}	7.368 × 10^{35}
0.419 – 2.800	-5.800 × 10^8	1.105 × 10^{15}	-8.297 × 10^{20}	2.601 × 10^{26}	-2.859 × 10^{31}

$$\frac{dF_0}{dr_p} = 1.373 U_{10}^{3.41} r_p^{-3} (1 + 0.057 r_p^{1.05}) \times 10^{1.19 e^{-B^2}}$$

$$B = \frac{0.38 - \log r_p}{0.65}$$

which provides the particle flux for particles at 80% RH, with radius r.

The implementation required the particle flux provided by Monahan (1986) to be translated into a sea salt mass flux. As sea salt is a wet aerosol after emission, we had to account for the fact that the dry radius determines the sea salt mass and that the wet radius determines the atmospheric lifetime. The relation between dry and wet radius varies with relative humidity, but as discussed above, for simplicity, we assumed a constant particle size. At a relative humidity of 80%, the particle radius r_p and dry particle radius r_d are related as follows:

r_p =F 2.0*r_d

Such a particle has a salt mass content m_p of:

$$m_p = \frac{4}{3}\pi\rho_{NaCl} r_d^3 = \frac{1}{6}\pi\rho_{NaCl} r_p^3$$

With ρ_{NaCl} being the density of salt (2.17 10^{-6} µg/m³). The salt mass flux is simply given as:

$$\frac{dM}{dr_p} = m_p \frac{dF}{dr_p}$$

so that the mass flux for the Monahan formulation becomes:

$$\frac{dM}{dr_p} = E \cdot f(U_{10}) \cdot g(r_p)$$

$$E = \frac{1.373}{6}\pi\rho_{NaCl}$$

$$f(U_{10}) = U_{10}^{3.41}$$

$$g(r_p) = (1 + 0.057 r^{1.05}) \cdot 10^{1.19 \exp(-B^2)}, B = \frac{0.38 - {}^{10}\log(r_p)}{0.65}$$

The mass flux is obtained by integrating equation x with respect to r_p. As the modelling of sea salt is usually performed in several size bins to account for the lifetime differences between particles of different sizes, the mass flux for each bin n is taken into account. The constant E and function f are independent of r_p and can be taken outside the integral:

$$M(n) = \int_{r_{n-1}}^{r_n} \frac{dM}{dr_p} dr_p$$

$$M(n) = E \cdot f(U_{10}) \cdot \int_{r_{n-1}}^{r_n} g(r_p) dr_p$$

$$M(n) = E \cdot f(U_{10}) \cdot I(n)$$

$$I(n) = \int_{r_{n-1}}^{r_n} g(r_p) dr_p$$

where r_n and r_{n-1} are the upper and lower limits of each bin. The numeric value of E is 1.56 10^{-6} and the value for $f(U_{10})$ is evaluated every hour, by using the meteorological parameters from the model.

The implementation of the Monahan parameterisation in the sea salt module consists of two parts. The first part integrates the size-dependent part (I) of the emission formulation over the size bins chosen for the simulation. The lowest size bin is integrated starting from 1.0 um. These calculations are only performed at the start of the simulation. The second part of the module contains the actual calculation of the emission strength and is called every hour. The total flux is scaled with the percentage of sea in the grid cell.

Annex C Dry deposition

C.1 Zhang scheme

Deposition velocity Vd is characterised by the gravitational settling velocity, which is mainly relevant for the larger particles, the aerodynamic resistance Ra and the surface resistance Rs. The formulation of Vg and Ra are well established, and based on physical processes. The formulation of Rs is empirical with parameters that are based on a few field studies. Different formulations have been used for different land-use classes. Within this study, the formulation by Zhang *et al.* (2001) has been tested as it has a uniform structure for all land-use classes, has an explicit dependence on aerosol size which makes it flexible, and is well compared with other formulations, leading to reasonable agreement within the validity of the various formulations.

$$V_d = V_s + \frac{1}{R_a + R_s}$$

The gravitational settling velocity is determined by the density of the particle ρ, the particle size, the gravitational acceleration g, the Cunningham correction factor C and the viscosity coefficient of air

$$V_g = \frac{\rho D_p^2 g C}{18\eta}$$

Zhang scheme:

$$R_s = \frac{1}{\varepsilon_0 u_* (E_B + E_{IM} + E_{IN}) R_1}$$

where ε is an empirical constant which is set to 3. The E's are the collection efficiencies for Brownian diffusion, impaction and interception.

Brownian diffusion depends on the Schmidt number Sc which is determined by the kinematic viscosity of air and the diffusivity of the particles in air. The exponent γ reflects the vegetation type.

$$E_B = Sc^{-\gamma}$$
$$Sc = \nu_{air} / Diff$$

Impaction is determined by the Stokes number St, the parameter α which depends on the vegetation type, and the exponent β which is set equal to 2. There are two parameterisations for the Stokes number, one for smooth surfaces and one for vegetated surfaces with A being the characteristic radius of the collectors.

$$E_{IM} = \left(\frac{St}{\alpha + St}\right)^{\beta} \quad \text{with}$$

$$St = \begin{cases} \dfrac{V_g u_*}{gA} & vegetated \\ \dfrac{V_g u_*^2}{\nu_{air}} & smooth \end{cases}$$

Interception also depends on the radius of the collectors A:

$$E_{IN} = \frac{1}{2}\left(\frac{D_p}{A}\right)^2$$

Interception is not applicable for smooth surfaces like sea, ice and desert.

Rebound. Larger particles may rebound after hitting the surface. The fraction of particles which stick to the surface is parameterised by

$$R = \exp(-St^{1/2})$$

For wet surfaces all particles stick to the surface and R is 1.

Deposition parameters as function of land-use class and five seasons **Table C.1**

LUC	grass	arable	permanent crops	coniferous forest	deciduous forest	water	urban	other	desert
A(mm) 1	2.0	2.0	2.0	2.0	5.0	-	10.0	-	-
2	2.0	2.0	2.0	2.0	5.0	-	10.0	-	-
3	5.0	5.0	2.0	2.0	10.0	-	10.0	-	-
4	5.0	5.0	2.0	2.0	10.0	-	10.0	-	-
5	2.0	2.0	2.0	2.0	5.0	-	10.0	-	-
alfa	1.2	1.2	1.2	1.0	1.0	100.0	1.5	50.0	50.0
gamma	0.54	0.54	0.54	0.56	0.56	0.50	0.56	0.54	0.58

C.2 Discussion

Below, we have remarked on the sensitivities in the deposition scheme. This is by no means intended to be an elaborate discussion on all the uncertainties and their implications, of which there are many.

The parameterisation of dry deposition is quite uncertain. Various parameterisations are used for different types of vegetation, and the used parameters themselves are not universal.

Here, we have not elaborated on the uncertainty in the parameterisation itself: comparisons of the Zhang parameterisation with other parameterisations and observations can be found in Zhang *et al*. (2001) and Petroff (2005).

Results are quite sensitive to the choice of roughness length Z0. An increase by a factor of 10 results in halving the concentration, since deposition becomes more effective. Therefore, a correct order of magnitude is important. For large water surfaces, the roughness length changes with wind speed and possibly with wave characteristics. Using the average Z0=0.002 m, often used in the literature, may lead to an underestimation of the concentration under very calm weather conditions, and to an overestimation of the concentration in the case of high wind speeds and rough seas. The latter conditions also lead to a large generation of sea salt, which will have a considerable added effect on those concentrations.

The density of the particle is mainly relevant for the larger particles, for which gravitational settling is important. For these particles, a doubling in density yields a near-doubling in concentration. For smaller particles, however, a doubling in the density causes a negligible difference.

Annex D Biogenic emission parameters

Table D1 shows the biogenic emission parameters used in Chapter 6.

Biomass density and emission parameters for isoprene and terpene for all **Table D.1**

Code	Name	From	Biomass[g/m2]	iso-coeff.	terp-coeff.(light)	terp-coeff.(mass)
1	Urban areas	Smiatek	0	0	0	0
2	Agriculture	Smiatek	1000	0	0	0.1
3	Grassland	Smiatek	400	0.1	0	0.1
4	Deciduous forest	Smiatek	300	10	0.2	0.2
5	Coniferous forest	Smiatek	1400	5	1.5	1.5
6	Mixed forest	Smiatek	850	5	1.5	1.5
7	Water	Smiatek	0	0	0	0
8	Marsh or wetland	Smiatek	0	0	0	0
9	Sand, bare rocks	Smiatek	0	0	0	0
10	Tundra	Smiatek	0	0	0	0
11	Permanent ice	Smiatek	0	0	0	0
12	Tropical forest	Smiatek	0	0	0	0
13	Woodland scrub	Smiatek	200	8	0	0.65
22	Abies alba	Koeble	1400	0.1	0	3
23	Abies borisii-regis	Koeble	1400	0.1	0	3
24	Abies cephalonica	Koeble	1400	0.1	0	3
25	Abies grandis	Koeble	1400	0.1	0	3
26	Acer campestre	Koeble	320	0.1	0	3
27	Acer monspessulanum	Koeble	320	0.1	0	3
28	Acer opalus	Koeble	320	0.1	0	3
29	Acer platanoides	Koeble	320	0.1	0	3
30	Acer sp.	Koeble	320	0.1	0	3
31	Alnus cordata	Koeble	320	0.1	0	1.5
32	Alnus glutinosa	Koeble	320	0.1	0	1.5
33	Alnus incana	Koeble	320	0.1	0	1.5
34	Alnus viridis	Koeble	320	0.1	0	1.5
35	Arbutus andrachne	Koeble	320	0.1	0	0
36	Arbutus unedo	Koeble	320	0.1	0	0
37	Betula pendula	Koeble	320	0.1	0	0.2
38	Betula pubescens	Koeble	320	0.1	0	0.2
39	Buxus semperviridis	Koeble	320	0.1	0	0
40	Carpinus betulus	Koeble	320	0.1	0	0.65
41	Carpinus orientalis	Koeble	320	0.1	0	0.65
42	Castanea sativa	Koeble	320	0.1	0	0.65
43	Cedrus atlantica	Koeble	700	0.1	0	0
44	Cedrus deodara	Koeble	700	0.1	0	0
45	Cercis siliquastrum	Koeble	320	0.1	0	0
46	Ceratonia siliqua	Koeble	200	0.1	0	0

Code	Name	From	Biomass[g/m2]	iso-coeff.	terp-coeff.(light)	terp-coeff.(mass)
47	Corylus avellana	Koeble	320	0.1	0	0
48	Cupressus sempervirens	Koeble	700	0.1	0	0.65
49	Erica arborea	Koeble	320	0.1	0	0
50	Erica manipuliflora	Koeble	320	0.1	0	0
51	Erica scoparia	Koeble	320	0.1	0	0
52	Eucalyptus sp.	Koeble	400	20	0	3
53	Fagus moesiaca	Koeble	320	0.1	0	0.65
54	Fagus orientalis	Koeble	320	0.1	0	0.65
55	Fagus sylvatica	Koeble	320	0.1	0	0.65
56	Fraxinus angustifolia	Koeble	320	0.1	0	0
57	Fraxinus excelsior	Koeble	320	0.1	0	0
58	Fraxinus ornus	Koeble	320	0.1	0	0
59	Ilex aquifolium	Koeble	320	0.1	0	0
60	Juglans nigra	Koeble	320	0.1	0	0
61	Juglans regia	Koeble	320	0.1	0	0
62	Juniperus communis	Koeble	700	0.1	0	0.65
63	Juniperus oxycedrus	Koeble	700	0.1	0	0.65
64	Juniperus phoenicea	Koeble	700	0.1	0	0.65
65	Juniperus thurifera	Koeble	700	0.1	0	0.65
66	Larix decidua	Koeble	300	0.1	0	1.5
67	Larix kaempferi	Koeble	300	0.1	0	1.5
68	Laurus nobilis	Koeble	300	0.1	0	0
69	Malus domestica	Koeble	300	0.1	0	0
70	Olea europaea	Koeble	200	0.1	0	0
71	Ostrya carpinifolia	Koeble	300	0.1	0	0
72	Other broadleaves	Koeble	300	0.1	0	0
73	Other conifers	Koeble	1000	0.1	0	0
74	Phillyrea latifolia	Koeble	300	0.1	0	0
75	Picea abies	Koeble				
76	Picea sitchensis	Koeble				
77	Pinus brutia	Koeble	700	0.1	0	3
78	Pinus canariensis	Koeble	700	0.1	0	3
79	Pinus cembra	Koeble	700	0.1	0	3
80	Pinus contorta	Koeble	700	0.1	0	3
81	Pinus halepensis	Koeble	700	0.1	0	0.65
82	Pinus leucodermis	Koeble	700	0.1	0	3
83	Pinus mugo	Koeble	700	0.1	0	3
84	Pinus nigra	Koeble	700	0.1	0	3
85	Pinus pinaster	Koeble	700	0.1	0	0.2
86	Pinus pinea	Koeble	700	0.1	0	6
87	Pinus radiata	Koeble	700	0.1	0	3
88	Pinus strobus	Koeble	700	0.1	0	3
89	Pinus sylvestris	Koeble				
90	Pinus uncinata	Koeble	700	0.1	0	3
91	Pistacia lentiscus	Koeble	320	0.1	0	3
92	Pistacia terebinthus	Koeble	320	0.1	0	3
93	Platanus orientalis	Koeble	320	34	0	0
94	Populus alba	Koeble	320	60	0	0
95	Populus canascens	Koeble	320	60	0	0
96	Populus hybrides	Koeble	320	60	0	0
97	Populus nigra	Koeble	320	60	0	0
98	Populus tremula	Koeble	320	60	0	0
99	Prunus avium	Koeble	300	0.1	0	0
100	Prunus padus	Koeble	300	0.1	0	0
101	Prunus serotina	Koeble	300	0.1	0	0
102	Pseudotsuga menziesii	Koeble	1000	0.1	0	1.5
103	Pyrus communis	Koeble	300	0.1	0	0
104	Quercus cerris	Koeble	320	0.1	0	1
105	Quercus coccifera	Koeble	500	0.1	20	0
106	Quercus faginea	Koeble	320	60	0	0.2
107	Quercus frainetto	Koeble	320	60	0	0.2
108	Quercus fructosa	Koeble	500	0.1	20	0

Code	Name	From	Biomass[g/m2]	iso-coeff.	terp-coeff.(light)	terp-coeff.(mass)
109	Quercus ilex	Koeble	500	0.1	20	0
110	Quercus macrolepsis	Koeble	320	60	0	0.2
111	Quercus patraea	Koeble	320	60	0	0.2
112	Quercus pubescens	Koeble	320	60	0	0.2
113	Quercus pyrenaica	Koeble	320	60	0	0.2
114	Quercus robur	Koeble	320	60	0	0.2
115	Quercus rotundifolia	Koeble	320	0.1	0	0
116	Quercus rubra	Koeble	320	60	0	0.2
117	Quercus suber	Koeble	500	0.1	0	0.2
118	Quercus trojana	Koeble	320	0.1	0	0
119	Robinia pseudoacacia	Koeble	320	34	0	0
120	Salix alba	Koeble	150	34	0	0
121	Salix caprea	Koeble	150	34	0	0
122	Salix cinerea	Koeble	150	34	0	0
123	Salix eleagnos	Koeble	150	34	0	0
124	Salix sp.	Koeble	150	34	0	0
125	Sorbus aria	Koeble	300	0.1	0	0
126	Sorbus aucuparia	Koeble	300	0.1	0	0
127	Sorbus domestica	Koeble	300	0.1	0	0
128	Sorbus torminalis	Koeble	300	0.1	0	0
129	Taxus baccata	Koeble	700	0.1	0	0
130	Thuya sp.	Koeble	700	0.1	0	0
131	Tilia cordata	Koeble	320	0.1	0	0
132	Tilia platyphyllos	Koeble	320	0.1	0	0
133	Tsuga sp.	Koeble	700	0.1	0	0
134	Ulmus glabra	Koeble	320	0.1	0	0.2
135	Ulmus laevis	Koeble	320	0.1	0	0.2
136	Ulmus minor	Koeble	320	0.1	0	0.2

75, [Biomass =F 800 g/m² if lat>60°];[1400 g/m² if (55°>lat>60°)];[1600 g/m² if lat < 55°]
76, [Biomass =F 800 g/m² if lat>60°];[1400 g/m² if (55°>lat>60°)];[1600 g/m² if lat < 55°]
89, [Biomass =F 500 g/m² if lat>60° else 700 g/m²]

Biomass density and emission parameters for isoprene and terpene for all land-use categories and 115 tree species.

Annex E Boundary conditions from TM5

Dutch levels of PM may be affected, to some extent, by sources from outside the model domain. Transport of pollutants from outside the European domain has been accounted for in LOTOS-EUROS by using monthly or annual mean concentrations. The disadvantage of these long term average concentrations is that one does not resolve the temporal variability in the concentrations outside Europe and, therefore, also not in the inflow into the model. Here, we implemented a module to incorporate the influx of pollutants, by using the TM5 global model. Below, we will demonstrate that the system works technically.

E.1 TM5 simulation

The TM5 model is a 3D atmospheric chemistry-transport model. It allows the definition of arbitrary zoom regions, which have a two-way nesting into the global model. Thus, simulations at relatively high spatial resolution (currently 1x1 degrees longitude-latitude) can be performed over selected regions, with boundary conditions always provided consistently from the global model. The TM5 model is an offline model, using preprocessed meteorological fields from ECMWF..The definition of vertical layers is linked to the 60 vertical layers of the ECMWF model. The tropospheric TM5 version uses a subset of 25 layers (mostly in the troposphere). For simulation years after 2006, the ECMWF model uses 91 vertical layers and, for TM5, a 34-layer subset has been created. The model includes all relevant processes for tropospheric chemistry, for example. chemistry, advection, emissions, dry and wet deposition, etc. The basic model operations (advection, convection, sources, chemistry) are solved by operator splitting. The model can be run as a single-tracer version (with offline chemistry) or with full CBM4-based chemistry. In addition, aerosol modules are available. For a TM5 model description we refer to Krol *et al.* (2005).

To obtain boundary conditions for LOTOS-EUROS, a dedicated model run was performed for 2005. For Europe, the simulation was performed by using three zooming levels: global grid on 6x4 degrees, zooming 3x2, and zooming 1x1. The intermediate zoom region with 3x2 resolution is employed to smooth the transition from the global grid (6x4) to the fine grid (1x1). For the simulation, the mixing ratio's of the necessary components for use in LOTOS-EUROS were stored on a three-hourly resolution in NetCDF files.

E.2 Coupling to LOTOS-EUROS

LOTOS-EUROS uses the boundary conditions to determine the incomming transport from outside the domain. Effectively, the model domain is expanded by one grid cell at each border (west, east, south, north, as well as at the model top) in which concentrations are set according to the boundary conditions. The TM5 output files are opened by the LOTOS-EUROS model, and every three hours the model reads the appropriate TM5 fields. The TM5 data are projected to the LOTOS-EUROS vertical levels and grid, and stored in the LOTOS-EUROS boundary conditions arrays. To obtain hourly fields, the TM5 data are interpolated linearly between the three-hourly data points.

For the simulation of other years, the possibility of using monthly mean TM5 concentration fields was also incorporated in the model description. In that case, the boundary conditions are kept constant for a full month. This option is not used within BOP.

E.3 Results

Two simulations were performed to illustrate the correct functioning and impact of the TM5 boundary conditions:
1. 'base' simulation with standard boundary conditions
2. 'TM5' simulation reading TM5 boundary conditions.

Below, three cases illustrate that the system works correctly: sulphate, dust and ozone.

Figure E.1 shows the monthly (July, 2005) average sulphate at ground level for the two runs, as well as the difference between these two fields. The new boundary conditions were larger by a factor of 10 than the original values in this period. Under the assumption that this was no bug in TM5 or in the conversion from TM5 to LOTOS-EUROS, this led to increased sulphate values all over Europe. The largest differences were found at the south and south-east side of the domain, where

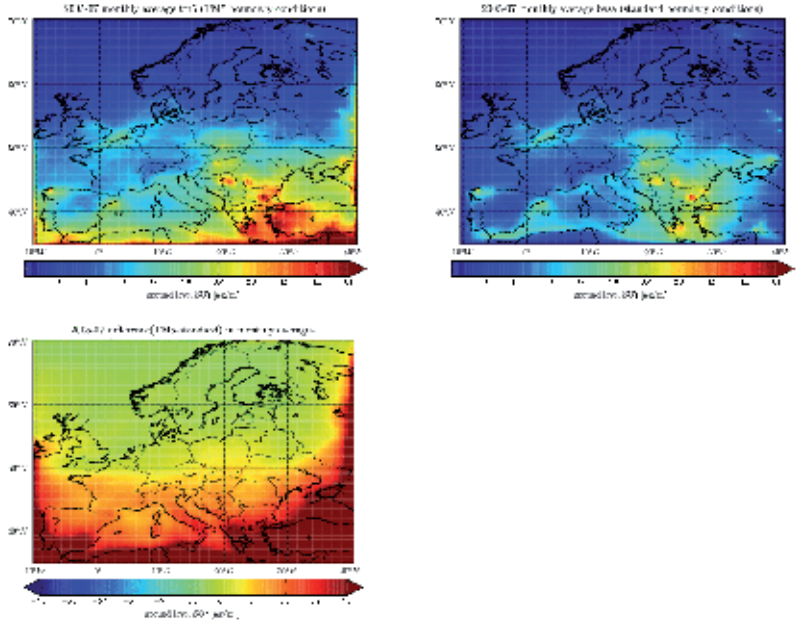

Monthly average sulphate concentrations at ground level, for July 2005, from LOTOS-EUROS runs with standard or TM5 boundary conditions. A one-cell row of halo cells at the edges of the grid illustrates the concentrations actually used at the boundary.

the new boundary conditions led to an increase in sulphate concentrations of more than 1 µg/m³.

The boundary conditions enable studies on PM contributions from outside Europe. As an example, the maximum daily average dust concentration in 2005, due to the dust boundary conditions taken from TM5, is shown in Figure E.2. Although the annual average concentration due to dust transport from outside Europe is very low (see Chapter 5), in the Netherlands there was one single day in 2005 with a contribution of 2-3 µg/m³. The plume that passed the Netherlands is shown in Figure E.2. In this case, the dust originated from the Sahara and was transported over the Atlantic and circulated towards western Europe around the Azores high pressure system.

Maybe the best test of incorporating boundary conditions is ozone. For ozone, a large set of chemically active substances make up the necessary boundary conditions to provide sound results. Figure E.3 shows the monthly (July, 2005) average ozone at ground level for the two runs, as well as the differences between them. The largest differences were found at the east side of the domain, where the new boundary conditions led to increased ozone concentrations of more than 5 ppb. For the concentrations across the European continent , this led to an enhanced gradient from west to east. In the inner part of the domain, the changes were limited to a few ppb. Above the North Sea and the western Mediterranean Sea, concentrations were 1-2 ppb lower. This could be partly explained by lower ozone values on the new boundaries, as seen in the north-west of Spain and for the western Mediterranean Basin. The lower concentrations in the North Sea area could not be explained by changed horizontal transport only; the impact of the upper boundary conditions and changes in other tracers probably contributed, too.

The simulations show that the new module for incorporation of TM5 boundary conditions works well.

E.4 Conclusion

Boundary conditions taken from TM5 for 2005, have been made available. By using these data, which have a higher time resolution, LOTOS-EUROS has boundary conditions available that better resolve the temporal variability in the concentrations outside Europe, compared to monthly or annual mean concentration fields. In addition, the LOTOS-EUROS model can be used to assess the impact of pollutants transported to the Netherlands from sources outside Europe.

Maximum mean daily dust concentrations over the European continent

Figure E.2

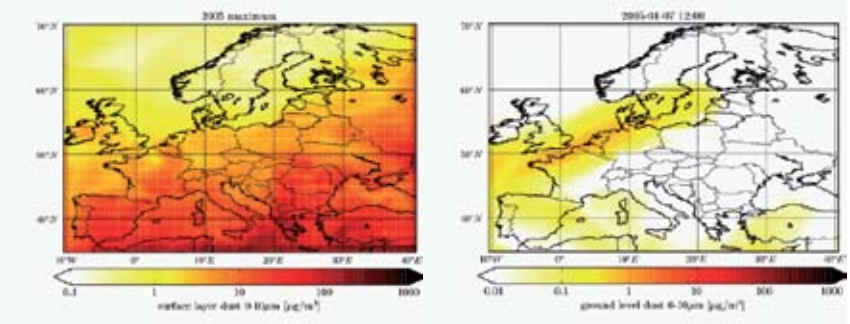

Maximum mean daily dust concentrations over the European continent, in 2005, due to import of dust, according to the TM5 model (right). The figure on the right shows the plume with the largest concentrations for the Netherlands.

Monthly average ozone concentrations at ground level

Figure E.3

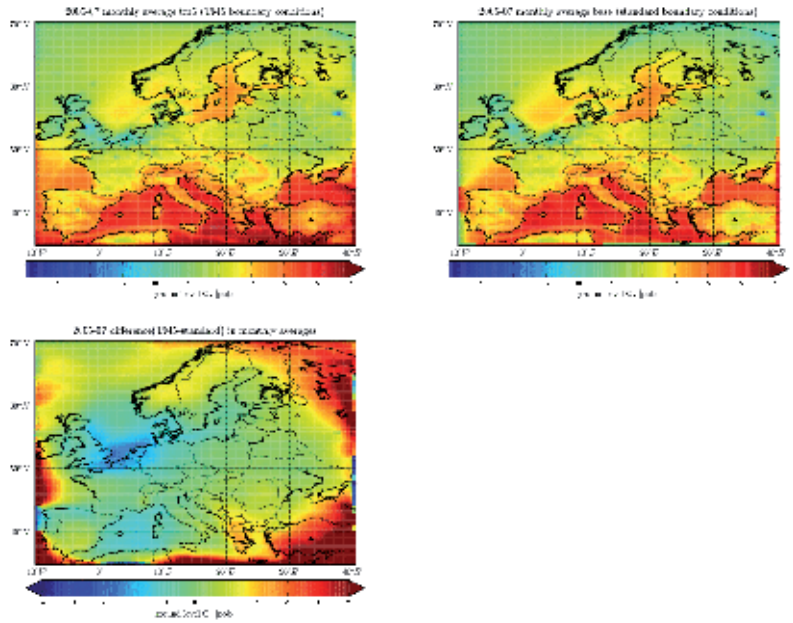

Monthly average ozone concentrations at ground level for July 2005, from LOTOS-EUROS runs with standard or TM5 boundary conditions. A one-cell row of halo cells at the edges of the grid illustrates the concentrations actually used as boundary condition.

Annex F Spatial distribution of PM components

In chapter 7 the Lotos-Euros model is compared with the Unified EMEP model and the OPS model in terms of country-averaged yearly mean over 2005 and source receptor matrices. In this Annex we compare the spatial distributions of the yearly mean over the Netherlands as computed by the Lotos-Euros and OPS models. No spatial distributions are available from the Unified EMEP model.

Since the OPS model works on a higher resolution (5 x 5 km² or 1 x 1 km²), computations with the Lotos-Euros model have been performed also on a higher resolution than the default. The high resolution of .125° x .063° longitude x latitude coincides with approximately 7 x 7 km² over the Netherlands, see also Chapter 3. In the following sections results for the secondary components NH_4^+, SO_4^{2-} and NO_3^- and the primary part PPM10 obtained by the Lotos-Euros model with the higher resolution are quantitatively compared with OPS results.

F.1.1 NH_4^+

There is not much similarity between the spatial distributions of NH_4^+ concentrations as computed by the Lotos-Euros and OPS models. Concentrations in the Lotos-Euros model are higher then in the OPS model: in most of the Netherlands at least 1.5 µg/m³ according to the Lotos-Euros model and around 1 to 1.25 µg/m³ in case of the OPS model. Also the maximum concentrations are located differently. According to the Lotos-Euros model the highest levels are found in south-eastern Netherlands and according to the OPS model in south-western Netherlands, especially in the industrial Rijnmond region. Unlike the dynamic chemistry modeling in the Lotos-Euros model, the OPS model treats the formation of NH_4^+ independent of the formation and concentration of NO_3^- and SO_4^{2-}.

F.1.2 NO_3^-

The patterns of the spatial distribution of NO_3^- computed by the Lotos-Euros and OPS models are quite similar, but the gradients by the OPS model are higher. The maximum in south-east-Netherlands is higher in case of the OPS model: 5 µg/m³ vs. 4 µg/m³ for the Lotos-Euros model. The minimum along the coast however, is lower for the OPS model than for the Lotos-Euros model: around 1 µg/m³ vs. 2.5 µg/m³, respectively.

F.1.3 SO_4^{2-}

Trends in the spatial patterns of SO_4^{2-} concentrations computed by the Lotos-Euros and the OPS model are similar: the northern part of the Netherlands has lower concentrations of SO_4^{2-} than southern part, but levels are lower in case of the OPS model. The highest level in case of the Lotos-Euros model in southern Netherlands is 2.5 µg/m³ with a peak in the south-western part (Zeeuws-Vlaanderen) above 2.5 µg/m³. In the OPS model results however, the highest level is 1.75 µg/m³.

F.1.4 PPM10

The gradient from north-Netherlands to south-Netherlands coincide well between the Lotos-Euros and OPS models and starts between 1 and µg/m³ in the north and increases to about 4-5 µg/m³ in the south. Also the lower concentrations between 3 and 4 µg/m³ in the province Zeeland in south-western Netherlands and the higher values above 5 µg/m³ in the Rijnmond region and Amsterdam appear in both models.

Much more spatial detail is found in the OPS model than in the Lotos-Euros model. The Lagrangian approach of the OPS model is specifically appropriate to describe the dispersion of primary pollutant emissions. The Lotos-Euros model is an Eulerian chemistry-transport model with a limited vertical resolution (4 layers) and is therefore more suitable to describe secondary components which have maximal concentrations after several hours of transport, dilution and chemical transformation.

F.1.5 Conclusions

The agreement between the high resolution results for the Netherlands from Lotos-Euros and OPS depends strongly on the component considered. Agreement of NH_4^+ is poor in pattern and absolute value. The OPS model shows high NH_4^+ concentrations in the industrial Rijnmond area in south-western Netherlands. This is not found in the Lotos-Euros model. The spatial patterns of NO_3^- and SO_4^{2-} show a reasonable agreement, although the absolute values differ. Especially

Spatial distribution of NH_4

Figure F.1

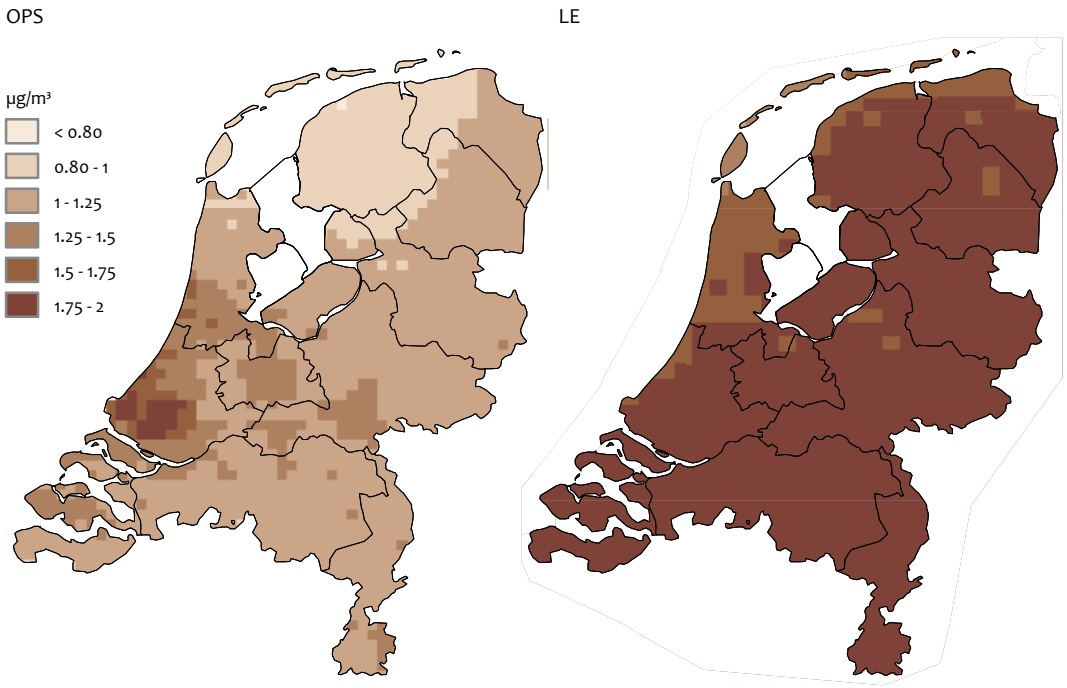

Spatial distribution of NO_3

Figure F.2

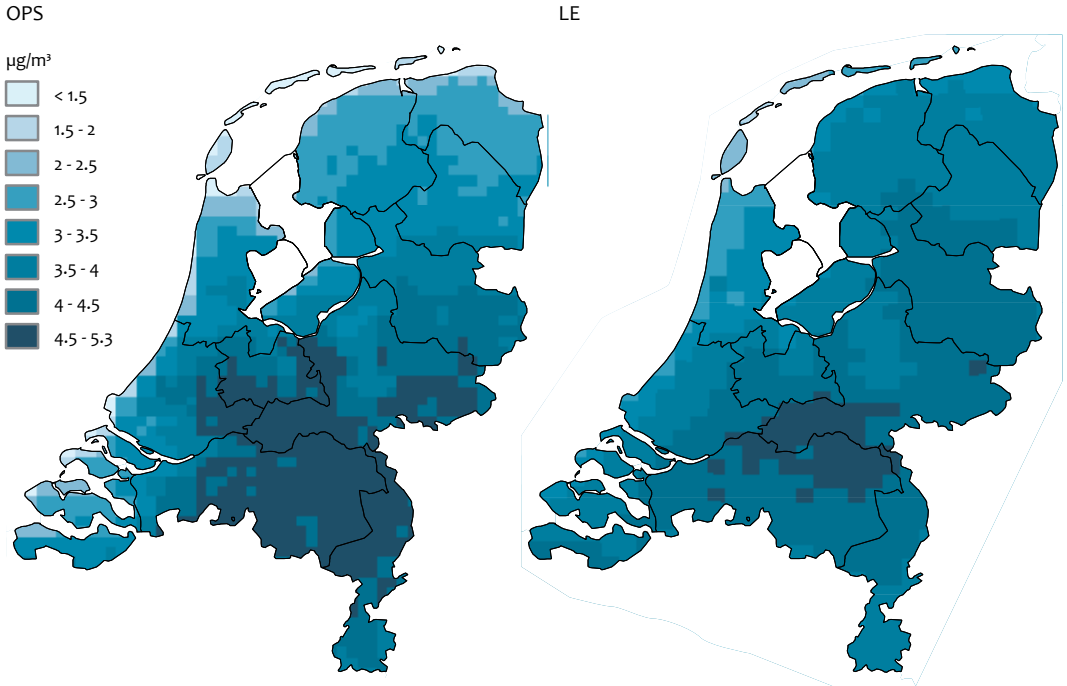

SO_4^{2-} concentrations obtained from the Lotos-Euros model are lower than from the OPS model. The best agreement in pattern as well as absolute values is found for PPM10.

The main reason for the discrepancy between the OPS and Lotos-Euros spatial distribution of the secondary components is found in the differences between the descriptions of the SIA formation in the two models. In the Lotos-Euros model the formation pathways of NH_4^+, SO_4^{2-} and NO_3^- are coupled in the parameterisation. In the OPS model the dependencies of the chemical formation rates of NH_4^+, SO_4^{2-} and NO_3^- on other species are parameterised by using prescribed background concentrations maps of SO_2, NO_x and NH_3.

Spatial distribution of SO_4

Figure F.3

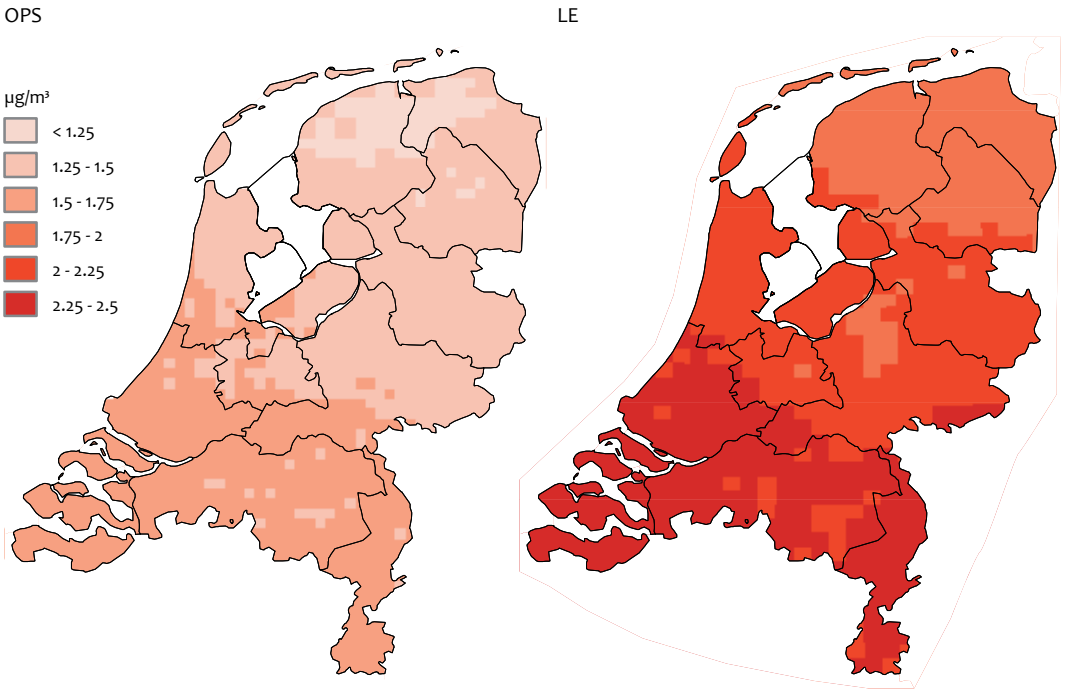

Spatial distribution of PPM_{10}

Figure F.4

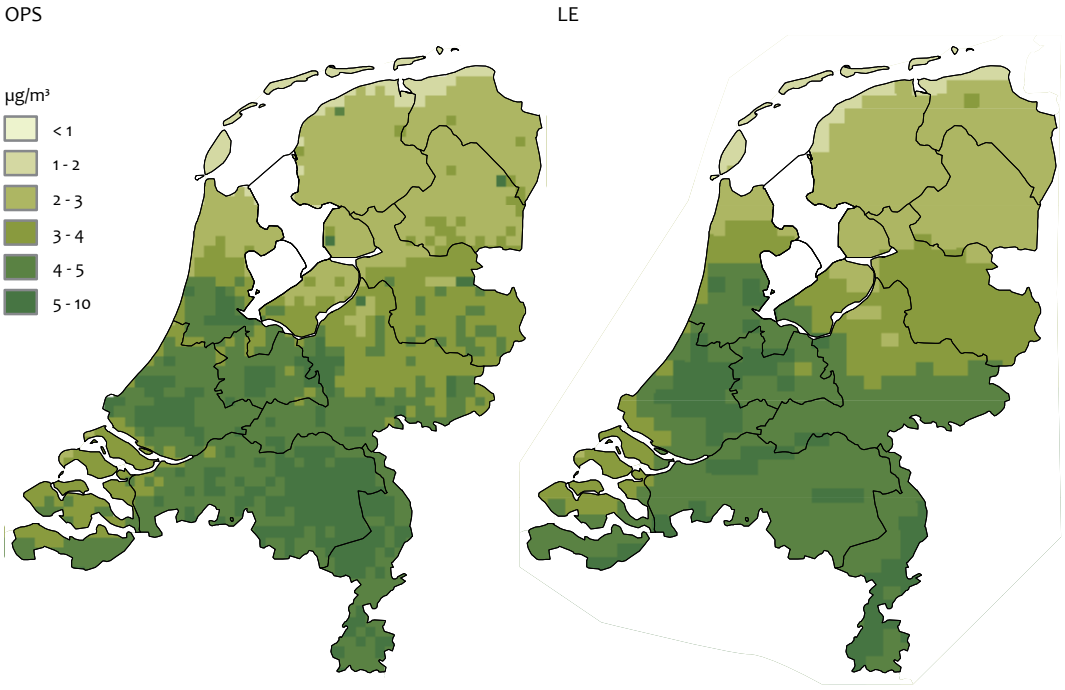

The spatial distribution of primary PM_{10} calculated with the OPS model shows more details than calculated with the Lotos-Euros model. This is due to the Lagrangian approach of the OPS model. The Lotos-Euros model is an Eulerian chemistry-transport model and is therefore more suitable to describe secondary components.

References

Aben, J.M.M., Hettelingh, J-P and Schöpp, W. (2005). RAINS-NL: An Integrated assessment model to support Dutch air quality policy making, In: Proc. 19th Intern. Conf. Informatics for Environmental Protection, pp 513-517, Brno. See also (http://www.mnp.nl/images/rainsnl_background_tcm60-21210.pdf)

Abu-Allaban, M., Gillies, J.A., Gerler, A.W., Clayton, R., Proffitt, D., Tailpipe, resuspended road dust, and brake-wear emission factors from on-road vehicles, Atmospheric Environment 37, pp 5283-5293, doi: 10.1016/j.atmosenv.2003.05.005, 2003.

Adelman, Z.E. (1999) 'A re-evaluation of the Carbon Bond-IV photochemical mechanism'. M.Sc. thesis, Department of Environmental Sciences and Eng., School of Public Health, Univ. of North Carolina, USA.

Alfaro, S.C., Gaudichet, A., Gomes, L., Maille, M., 1997. Modelling the size distribution of a soil aerosol produced by sandblasting. J. Geophys. Res. 102, 11239–11249.Alfaro et al, 1997

Alfaro, S. C., A. Gaudichet, L. Gomes and M. Maill´e, 1998: Mineral aerosol production by wind erosion: Aerosolparticle si zes and binding energies. *Geophys. Res. Lett.*, 25(7), 991–994.

Alfaro, S.C., Gomes, L., 2001. Modelling mineral aerosol production by wind erosion: emission intensities and aerosol distributions in source areas. J. Geophys. Res. 106, 18075– 18084.

Asman, W.A.H. and J.A. Van Jaarsveld, 1990. A variable-resolution transport model applied for NH_x in Europe. Atmos. Environ., 26A, 445-464.

Bagnold, R.A., 1941. The Physics of Blown Sands and Desert Dunes. Methuen, London, 241pp.

Barbu, A., Segers, A., Schaap, M., Heemink, A. Builtjes, P.J.H. (2008), A multi-component data assimilation experiment directed to sulphur dioxide and sulphate over Europe, Atmospheric Environment, in press.

Beekmann, M., A. Kerschbaumer, E. Reimer, R. Stern, D. Möller, PM measurement campaign HOVERT in the Greater Berlin area: model evaluation with chemically specified particulate matter observations for a one year period, Atmos. Chem. Phys., 7, pp 55-68, www.atmos-chem-phys.net/7/55/2007/, 2007.

Birmili, W., Schepanski, K., Ansmann, A., Spindler, G., Tegen, I., Wehner, B., Nowak, A., Reimer, E., Mattis, I., Müller, K., Brüggemann, E., Gnauk, T., Herrmann, H., Wiedensohler, A., Althausen, D., Schladitz, A., Tuch, T., Löschau, G. (2008), A case of extreme particulate matter concentrations over Central Europe caused by dust emitted over the southern Ukraine, Atmospheric Chemistry and Physics, 8 (4), pp. 997-1016.

Builtjes, P.J.H., van Loon, M., Schaap, M., Teeuwisse, S., Visschedijk, A.J.H., Bloos, J.P. (2003) 'Project on the modelling and verification of ozone reduction strategies: contribution of TNO-MEP', *TNO-report, MEP-R2003/166*, Apeldoorn, The Netherlands.

Chamley, H, Clay Sedimentology, Spring-Verlag, Berlin, 1989.

Chatenet, B., M. Marticorena, L. Gomes and G. Bergametti, 1996: Assessing the microscopic size distributions of desert soils erodible by wind. *Sedimentology*, 43(5), 901–911.

Claiborn, C., A. Mitra, G. Adams, L. Bamesberger, G. Allwine, R. Kantamaneni, B. Lamb, H. Westberg, Evaluation of PM10 emission rates from pave and unpaved roads using tracer techniques, Atmospheric Environment 29, pp. 1075-1089, 1995.

Day, D.E. and Malm, W.C. (2001), 'Aerosol light scattering measurements as a function of relative humidity: a comparison between measurements made at three different sites', *Atmos. Env.*, 35, 5169-5176.

Denby, B., Schaap, M., Segers, A., Builtjes, P., Horalek,J. (2008), Comparison of two data assimilation methods for assessing PM10 exceedances on the European scale, Atmospheric Environment 42, 7122-7134.

Dühring, I., A. Lohmeyer, Validierung von PM10-Immisionsberechnungen im Nahbereich von Strassen und Quantifizirung der Feinstaubbildung von Strassen, Ingenieurbüro Dr.-Ing. Achim Lohmeyer, Karlsruhe und Dresden, 2001.

ECMWF (2005). European Centre for Medium-Range Weather Forecasts. Website: www.ecmwf.int.

EMEP/CORINAIR, 2004. Emission Inventory Guidebook, third ed. September 2003 update 2004/01/19. Technical Report No. 30. See also / http://reports.eea.eu.int/EMEPCORINAIR4/enS.

EP (2001). Directive 2001/81/EC of the European Parliament and of the Council of 23 October 2001 on national emission ceilings for certain atmospheric pollutants, European Community. OJ L 309: 22-30.

Erisman, J.W., van Pul, A., Wyers, P. (1994) 'Parametrization of surface-resistance for the quantification of atmospheric deposition of acidifying pollutants and ozone', *Atmos. Environ.*, Vol. 28, 2595-2607.

Etyemezian., V., H. Kuhns, J. Gillies, J. Chow, K. Hendrickson, M. McGown, M. Pitchford, Vehicle-based road dust emission measurement – Part III: effect of speed, traffic volume, location, and season on PM10 road dust emissions in the Treasure Valley, ID, Atmospheric Environment 37, pp 4583-4593, doi: 10.1016/S1352-2310(03)00530-2, 2003.

EU (2008), Directive 2008/50/EC of the European Parliament and of the Council on ambient air quality and cleaner air for Europe. EU, 21 May 2008.

Fagerli, H., Simpson, D. and Tsyro, S. The Norwegian Meteorological Institute (2004). Transboundary acidification, eutrophication and ground level ozone in Europe, Unified EMEP model: Updates, EMEP Status Report 1/2004, The Norwegian Meteorological Institute, 11-18.

Fécan, F., Marticorena, B., Bergametti, G., 1999. Parameterization of the increase of the aeolian erosion threshold wind friction velocity due to soil moisture for semi arid areas. Ann. Geophys. 17, 149–157.

Funk, R., W. Engel, C. Hoffmann, and H. Reuter, Influence of soil type and soil moisture on PM emissions form soils during tillage, Landbauforshung Völkenrode Special Issue 308, pp. 157-163, 2008.

Gaffney, P, H. Yu, Computing Agricultural PM10 Fugitive Dust Emissions Using Process Specific Emission Rates and GIS, Dust Conference 2007, Maastricht, The Netherlands, 2007.

Gehrig, R., M. Hill, B. Buchmann, D. Imhof, E. Weingarter, U. Baltensprenger, Separate determination of PM10 emission factors of road traffic for tailpipe emissions and emissions form abrasion and resuspension processes, International Journal for Environment and Pollution 22, pp. 312- 32, 2004.

Gerber, H.E. (1985), Relative-humidity parameterization of the Navy aerosol model (NAM), NRL Rep. 8956, Natl. Res. Lab., Washington DC.

Gertler, A., H. Kuhns, M. Abu-Allaban, C. Damm, J. Gillies, V. Etyemezian, R. Clayton, D. Proffitt, A case study of the impact of Winter road sand/salt and street sweeping on road dust re-entrainment, Atmospheric Environment 40, pp. 5976-5985, doi: 10.1016/j.atmosenv.2005.12.047, 2006.

Gillies, J.A., V. Etyemezian, H. Kuhns, D. Nikolic, D.A. Gillette, Effect of vehicle characteristics on unpaved road dust emissions, Atmospheric Environment 39, 2341-2347, doi: 10.1016/j.atmosenv.2004.05.064, 2005.

Gomes, L., Arru´e, J.L., Lo´pez, M.V., Sterk, G., Richard, D., Gracia, R., Sabre, M., Gaudichet, A., Frangi, J.P., 2003. Wind erosion in a semi-arid agricultural area of Spain: the WELSONS project. Catena 52, 235– 256.

Harrison, R.M., Yin, J., Mark, D., Stedman, J., Appleby, R.S., Booker, J., Moorcroft, S., 2001. Studies of the coarse particle (2.5-10µm) component in UK urban atmospheres. Atmospheric Environment 35(21), 3667- 3679.

Hinz, T., R. Funk, Particle Emissions of soils induced by agricultural field operations, Dust Conference 2007, Maastricht, The Netherlands., 2007.

Hodzic, A., Vautard, R., Chepfer, H., Goloub, P., Menut, L., Chazette, P., Deuzé, J.L., Apituley, A., Couvert, P. (2006), Evolution of aerosol optical thickness over Europe during the August 2003 heat wave as seen from CHIMERE model simulations and POLDER data, Atmospheric Chemistry and Physics, 6, pp. 1853-1864.
Hoogerbrugge, R., J. Matthijsen, H. van Jaarsveld, M. Schaap, H. Denier van der Gon (2005), Aanbeveling voor een voorlopige regeling voor de correctie van fijn stof (PM10) concentraties voor de bijdrage van zeezout., 14 juli 2005, www.rivm.nl/milieuportaal/dossier/fijnstof/bronnen
Hoogerbrugge, R., H. Denier van der Gon and J. Matthijsen (2009) Particulate Matter Trends in the Netherlands, PBL report nr. 500099014, Netherlands Environmental Assessment Agency, Bilthoven.
IIASA. (2007). "GAINS." from www.iiasa.ac.at/web-apps/apd/gains/.
INFRAS, HBEFA Handbuch Emissionsfaktoren des Strassenverkehrs. Version 2.1. INFRAS, UBA Berlin, UBA Wien, BUWAL.
Iversen, J.D., White, B.R., 1982. Saltation threshold on Earth, Mars, and Venus. Sedimentology 29, 111–119.
JRC (2008). Eurodelta-II: Evaluation of a Sectoral Approach to Integrated Assessment Modelling including the Mediterranean Sea, EUR 23444 EN - 2008, JRC.
Kantamaneni, R., G. Adams, L. Bamesberger, E. Allwine, H. Westberg, B. Lamb, C. Claiborn, The measurement of roadway PM10 emission rates using atmospheric tracer ratio techniques, Atmospheric Environment 30, pp. 4209-4233, 1996.
Kerschbaumer, A. and Reimer, E. (2003) 'Preparation of Meteorological input data for the RCG-model', *UBA-Rep. 299 43246,* Free Univ. Berlin Inst for Meteorology (in German).
Ketzel, M., G. Omstedt, C. Johansson, I. Düring, M. Pohjola, D. Oettl, J. Gidhagen, P. Wåhlin, A. Lohmeyer, M. Haakana, R. Berkowicz, Estimation and validation of PM2.5/PM10 exhaust and non-exhaust emission factors for practical street pollution modeling, Atmospheric Environment 41, pp. 9370-9385, doi: 10.1016/j.atmosenv.2007.09.005, 2007.
Kiehl, J. T., and B. P. Briegle, (1993), 'The relative roles of sulphate aerosols and greenhouse gases in climate forcing', *Science*, *260*, 311-314.
Koeble, R., and G. Seufert (2001), Novel maps for forest tree species in Europe, Proceedings of the conference "a changing atmosphere", Sept 17-20, Torino, Italy.
Krol, M., Houweling, S., Bregman, B., van den Broek, M., Segers, A., van Velthoven, P., Peters, W., Dentener, F., and Bergamaschi, P. (2005). The two-way nested global chemistry-transport zoom model TM5: algorithm and applications. Atmos. Chem. Phys., 5(2):417-432.
Kuhlbusch T.A.J., John, A.C., Fissan, H., 2000. Korngrößenabhängige Untersuchungen von Schwebstaub und Inhaltsstoffen. Final report for Ministerium fuer Umwelt, Raumorndung und Landwirtschaft, NRW (available at: www.uni–duisburg.de/FB9/AMT), 2000.
Kupiainen K., Tervahattu H., and Räisänen M., 2003. Experimental Studies about the Impact of Traction Sand on Urban Road Dust Composition. *The Science of the Total Environment* 308, 175-184.
Kupiainen K.J., Tervahattu H., Räisänen M., Mäkelä T., Aurela M., and Hillamo R., 2005. Size and Composition of Airborne Particles from Pavement Wear, Tires, and Traction Sanding. *Environmental Science & Technology*
Kuhns. H., V. Etyemezian, M. Green, K. Hendrickson, M. McGown, K. Barton, M. Pitchford, Vehicle-based road dust emission measurement – Part II: Effect of precipitation, wintertime road sanding, and street sweepers on inferred PM10 emission potentials form paved and unpaved roads, Atmospheric Environment 37, pp. 4573-4582, , doi: 10.1016/S1352-2310(03)00229-6, 2003.
Laurent, B., Marticorena, B., Bergametti, G., Chazette, P., Maignan, F., Schmechtig, C., 2005. Simulation of the mineral dust emission frequencies from desert areas of China and Mongolia using an aerodynamic roughness length map derived from the POLDER/ADEOS 1 surface products. J. Geophys. Res. 110, D18S04. doi:10.1029/2004JD005013.
Leeuw, G. de, Neele, F.P., Hill, M., Smith, M.H., Vignati, E. (2000) , Production of sea spray aerosol in the surf zone, J. Geophys. Res., 105,
Lenschow, P., Abraham, H. J., Kutzner, K., Lutz, M., Preu, J.D., Reichenbacher, W., 2001. Some ideas about the sources of PM10. Atmospheric Environment 35: 23-33.
Lewis, E.R., and Schwartz, S.E. (2004), Sea Salt Aerosol production, AGU, Washington DC
Liu M.K., Durran D. (1977). 'Development of a regional air pollution model and its application to the Northern Great Plains'. *US-EPA* (EPA-908/1-77-001).
LML, 2008. Landelijk Meetnet Luchtkwaliteit (National Air Quality Monitoring Network of the Netherlands), http://www.lml.rivm.nl
Logan, J. (1999) 'An analysis of ozonesonde data for the troposphere, recommendations for testing 3-D models and development of a gridded climatology for tropospheric ozone', *J. Geophys. Res. 104,* Vol 16.
Lohmeyer, A., Bächlin, W., Düring, I., Modelling of vehicle induced non-exhaust PM10 emissions, Proceedings of the PM Emission Inventories Scientific Workshop, 18 October 2004.
Loosmore, G.A., J.R. Hunt, Dust resuspension without saltationl, J. Geophys. Res. 105, No. D16, pp.20,663-20,671, 2000.
Manders, A., L. Nguyen and R. Hoogerbrugge, Evaluatie van RIVM-modellen voor de ozon- en fijnstofverwachting, RIVM report no. 680704004, 2008
Manders et al., (2009). The contribution of sea salt to PM10 and PM2.5 in the Netherlands, PBL report nr. 500099004, Netherlands Environmental Assessment Agency, Bilthoven.
Marticorena, B., Bergametti, G., Gillette, D.A., Belnap, J., 1997. Factors controlling threshold friction velocity in semiarid and arid areas of the United States. J. Geophys. Res. 102, 23277–23287.
Mensink, C. and L. Janssen, 1996. Implementatie van het Operationeel Prioritaire Stoffen (OPS) model in Vlaanderen. VITO-rapport no E&M. ERB9602, Mol, België.
Mie, G., (1908), 'Beiträge zur optik trüber medien', *speziell kolloidaler metallösungen, An. Phys. Leipzig*, 25, 377-445.
Monahan, E.C., Spiel, D.E., Davidson, K.L. (1986) 'A model of marine aerosol generation via whitecaps and wave disruption', In *Oceanic Whitecaps and their role in air/sea exchange*, edited by Monahan, E.C, and Mac Niocaill, G., pp. 167-174, D. Reidel, Norwell, Mass., USA.
Moosmuller, H., Gillies, J.A., Rogers, C.F., DuBois, D.W., Chow, J.C., Watson, J.G., Langston, R., 1998. Particulate emission rates for unpaved shoulders along paved roads. Journal of the Air and Waste Management Association 48, 174–185.
Nenes, A., Pilinis, C., and Pandis, S. N. (1999) 'Continued Development and Testing of a New Thermodynamic Aerosol Module for Urban and Regional Air Quality Models', *Atmos. Env.*, Vol. 33 , pp.1553-1560.
Nicholson K.W., 1988. A Review of Particle Resuspension. *Atmospheric Environment* 22(12), 2639-2651.
Omstedt, G., Bringfelt, B., Johansson, C., A modell for vehicle-induced non-tailpipe emissions of particles along Swedisch roads, Atmospheric Environment 39, pp 6088-6097, doi: 10.1016/j.atmosenv.2005.06.037, 2005
Öttl, D, R. Funk, PM emission factors for farming activities by means of dispersion modeling, Landbauforshung Völkenrode Special Issue 308, pp. 173-177, 2008.
Pierce, J.R., and Adams, P.J. (2006), Global evaluation of CCN formation by direct emission of sea salt and growth of ultrafine sea salt, J. Geophys. Res., 111,
Poppe, D., Andersson-Sköld, Y., Baart, A., Builtjes, P.J.H., Das, M., Fiedler, F., Hov, O., Kirchner, F., Kuhn, M., Makar, P.A., Milford, J.B., Roemer, M.G.M., Ruhnke, R., Simpson, D., Stockwell, W.R., Strand, A., Vogel, B. and Vogel, H. (1996) 'Gas-phase reactions in atmospheric chemistry and transport models: a model intercomparison', *EurotracReport. ISS*, Garmisch-Partenkirchen.
Putaud, Jean-P.,Frank Raes, Rita Van Dingenen, Erika Brüggemann, M. -Cristina Facchini, Stefano Decesari, Sandro Fuzzi, Robert Gehrig, Cristoph Hüglin, Paolo Laj, Gundi Lorbeer, Willy Maenhaut, Nikolaos Mihalopoulos, Konrad Müller, Xavier Querol, Sergio Rodriguez, Jürgen Schneider, Gerald Spindler, Harry ten Brink, Kjetil Tørseth, Alfred
Querol, X., A. Alastuey, C.R. Ruiz, B. Artiñano, H.C. Hansson, R.M. Harrison, E. Buringh, H.M. ten Brink, M. Lutz, P. Bruckmann, P. Straehl, J. Schneider, Speciation and origin of PM10 and PM2.5 in selected European cities, *Atmos.Envir.38, Issue 38*, pp *6547-6555, 2004.*
Schaap, M., van Loon, M., ten Brink, H.M., Dentener, F.D., Builtjes, P.J.H. (2004a) 'Secondary inorganic aerosol simulations for Europe with special attention to nitrate', *Atmos. Phys. Chem.*, Vol. 4, pp.857-874.
Schaap, M., Denier Van Der Gon, H.A.C., Dentener, F.J., Visschedijk, A.J.H., van Loon, M., Ten Brink, H.M., Putaud, J-P., Guillaume, B., Liousse, C. and Builtjes, P.J.H. (2004b) 'Anthropogenic Black Carbon and Fine Aerosol Distribution over Europe'*J. Geophys. Res.,* Vol. 109, D18201, doi: 10.1029/2003JD004330.
Schaap, M. and H.A.C. Denier van der Gon, On the variability of Black Smoke and carbonaceous aerosols in The Netherlands, Atmos. Env. 41, 5908-5920, 2007
Schaap, M., M. Roemer, F. Sauter, G. Boersen, R. Timmermans, P.J.H. Builtjes (2005), 'LOTOS-EUROS Documentation', *TNO report B&O 2005/297*, TNO, Apeldoorn, the Netherlands.
Schaap, M., Vautard, R., Bergstrom, R., van Loon, M., Bessagnet, B., Brandt, J., Christensen, J.H., Cuvelier, K., Foltescu, V., Graff, A., Jonson, J.E., Kerschbaumer, A., Krol, M., Langner, J., Roberts, P., Rouil, L., Stern, R., Tarrason, L., Thunis, P., Vignati, E., White, L., Wind, P., Builtjes, P.J.H. (2009), Evaluation of long term aerosol simulations from seven regional air quality models and their ensemble in the EURODELTA study, submitted to Atmos. Environ.
Sehmel, G.A., 1973. Particle Resuspension from and Asphalt Road Caused by Car an

Seinfeld, J.H., and Pandis, S.N., Atmospheric chemistry and physics, Wiley, 1998
Shao, Y., Raupach, M.R., Findlater, P.A., 1993. Effect of saltation bombardment on the entrainment of dust by wind. J. Geophys. Res. 98, 12719–12726.
Simpson, D., Guenther, A.., Hewitt, C.N., and Steinbrecher, R., 1995: Biogenic emissions in Europe 1. Estimates and uncertainties, J. Geophys. Res., 100, No. D11, 22875-22890.
Simpson, D., Stockwell, W.R., Strand, A., Vogel, B., Vogel, H. (1996) 'Gas-phase reactions in atmospheric chemistry and transport models: a model intercomparison', *Eurotrac report. ISS*, Garmisch-Partenkirchen.
Simpson, D., Winiwater, W., Borjesson, G., Cinderby, S., Ferreiro, A., Guenther, A., Hewitt, C.N., Janson, R., Aslam, M., Owen, S., Pierce, T.E., Puxbaum, H., Shearer, M., Skiba, U., Steinbrecher, R., Tarrason, L., Oquist, G., 1999: Inventorying emissions from nature in Europe. Journal Geophy. Res., Vol. 104, 8113-8152.
Simpson, D., Fagerli, H., Jonson, J.E., Tsyro, S., Wind, P., and Tuovinen, J-P (2003), 'Transboundary Acidification, Eutrophication and Ground Level Ozone in Europe, Part 1: Unified EMEP Model Description', *EMEP Report 1/2003*, Norwegian Meteorological Institute, Oslo, Norway.
Stalpers, S.I.P. (2003), Modeling the sea salt fraction of particulate matter with the atmospheric transport model EUROS, Reports Environmental Studies nr 229, Katholieke Universiteit Nijmegen, 2003.
Stern, R., Builtjes, P., Schaap, M., Timmermans R., Vautard, R.; Hodzic, A., Memmesheimer, M., Feldmann, H.; Renner, E., Wolke, R., Kerschbaumer, A. (2008): A model inter-comparison study focussing on episodes with elevated PM10 concentrations, *Atmos. Environ, 42, 4567-4588*
Strader, R.; Lurmann, F.; Pandis, S. N. *Atmos. Environ.1999, 33*, 4849.
Tang I. N., (1997), Thermodynamic and optical properties of mixed-salt aerosols of atmospheric importance,*J. Geophys. Res.*, 102 (D2), 1883-1893.
Tarrasón, L., Fagerli, H., et al. The Norwegian Meteorological Institute (2008). Transboundary acidification, eutrophication and ground level ozone in Europe in 2006, status report 1/2008, The Norwegian Meteorological Institute.
Tarrasón, L., Jonson, J. E., et al. The Norwegian Meteorological Institute (2007). Transboundary acidification, eutrophication and ground level ozone in Europe in 2005, status report 1/2007, The Norwegian Meteorological Institute.
Tegen, I., Hollrig, P., Chin, M., Fung, I., Jacob, D., Penner, J., (1997), 'Contribution of different aerosol species to the global aerosol extinction optical thickness: Estimates from model results', *J. Geophys. Res.* 102, 23,895-23,915.
Ten Brink, H., Maenhaut, W., Hitzenberger, R., Gnauk, T., Spindler, G., Even, A., Chi, X., Bauer, H., Puxbaum, H., Putaud, J.-P., Tursic, J., Berner, A. (2004), INTERCOMP2000: The comparability of methods in use in Europe for measuring the carbon content of aerosol, Atmospheric Environment, 38 (38), pp. 6507-6519
Thorpe, A., R. M. Harrison, P.G. Boulter, I.S. McCrae, Estimation of particle resuspension source strength on a major London Road, Atmospheric Environment 41, pp. 8007-8020, doi: 10.1016/j.atmosenv.2007.07.006, 2007.
Thunis, P. and C. Cuvelier (eds.) (2008). EURODELTA – II, Evaluation of a Sectoral Approach to Integrated Assessment Modelling including the Mediterranean Sea, EUR 23444 EN – 2008, Luxembourg: Office for Official Publications of the European Communities.
Tsyro, S.G. (2005), To what extent can aerosol water explain the discrepancy between model calculated and gravimetric PM10 and PM2.5?, Atmospheric Chemistry and Physics, 5 (2), pp. 515-532.
Marticorena, B., Bergametti, G., 1995. Modeling the atmospheric dust cycle: 1. Design of a soil derived dust production scheme. J. Geophys. Res. 100, 16415–16430.
Van Jaarsveld J.A., 1989. Berekening van concentraties in de Nederlandse buitenlucht met behulp van het OPS model; Benzeen en Tolueen (in Dutch). RIVM report 228475010, Bilthoven, The Netherlands.
Van Jaarsveld J.A. and F.A.A.M. de Leeuw, 1993. An operational atmospheric transport model for priority substances. Environmental software, 8, 91-100.
Van Jaarsveld J. A., 1995. Modelling the long-term atmospheric behaviour of pollutants on various spatial scales. Ph.D. Thesis, Utrecht University, the Netherlands
Van Jaarsveld, J.A., 2004. The Operational Priority Substances model, description and validation of OPS-Pro 4.1, MNP report 500045001, Bilthoven, The Netherlands. (http://www.rivm.nl/bibliotheek/rapporten/500045001.pdf) (see also: http://www.mnp.nl/ops)
Van Jaarsveld and Klimov, (2009). Modelling the impact of sea-salt particles on the exceedances of daily PM10 air quality standards in the Netherlands, Int. J. of Environment and Pollution, excepted for publication.
Vautard, R., et al., Skill and uncertainty of a regional air quality model ensemble, Atmospheric Environment (2008), doi:10.1016/j.atmosenv.2008.09.083
Van Loon, M., et al, EMEP rapport, 2005, Modelling base cations in Europe
Velders, G.J.M., J.M.M. Aben, W.F. Blom, J.D. van Dam, H.E. Elzenga, G.P. Geilenkirchen. P. Hammingh, A. Hoen, B.A. Jimmink, R.B.A. Koelemeijer, J. Matthijsen, C.J. Peek, C.B.W. Schilderman, O.C. van der Sluis, W.J. de Vries, 2008, Concentratiekaarten voor grootschalige luchtverontreiniging in Nederland. Rapportage 2008, MNP report 500088002 (in Dutch), Bilthoven, The Netherlands. (http://www.rivm.nl/bibliotheek/rapporten/500088002.pdf)
Veldt, C. (1991) 'The use of biogenic VOC measurements in emission inventories', *MT-TNO Rep* 91-323.
Venkatram, A., D. Fitz, K. Bumiller, S. Du, M. Boeck, C. Ganguly, Using a dispersion modell to estimate emission rates of particulate matter from paved roads, Atmospheric Environment 33, pp. 1039-1102, 1999.
Visschedijk, A.J.H. and H.A.C. Denier van der Gon (2005) 'Gridded European anthropogenic emission data for NOx, SOS, NMVOC, NH3, CO, PM 10, PPM 2.5 and CH4 for the year 2000'. *TNO-Rep B&O*-A R 2005/106.
Wagner, F., Amann, M. and Schöpp, W. (2007). The GAINS Optimization Module as of 1 February 2007. IIASA Interim Report IR-07-004. (http://www.iiasa.ac.at/Admin/PUB/Documents/IR-07-004.pdf)
Walcek, C.J. (2000) 'Minor flux adjustment near mixing ratio extremes for simplified yet highly accurate monotonic calculation of tracer advection', *J.Geophys. Res.*, Vol. 105, D7, pp.9335-9348.
WebDab (2007). WebDab 2007 EMEP activity data and emission database. Website: webdab.emep.int.
WebDab (2008). EMEP modelled air concentrations and depositions. Website: http://webdab.emep.int/Unified_Model_Results/AN/.
Weijers, E.P. et al. (2009) Secondary Inorganic Aerosol in the Netherlands, PBL report nr. 500099006, Netherlands Environmental Assessment Agency, Bilthoven.
Whitten, G., Hogo, H., Killus, J. (1980) 'The Carbon Bond Mechanism for photochemical smog', *Env. Sci. Techn.*, Vol. 14, pp.14690-14700.
Witek, M.L.., Flatau, P.J., Teixeira, J., Westphal, D.L. (2007), Coupling an ocean wave model with a global aerosol transport model: A sea salt aerosol parameterisation perspective, Geophys.res let., 34, 2007
Yamartino, R. J., Flemming, J. and Stern, R.M. (2004) 'Adaption of analytic diffusivity formulations to eulerian grid model layers finite thickness', *27th ITM on Air Pollution Modelling and its Application.* Banff, Canada, October 24-29, 2004.
Yu, S., Mathur, R., Schere, K., Kang, D., Pleim, J., Young, J., Tong, D., Pouliot, G., McKeen, S.A., Rao, S.T. (2008), Evaluation of real-time PM2.5 forecasts and process analysis for PM2.5 formation over the eastern United States using the Eta-CMAQ forecast model during the 2004 ICARTT study, Journal of Geophysical Research D: Atmospheres, 113 (6), art. no. D06204, DOI: 10.1029/2007JD009226
Zhang, L., Gong, S., Padro, J. and Barrie, L. (2001), A size-segregated particle dry deposition scheme for an atmospheric aerosol module, Atmos. Env, 35, 549-560
Zhang, K.M., Knipping, E.M., Wexler, A.S., Bhave, P.V, Tonnesen, G.S. (2005), Size distribution of sea-salt emissions as a function of relative humidity, Atmos Env., 39,

Improved model system for Particulate Matter

This report is a technical background document about modelling of Particulate Matter. For policy support, it is necessary to quantify the relation between emissions, atmospheric conditions and concentrations of air pollutants. In the Netherlands, two models are used for this purpose. This document describes the two models and their recent developments accomplished within the BOP research programme. The LOTOS-EUROS model calculates air quality on a European scale and the OPS model focuses on the Netherlands. The LOTOS-EUROS model was validated against observations and further developed by including improved and new parameterisations for the contribution of sea salt, mineral dust and biogenic secondary organic aerosol to particulate matter. In addition, a coupling was realised between the global air quality model TM5 and LOTOS-EUROS. Finally, the LOTOS-EUROS model and the OPS model were tested in an intercomparison together with the unified EMEP model for ammonium, nitrate, sulphate and fine primary particles.

This technical background report is a BOP publication produced under the auspices of TNO.

The Netherlands Research Program on Particulate Matter (BOP) is a national program on PM_{10} and $PM_{2.5}$. It is a framework of cooperation involving the Energy Research Centre of the Netherlands (ECN), the Netherlands Environmental Assessment Agency (PBL), the Environment and Safety Division of the National Institute for Public Health and the Environment (RIVM) and TNO Built Environment and Geosciences.

P.O. Box 303, 3720 AH Bilthoven, The Netherlands